NOTICES

When Government drawings, specifications, or other data are used for any purpose other than in connection with a definitely related Government procurement operation, the United States Government thereby incurs no responsibility nor any obligation whatsoever; and the fact that the Government may have formulated, furnished, or in any way supplied the said drawings, specifications, or other data, is not to be regarded by implication or otherwise as in any manner licensing the holder or any other person or corporation, or conveying any rights or permission to manufacture, use, or sell any patented invention that may in any way be related thereto.

The nature of this research program requires the evaluation of a certain number of products under conditions peculiar to the research equipment and environments investigated. Many of the materials subjected to experiments were not developed or intended by the manufacturer for the conditions to which they have been subjected. Any failure or poor performance of a material is, therefore, not necessarily indicative of the utility of this material under less stringent conditions or for other applications.

Qualified requesters may obtain copies of this report from the Defense Documentation Center (DDC), (formerly ASTIA), Cameron Station, Bldg. 5, 5010 Duke St., Alexandria, Virginia, 22314.

This report has been released to the Office of Technical Services, U. S. Dept. of Commerce, Washington 25, D. C., in stock quantities for sale to the general public.

Copies of this report should not be returned to the Research and Technology Division, Wright-Patterson Air Force Base, Ohio, unless return is required by security considerations, contractual obligations, or notice on a specific document.

FOREWORD

This report was prepared by Mechanical Technology, Incorporated, Latham, New York, under AF Contract No. AF 33(657)-10694. The work was initiated under Project 3044, "Aerospace Lubrication," Task 304402, "Missile and Space Vehicle Propulsion Lubrication Engineering." The program was administered by AF Aero Propulsion Laboratory, Research and Technology Division, Wright-Patterson Air Force Base, Ohio with M. A. Sheets acting as project engineer.

The research was conducted from March 1963 to March 1964 by P. Lewis and J. Meacher, the authors.

This research is part of a continuing effort to obtain high speed, high temperature bearings for power conversion equipment for flight vehicles.

ABSTRACT

This report describes the first year's effort on a program that has as its objective the development of nitrogen gas lubricated journal and thrust bearings that have the best potential for stable operation at temperature to 1900 F and speeds to 60,000 RPM with low flow rates. The program concentrated on attaining quantitative performance data on dynamic rotor bearing behavior. The report summarizes materials selection, bearing types, equipment design, instrumentation, and experimental work.

This technical documentary report has been reviewed and is approved.

H. E. AMLI, Asst. Chief
Technical Support Division
AF Aero Propulsion Laboratory

TABLE OF CONTENTS

LIST OF TABLES

LIST OF ILLUSTRATIONS

LIST OF ILLUSTRATIONS (Contd.)

RECTANGULAR PAD ANALYSIS NOMENCLATURE

a	=	orifice radius, in.
b	=	pocket width, in.
B	=	pad width, in.
C	=	bearing clearance at neutral position, in.
k	=	stiffness, #/in.
ℓ	=	pocket length, in.
L	=	pad length, in.
M	=	mass flow thru an orifice, $\frac{\#\text{-sec}}{\text{in.}}$
M_t	=	total mass flow thru the pad, $\frac{\#\text{-sec}}{\text{in.}}$
N	=	number of orifices
P	=	dimensionless local pressure
P_a	=	ambient pressure, psia
P_p	=	dimensionless pocket pressure
P_s	=	supply pressure, psia
P_o	=	dimensionless local pressure at = 0
P_1	=	dimensionless pressure of the first order term shown in Eq. 3.
q	=	dimensionless flows
R	=	gas constant $\frac{\text{in.}^2}{\text{sec.}^2\ {}^{o}\text{R}}$
T	=	absolute temperature ^{o}R
V	=	supply pressure ratio = P_s/P_a
W	=	bearing load per pad, #
X, Z	=	coordinates shown in Figure 1, in.
α	=	orifice coefficient
ϵ	=	eccentricity ratio
λ	=	constant defined in Eq. 12
Λ_s	=	constant defined in Eq. 11
Λ_t	=	feeding parameter defined in Eq. 10
μ	=	viscosity $\frac{\#\text{-sec.}}{\text{in.}^2}$

INTRODUCTION

Requirements for equipment which must operate at high temperatures and high speeds, have prompted investigations on gas-lubricated bearings to establish the potential usefulness of this technique. The gas bearing has many characteristics which recommend it for such applications. Some of these are:

1. No deterioration at high temperatures.
2. Phase stability
3. Beneficial physical property for load capacity (viscosity increases with temperature).
4. Low friction.

The investigations carried on to date have given qualitative evidence that gas bearings can be applied to high-temperature, high-speed applications. However, in order to apply gas bearings to specific designs, quantitative information must be obtained on their performance characteristics.

The research work called for in AF 33(657)-10694 has as its objective the development of nitrogen gas-lubricated journal and thrust bearings that have the best potential for stable operation over the following ranges of operating conditions:

Ambient Temperature: 80 to 1900 F

Speed: 0 to 60,000 RPM

Supply Pressure: to 300 psig

The bearings must support static, unidirectional loads (not rotor mass of up to 100 pounds radial and thrust. Gas flow should not exceed 40 pounds per hour under any operating condition. One additional requirement is to consider situations where the factor controlling performance is dynamic, multidirectional loading, in place of static unidirectional loading. Unless proven impractical for the requirements, the bearing sizes should be no larger than:

1-1/2" diameter x 1-1/2" long radial bearing

1-1/2" diameter thrust bearing

A further requirement has been added: that the design characteristics consider the support of rotor masses from 3 to 30 pounds. This latter is particularly important with respect to dynamic rotor behavior.

This report summarizes the efforts on the subject contract during the first year covering the period March 31, 1963, to March 31, 1964. It includes program approach, design considerations, materials selection, test equipment, instrumentation, and experimental work.

Manuscript released by authors 20 March 1964, for publication as an RTD Technical Documentary Report.

PROGRAM APPROACH

Certainly, the first step in any investigation is to define the major problem areas. These are summarized briefly as follows:

1. Obtain required load-carrying capacity at minimum flow rates.
2. Maintain stable rotor-bearing behavior over the required range.
3. Select materials with suitable properties.
4. Consider and compensate for geometry changes due to thermal gradients, growth and distortion.
5. Consider possible deterioration of restrictor and flow passages due to high gas velocity and impingement (long life consideration).

The investigative program must then select the approaches which hold the greatest promise for providing solutions and reliable quantitative design information. The general steps are described briefly as follows:

1. Designs which will provide the required load capacity.
2. Designs and analyses of designs which will be stable under the range of speeds, and magnitude and types of loading.
3. General design characteristics where possible such as:
   a) adjustable features for growth and alignment
   b) minimum erosion
   c) minimize variations of performance due to geometry changes
   d) suitable mounting techniques
4. Materials selection
5. Consideration of system components
6. Suitable evaluation equipment and instrumentation necessary to establish operating characteristics.

The anticipated complexity of the designs, expense of materials, and difficulties of fabrication make it increasingly important to do the experimental work on designs that will yield the greatest potential and the most useful quantitative design information. This makes it necessary to combine experimental work and analysis in a well-coordinated program. Application of available design analyses will make it possible to eliminate less promising candidates, thereby reducing costly "cut and try" experimentation. This procedure permits putting the maximum amount of program resources into more promising approaches.

Prior work (Reference 1) has been conducted to develop bearings for the above-described conditions. In this work, short duration runs were achieved using an Al_2O_3 rotor with integral turbine drive, a single journal bearing loaded by hydrostatic loader pads at the ends of the journal. Instability of the pneumatic hammer type was encountered when a pocket type thrust bearing was used, leading

to a redesign of this bearing into one that had a "race track" groove fed from the central feeding tube by means of three "spokes." After some further machining of the thrust face which, in effect, reduced the initial depth of the grooves, the pneumatic hammer type instability was suppressed. For a variety of reasons, including: (a) the above-mentioned pneumatic instability, (b) limited heater life, (c) "thermal shock" cracking of rotor, and (d) foreign particles, (e) other, sometimes undetermined, reasons for failing to achieve or maintain full speed, the durations of the high-temperature runs were short. Tests were also run at high temperature and speed, but without load application in a specially designed spin rig. Also, tests were conducted with load application, but at temperatures of up to 1500 F, with an Inconel X rotor.

Despite the relatively short duration of the high-temperature, high-speed runs achieved in the prior work, it can be tentatively concluded that no unforeseeable limitations on operation under the conditions spelled-out in the specifications were encountered. Instead, achievement of the very stringent requirements will depend on attaining solutions to a number of extremely difficult technical problems including:

1. Development of gas bearing designs that are near optimum from the standpoint of minimum flow for the specified load and size. Such designs must, however, be consistent with the use of clearance sizes and restrictor types and sizes that are realistic over the entire temperature range.

2. Development of gas bearing designs that can withstand the large temperature range. This can be achieved, for example, either:

   a) if thermal expansion of all parts is exactly matched at all critical points, or

   b) if through certain design features, differential thermal expansions are absorbed by compliant or adjustable members.

3. Rotor centrifugal growth must be allowed for without either (a) excessive gas flow under some operating conditions, or (b) marginally small film thickness under other conditions.

4. Development of gas bearing designs that are free from instabilities throughout the pressure and speed ranges. Unless specifically suppressed in the design, instabilities of the pneumatic hammer type or of the Fractional Frequency type may be encountered in the ranges described.

5. Selection of bearing, restrictor and rotor materials that are satisfactory over the full temperature range from, at least, the standpoints of dimensional stability, expansion rates, high temperature strength, manufacturability and compatibility.

6. Adequate life (through both material selection and design features) of the restrictor and flow passages under high velocity, high-temperature gas and possible impingement or jetting.

7. Design and construction of heaters and other auxiliary components of the 1900 F test rig, for economy and adequate life.

8. Adaptation or development of adequate instrumentation for the high-temperature tests, including monitoring of the film thickness (rotor dynamics) and attitude angles. Such measurements are essential if meaningful conclusions on causes of operating difficulties and means of correcting them are to be drawn from the tests.

In the contract, the selection of hydrodynamic (self-acting) or hydrostatic (externally pressurized) gas bearings is left open, depending on which type can be shown to be not suitable. Actually, consideration of the loads and sizes specified indicates that hydrodynamic pressures alone are not sufficient, except under very marginal operating conditions. Some improvement in hydrodynamic load capacity could be achieved by operation in a pressurized ambient, but this would be at the cost of increased instability problems. On the other hand, the speed range of the application is sufficiently high that hydrodynamic effects will be significant even with hydrostatic bearings. (Unless, of course, designs are used which almost totally suppress these effects by means of very extensive and deep pockets or venting of the hydrodynamic pressure generating regions. Such designs, however, would be expensive in terms of gas flow, probably in excess of the allowable value, low stiffness, as well as inviting pneumatic hammer problems.) Thus, it has been decided that the bearings that evolve from this development will be of the hybrid (i.e. combined hydrodynamic, hydrostatic) type. While hybrid bearings are economical from the standpoint of flow, they must be carefully designed to suppress both pneumatic hammer and fractional, frequency-whirl type instabilities.

Design to support a static load with nominal supply pressures and flow is relatively straightforward. However, the definition of the stable operating range is more difficult and has received considerably less attention. In this instance the rotor mass to be supported and its geometry are the critical items. The interaction of the rotor-bearing system determines the stable operating range.

The area of stability was selected as a major item for emphasis in this program. There are two possible approaches:

1. to conduct an exhaustive investigation on a simple geometry, or

2. to select a new geometry in the hopes of eliminating the problem.

Without some further consideration, a restrictive decision on one or the other was not promising. A restrictive evaluation on the simple geometry would result in information on a design which would have definite limitations. By the same token, the new geometry has a series of unknown characteristics which remain to be established. In addition, design requirements will vary over a wide spectrum.

In order to review the basis for such a decision, a preliminary analysis and review of available experimental data on stability was made. (A summary is included in this report.) It indicated that the simple geometry had a definite range of applicability, but that the method for achieving the maximum value from this design required definition. The indications were that this would represent a fair portion of the application range.

It was necessary to select a design to cover a greater portion of the application range or for use with larger rotor masses. Based upon the best available information, the flexure mounted hybrid pad bearing was selected for consideration in this program. This bearing type should extend the range of operation beyond that possible with the 360 degree bearing.

The decision was to define the range of the 360 degree bearing in regard to the support of specific rotor masses. The information would be put in general form such that definite guidelines would be available to the designer. One other feature which becomes available is a datum established by the 360 degree bearing to evaluate the performance of the other design concepts. The flexure-mounted hybrid pad would be constructed and evaluated after the 360 degree bearing. In this manner, information relative to a wide range of applications will be forthcoming.

Considerable attention was devoted to the design of suitable equipment and the selection of instrumentation.

In order to establish a realistic experimental program, the preliminary analyses and evaluation of available experimental evidence were used to select the variables and the ranges to be explored in this program.

In summary, the program was designed to concentrate on the following.

1. The program is directed toward bearing development which is applicable to the support of practical rotor systems. To this end, rotor systems supported by two bearings will be evaluated. The dynamic characteristics of such systems will receive major attention.

2. Evaluations will start with optimum and near optimum designs in order to establish the validity of the stability criteria.

3. Normally, a single regime of compensation will be used, and the ranges considered will not unless by intent cause changes in the mode of compensation (from orifice to inherently compensated).

4. Care will be taken to avoid extraneous rig effects, e.g., contamination from the gas heaters and influences from a third loader bearing. Normally, the loader bearing will not be in the system during evaluations for stability. However, it is designed for extremely low stiffness, should it be necessary during such tests. Careful mounting will minimize the possibility of misalignments due to distortion.

5. Thermal and centrifugal effects will be included in the evaluation and interpretation of results.

6. Although the double row bearing has been selected for initial evaluation, an overall design concept like the partial arc will be brought along.

The sections which follow discuss these items in detail.

BEARING TYPES AND DESIGN

Bearing Types

As will be shown later in this section, the 360 degree externally pressurized bearing which will support a 15 pound rotor mass per bearing at 60,000 RPM will require high supply pressure, small clearances, and small orifices. The last two factors are not the most desirable from the standpoint of high-speed operation over a range of temperatures.

It appeared desirable to compare the bearing types on the basis of the factors which are considered most important from the standpoint of program objectives and future applications. Table 1 summarizes the status of the evaluation. Figure 1 schematically shows schematically the various bearing types. Although such a rating is of necessity arbitrary, these are sufficiently realistic for comparative purposes. As Table 1 is examined from the standpoint of all the items, three of the bearing types would be very comparable: a flexibly mounted 360 degree hybrid bearing, a pivoted pad hybrid bearing, and flexible mounted hybrid pad. If the comparison is made, based solely on the ability to meet operating objectives (the first five items), the two hybrid pad types are the primary choices.

Some explanation of some of the ranking and reasoning behind it is in order at this point.

360 Degree Hybrid Bearing - This bearing is by far the most susceptible to instability. The rigidly mounted type is sensitive to misalignment, rotor thermal gradients, and housing distortions. Its simplicity generally makes it attractive for consideration. However, when higher rotor masses and high speeds are involved, this type is severely limited.

The flexibly-mounted version will generally decrease the threshold speed at which fractional frequency-whirl will be encountered, since additional radial flexibility is placed in the system. However, the ability of such a system to align is improved many fold. In addition, the cylindrical shell is isolated thermally from the housing and will follow shaft gradients and will not readily reflect housing distortions. The cylindrical shell also resists geometrical distortions better than sectors or other shapes.

Hybrid Pad - Pivoted - The pivoted pad type bearing has proven itself to be successful for high-speed stable operation. This is attributed to the inability of the pad to sustain a tangential load. Where the pivot is a sphere or gimbal mount, the ability to align is excellent. The ability to tolerate gradients is good, particularly where these can be accommodated by pivoting. Some thermal isolation is achieved. However, this type would be susceptible to radial movements. Although perhaps a lesser point, the pad or cylindrical sector is not as resistant to distortion as a full cylinder. Major considerations are the loading and rubbing contact of the pivots, and the problem of bringing the gas supply to the pad without incurring the penalties of high leakage flow and restriction of pad motion.

TABLE 1

RANKING OF THE BEARING TYPES

	Bearing Type	Stability	Alignment	Tol. to Distortion Thermal Gradients	Stiffness	Flow	Mfg.Diff.	Design Complexity
a.	Hybrid 360 Rigid	3*	4	4	1	1	1	1
b.	Hybrid 360 Flex. Mt.	4	2	1	2	1	2	2
c.	Hybrid Pad Pivoted-Normal Pivot	1	1	2	1	2	3	4
d.	Hybrid Pad Hydrostatic Pivot	2**	1	2	2	3	4	4
e.	Hybrid Pad Flex. Mt.	2	1	1	1	2	3	3
f.	Hybrid 360 Hydrostatic 360	2**	2	2	2	3	2	4
g.	Hybrid 360 Hydro. Spher.	2**	1	2	2	3	3	4

* Lowest number corresponds to the most desirable.

** Considers also the pneumatic hammer type of instability.

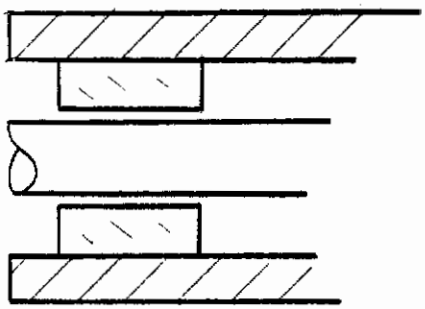

a. Hybrid 360° Bearing Rigidly Mounted in the Housing

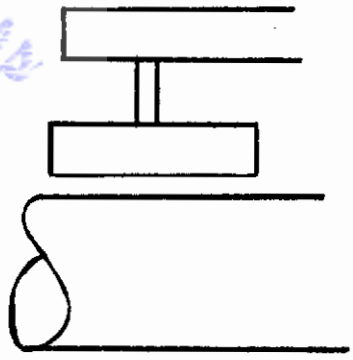

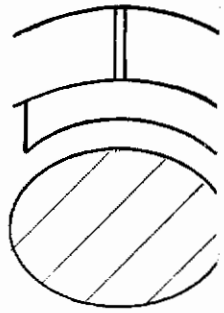

e. Hybrid Pad with a Flexible Mounting

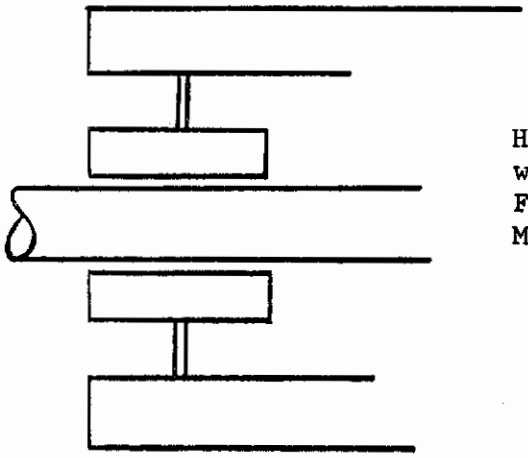

b. Hybrid 360° with Flexible Mounting

f.

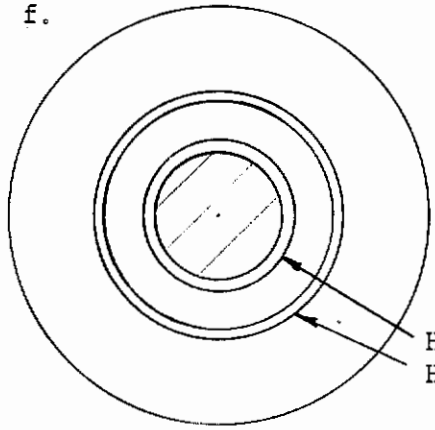

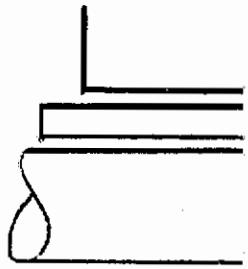

Hybrid 360°
Hydrostatic 360°

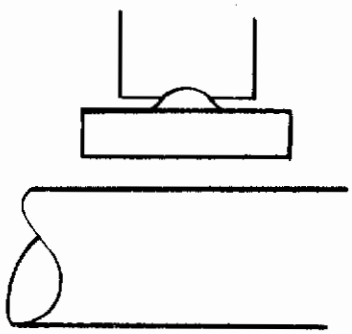

c. Hybrid Pivoted Pad

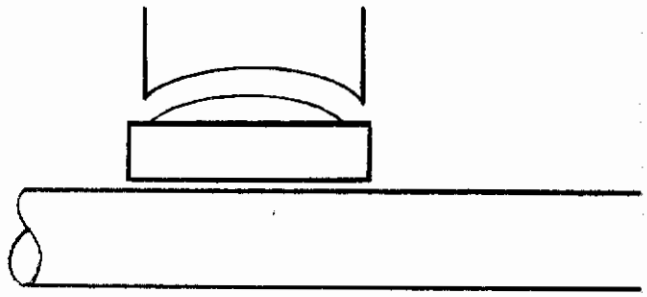

g. Hybrid 360° Hydrostatic Spherical

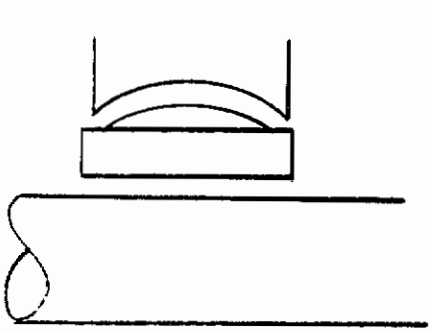

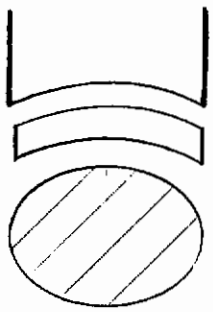

d. Hybrid Pad with Hydrostatic Pivot

Fig. 1 Bearing Types Considered in Table 1.

A variation of this theme would be to utilize a hydrostatic pivot. Certainly this would remove the problem of rubbing contact and possible material creep under the contact loading. In all probability, this design would result in a more massive pad of higher inertia which would not be desirable. Flow is increased and the supply of gas to the pad is not simplified. It is possible that under a wide variation in loading, a pneumatic hammer type of instability could be encountered.

The second variation would replace the pivot with a column which is radially stiff but flexible to bending deflection. It will be noted in Table 1 that the ranking for stability has been decreased since the pad could sustain a tangential force by virtue of the moment on the column. However, if sufficient bending flexibility can be incorporated into the column, this should not be a major factor. A hollow column or post would provide the mechanism for gas supply to the pad without additional restraint. The post must be considered with respect to fatigue life and possible creep which would change the radial position of the pad. In the design several possible resonances must be considered. Preliminary design calculations on such a design (Figure 2) indicate feasibility.

Hybrid-Hydrostatic Combination - This concept would utilize the hybrid bearing for primary shaft support and a hydrostatic (non-rotating) bearing outside of the hybrid bearing. This concept is an extension of the theory which would incorporate flexibility and damping in the bearing support structure to damp out vibration. The hydrostatic bearing is designed to provide suitable spring and damping characteristics to accomplish this. Figure 3 shows how the ratio of running speed-to-rigid body resonance is affected by spring and damping characteristics of the two bearings. Preliminary design calculations on the double cylindrical configuration indicate that this can be accomplished with practical clearances and sizes. However, the gas supply to the inner bearing (hybrid) presents a problem. In addition, the 360 degree cylindrical hybrid bearing is not truly thermally isolated from the housing as is the flexibly-mounted hybrid bearing. The ability to align is limited. Because of the number of components and functions,this is a complex arrangement.

Substitution of a spherical, hydrostatic support for the 360 degree support greatly improves the ability to align and adjust, but leaves the other features reasonably similar.

Although several design and manufacturing problems remain to be overcome, the hybrid pad or sector on a flexible post which also serves as a gas supply tube appears the most promising at this time.

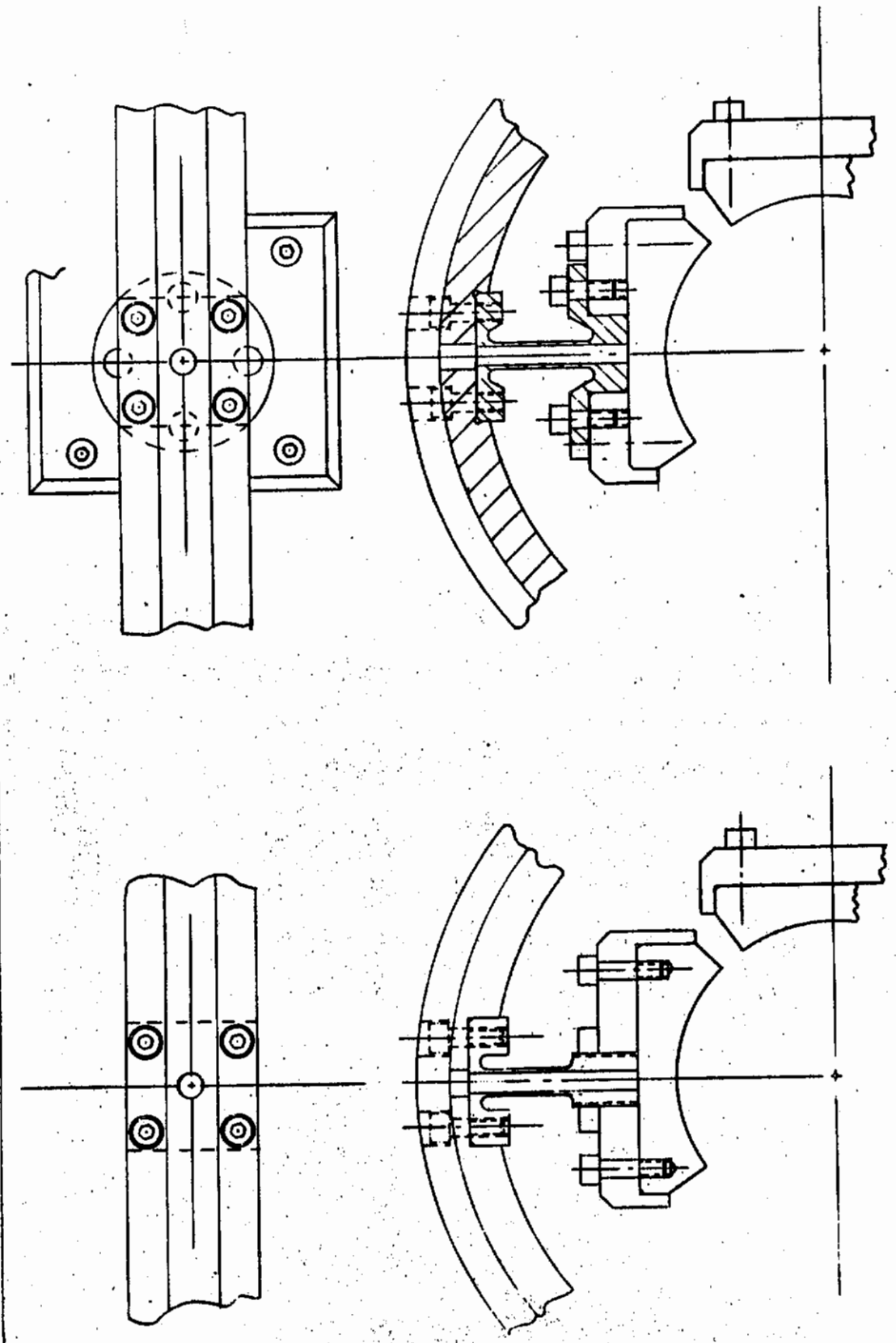

Fig. 2. Flexibly Mounted Hybrid Pad - Preliminary Design

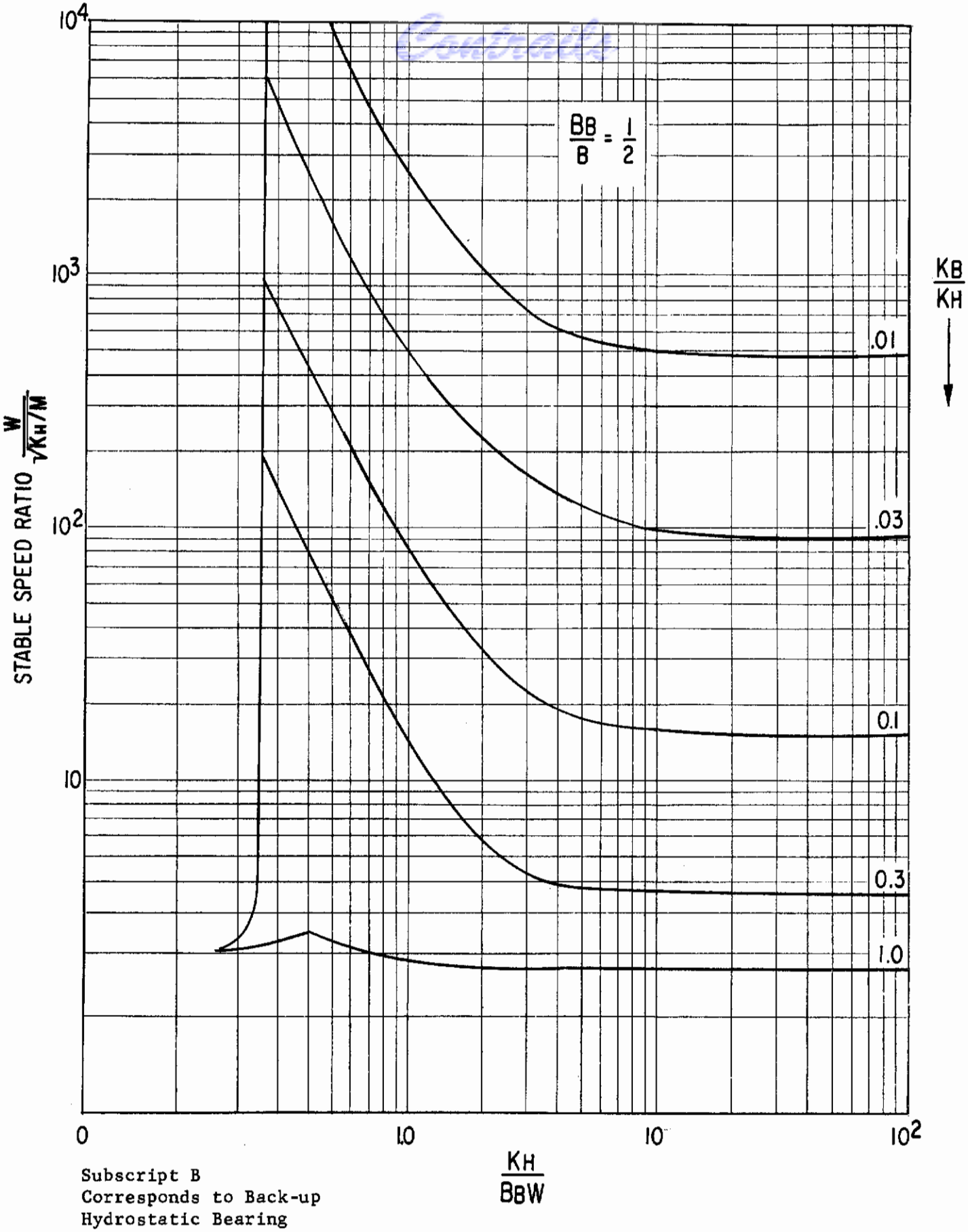

Figure 3. Theoretical Speed Capability of Hybrid Bearing with a Flexible Damped Support.

Load Capacity and Gas Flow

As previously mentioned, it is felt that externally pressurized bearings will be required in view of the specified loads and bearing sizes. A major consideration here will be to achieve a design that is adequate over the wide temperature range (and hence viscosity and density ranges) required, without excessive flow or marginal film thickness at any condition. Because of this wide temperature range, it is not practical to anticipate a design that will be optimum from the standpoint of minimum flow for a given load capacity over the whole range. Instead, the matching of restrictor system and bearing clearance should be such that the range of operation scans the optimum point with relatively flat design regions on both sides of it.

In order to gage the potential flow requirement in the present development, some preliminary calculations were made for an orifice journal bearing of the size described. These calculation results are summarized in Table 2 and are plotted in Figure 4. These show the major effects of (a) clearance and (b) temperature effects on the fluid properties. Note that these preliminary calculations did not involve optimum matching of restrictors and clearances, so that it appears that the 40 lbs/hr maximum flow specified can be achieved.

The preliminary calculations of Table 2 were made for a single-row orifice feed. The load capacity and stiffness were optimized at 80 F. Obviously, the selection of this design point would not suffice over the required temperature range. Load capacity and resistance to misalignment can be improved by using two rows of orifices. Results of the calculations on this type are included. Further, orifices in series or combined orifice and inherent compensation can, if necessary, be used in order to achieve optimum matching of restrictor and clearance characteristics without resorting to too few or too small orifices.

Orifice-fed bearings are, of course, only one possible type of bearing for this development. Other types were:

(1) Porous Material Bearings - These bearings generally can be designed to possess higher load capacity for a given size and flow. However, the lack of porous materials, suitable for the temperature range and the inherent problem of flow control eliminated them from further consideration.

(2) Step-type Bearings - While these designs are generally not optimum from the standpoint of low flow, they were considered because experience with them in the 80 to 1900 F temperature range has been obtained in the prior work (Reference 1).

Externally pressurized, double-row orifice journal bearings were selected. In order to arrive at a bearing design, it is necessary first to set up the design conditions. In the present analysis, the influence of the thermal expansion upon the bearing clearance will not be considered. Since it is more properly a part of the actual mechanical design, it will be left for future investigation. Hence, under the assumption of constant clearance over the operating temperature range, the design conditions may be listed as:

TABLE 2

PRELIMINARY HYDROSTATIC BEARING CALCULATIONS

1-1/2" Dia. x 2" lg. Journal Bearing
Single row orifice feed
Load: 100 lbs.
Gas: nitrogen
Pressure Ratio 20; Ambient Pressure 14.7 psia

Radial Clearance inches	Temperature ^{o}F	Ecc. Ratio	Flows lbs./hr.	Stiffness lb./inch
0.0003	80	0.25	1.6	1.33×10^6
0.0003	1000	0.35	0.6	0.95×10^6
0.0003	1900	0.78	0.3	0.32×10^6
0.0006	80	0.25	12.4	0.67×10^6
0.0006	1000	0.35	4.4	0.47×10^6
0.0006	1900	0.78	2.3	0.16×10^6
0.0009	80	0.25	41.8	0.44×10^6
0.0009	1000	0.35	14.9	0.32×10^6
0.0009	1900	0.78	7.8	0.11×10^6
0.0012	80	0.25	99	0.33×10^6
0.0012	1000	0.35	35	0.24×10^6
0.0012	1900	0.78	19	0.08×10^6

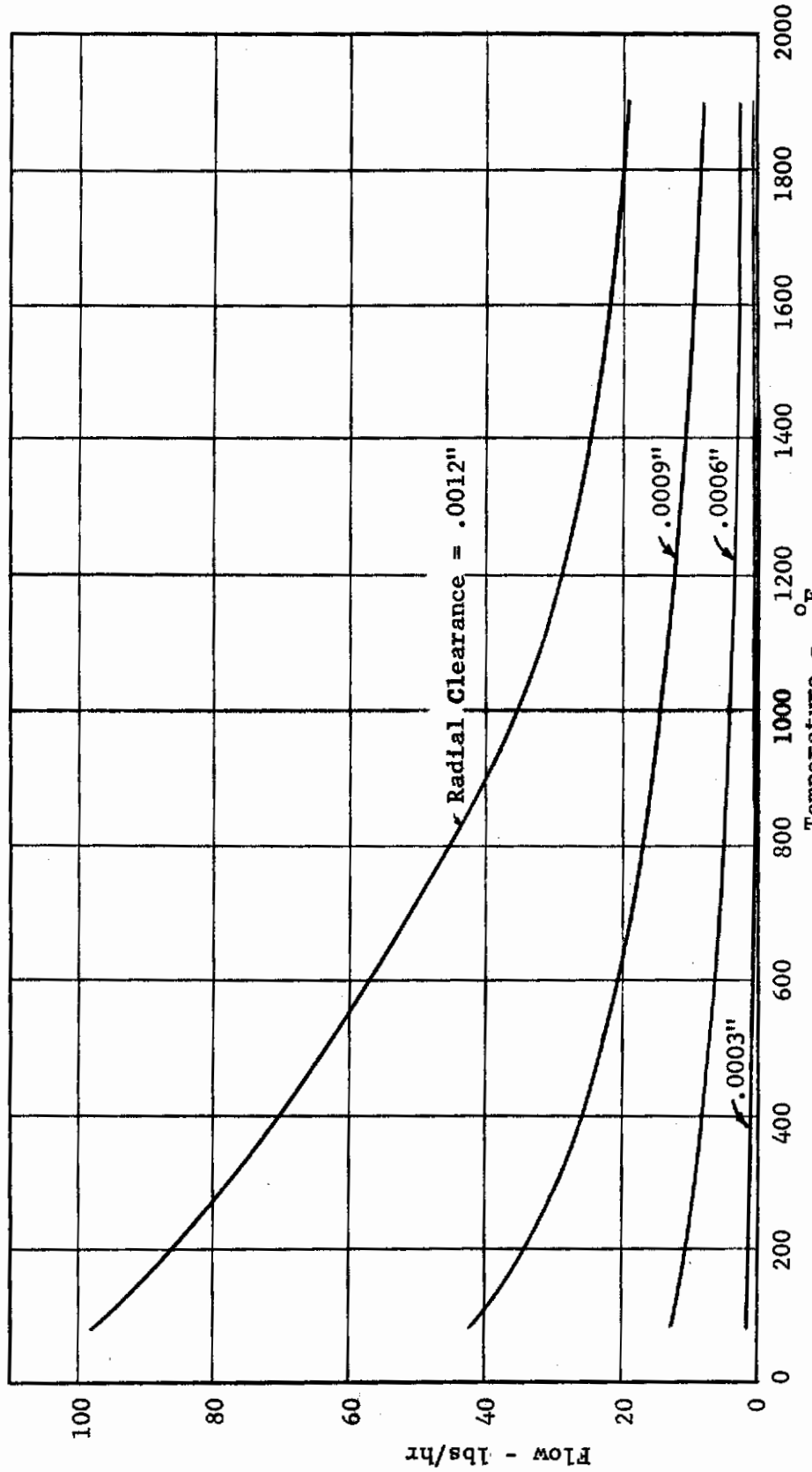

Figure 4. Preliminary Flow Calculations

1. Mass flow less than 40 lbs/hr.

2. Gas temperature from 0 to 1900 F.

3. Stiffness sufficiently high to prevent instability within the speed range 0 to 60,000 RPM.

4. Maximum available supply pressure is 300 psi.

The bearing has a diameter of 1.5 inches and a length of 1.5 inches. It is fed through two rows of orifices, symmetrically located midway between the middle of the bearing and the ends. Based on this configuration, calculations have been performed to compute the dimensionless load as a function of the feeding parameter Λ_s for several values of the ratio between supply pressure P_s and ambient pressure P_a. The feeding parameter expresses the ratio between the bearing flow resistance and the orifice resistance and, therefore, depends on the viscosity, the temperature, the gas, the total orifice area, the clearance and the supply pressure. The underlying analysis assumes that the load is a linear function of displacement, i.e., of eccentricity ratio ϵ so that the stiffness is obtained directly. The results are plotted in two diagrams, one for load and one for flow. It is seen that there is a maximum obtainable load which occurs at $\Lambda_s = 1.5$. To select the design, the variation in Λ_s due to temperature is needed. The viscosity can be approximated by:

$$\mu = 1.7 + 2.2 \cdot 10^{-3} \cdot T \quad 10^{-9} \frac{\text{lbs.sec.}}{\text{in}^2} \quad (T \text{ in } {}^{\circ}R)$$

Thus, the feeding parameter can be written:

$$\Lambda_s = \frac{6\mu N a^2}{P_s C^3} \quad T = \frac{6Na^2}{P_s C^3} \cdot 10^{-9} \quad 1.7 + 2.2 \cdot 10^{-3} T \quad T$$

Letting T vary from $500^{\circ}R$ to $2360^{\circ}R$ results in Λ_s varying by a factor of 5.3. Select $\Lambda_s = .4$ at $500^{\circ}R$ ($40^{\circ}F$) yielding a dimensionless load of .55.

To ensure stability, the first rotor critical speed must be at least half the top running speed of 60,000 RPM. Assuming a rotor mass M per bearing of 15 pounds the corresponding stiffness becomes:

$$K > M\omega_{crit}^2 = \frac{15}{386} (3,500)^2 = 5 \cdot 10^5 \text{ lbs/in}$$

From the result for the dimensionless load:

$$K = \frac{w}{C_\epsilon} = \frac{D.L\ (P_s - P_a)}{C} \cdot .55$$

With D = L = 1.5 inch, set $P_s - P_a$ = 300 psig and the radial clearance $C = .5 \cdot 10^{-3}$ inches to get

$$K = 742{,}000 \text{ lbs/in}$$

which meets the requirement.

The flow is determined from the second diagram:

at $500^\circ R$ ($40^\circ F$, $\Lambda_s = .4$): Q = 6.6 lbs/hr.

at $2360^\circ R$ ($1900^\circ F$, $\Lambda_s = 2$): Q = 2.4 lbs/hr.

which is well below the limit of 40 lbs/hr.

The size of the orifices is computed from the chosen value of Λ_s:

Orifices per row	Orifice diameter, inch
8	$4.5 \cdot 10^{-3}$
12	$3.7 \cdot 10^{-3}$
16	$3.2 \cdot 10^{-3}$

Summary

With the above described configuration of the double row, externally pressurized bearing and:

Radial clearance: $C = .5 \cdot 10^{-3}$ inch

Supply pressure: P_s = 300 psia

Orifice dimensions, see table above.

the bearing has a stiffness of 742,000 lbs/in. (40 F) to 1,000,000 lbs/in (1900 F) and a mass flow of 6.6 lbs/hr. (40 F) to 2.4 lbs/hr. (1900 F). This should ensure stable operation up to 60,000 RPM for a rotor weight of 15 pounds per bearing. The calculation assumes that the bearing clearance is not significantly affected by temperature.

The effect upon load-carrying capacity of the rotational speed is negligible because of the high supply pressure. The compressibility number is:

$$\Lambda = 16.2 \text{ (40 F) to } 39.8 \text{ (1900 F)}$$

In addition, this calculation shows that the single row bearing has too low a load-carrying capacity to meet the design requirements.

These charts can be used to consider the designs for the high-temperature rig which will not have as large a mass. The general design charts are shown in Figures 5 and 6.

Stability

Instability has been the major problem area encountered in gas bearing work and it is one of the factors that has limited their applications to date. Analytical approaches to the problem of instability have been only partly successful because of the non-linearity of the fluid film equations (with compressible fluids) and because of the large variety of possible geometries. Often, in view of the difficulties of the problem, complex mathematical techniques were used and a clear physical picture of "events" in the fluid film could not be given. Despite these difficulties, considerable progress has been achieved in this area. As a result of work which has been both theoretical and experimental, the important geometrical and other parameters that tend to suppress instabilities are well known and it is frequently possible to ascertain during design whether a particular rotor-bearing system will be stable in its operating range.

A frequently encountered instability in externally pressurized bearings is "pneumatic hammer." This is a self-excited oscillation of the fluid system that can occur with or without rotation. Analogous phenomena have been encountered in valves, gas regulators and other components of pneumatic control systems. While several factors influence the occurrence of pneumatic hammer, the principal cause of it is the low stiffness of a gas-filled pocket. Because of compressibility, large storage of potential energy can be effected and rapid, oscillatory interchange of kinetic and potential energies can occur with little energy dissipation. In order for the present development to be successful, it will be necessary to ensure that pneumatic hammer is suppressed throughout the range of operating pressures. An extensive fundamental treatment (either theoretical or experimental) of pneumatic hammer is clearly outside the scope of this bearing development. However, the criteria of Reference 2 will be used for design review.

Pneumatic hammer is only one of the instabilities that are encountered in gas bearing operations, particularly in view of the high speed required here. The occurrence of instabilities is a function of:

1 Fluid Properties (viscosity, density),
2 Supply Pressure and Pressure Ratio,
3 Load and Speed,
4 Bearing and Restrictor Geometry, size and clearance ratio,
5 Bearing Mounting,
6 Rotor Mass,
7 Rotor Polar and Transverse Moments of Inertia,
8 Rotor Flexibility.

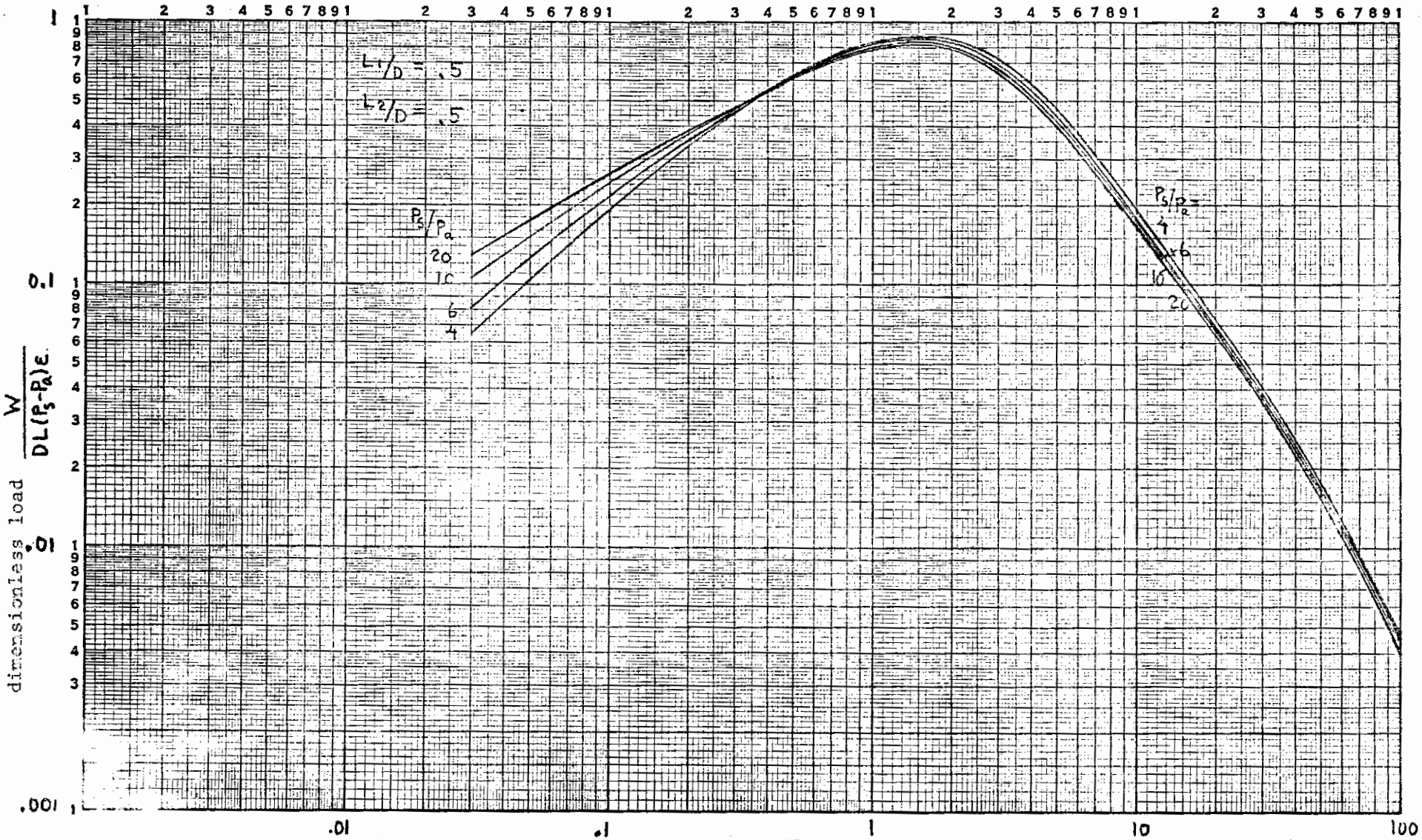

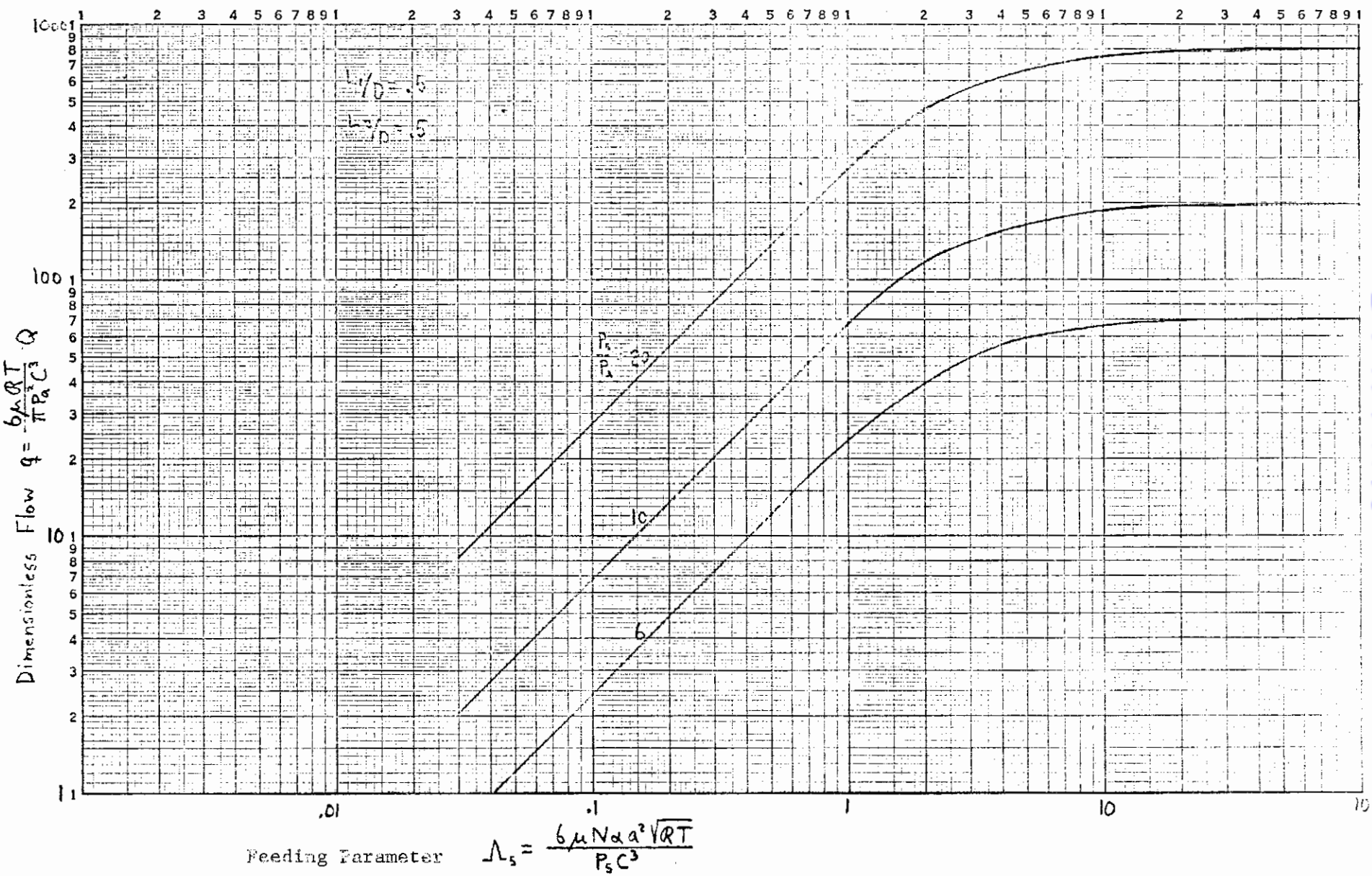

Figure 6. Flow - Double Row Hydrostatic Bearing

6-6-63

In the present development, the rotors used will be rigid, in that coupling of the rotor and fluid film elasticities need not be considered. (the use of rigid rotors will also ensure that any flexible critical speeds will be well above the planned speed range.)

The hybrid bearing, in particular, because of its potential for high load and high speed with minimum flow has received considerable attention under steady state and dynamic conditions. Rotation and the subsequent generation of hydrodynamic pressures influences performance of externally pressurized bearings as follows:

1. Added load capacity
2. Change in attitude angle
3. Potential instability

The extent to which hydrodynamic pressures will contribute to load capacities in the present program will be experimentally established for selected cases. Based on previous work (References 3 and 4), it appears that this can be a significant amount. For example, Figures 7 and 8 reproduced from Reference 4, show this influence on load capacity and attitude angle, for a specific orifice fed bearing. Guidance from such theoretical and experimental work on hybrid bearings are being applied to reduce the time and cost of designing suitable low flow bearings for the present development.

From the standpoint of stability, the generation of hydrodynamic pressures results in a threshold speed above which, fractional-frequency whirl sets in. This instability is analogous to half-frequency whirl of purely hydrodynamic bearings, except that the whirl frequency is some fraction (less than 1/2) of running speed. The onset of this instability often escapes attention (unless continuous monitoring of the fluid film thickness is made) until the whirl amplitudes increase to a destructive magnitude. For this reason, it is important that selected geometries, speed ranges and pressure ratios be proved out first in room temperature runs where there is no problem with film thickness measurement. In addition, development of high temperature film thickness gages is extremely important in this development for detection of incipient whirl in high temperature studies.

Experimental determination of the effects of the various parameters previously listed, on inception of fractional-frequency whirl have already been performed in a recent work (Reference 5).

In the above discussion, we have attempted to mention some of the stability problems associated with development of high speed, externally pressurized gas bearings. Table 3 summarizes the design parameters which require attention in such development.

As a starting point for a stable design, one must consider the fact that such bearings will normally operate at low eccentricity ratios and pressurized central regions. This tends to make the hydrodynamic behavior more nearly incompressible. Consideration of such a system leads to the conclusion that the system will be unstable whenever the rotative speed exceeds twice the lowest natural frequency since the fluid film damping goes negative at this point. Although certain investigations (Reference 5, 6, and 7) have shown results where the ratio of rotative speed (onset of instability) to the lowest natural frequency far exceeds two, a check of the optimized design correlates reasonably well.

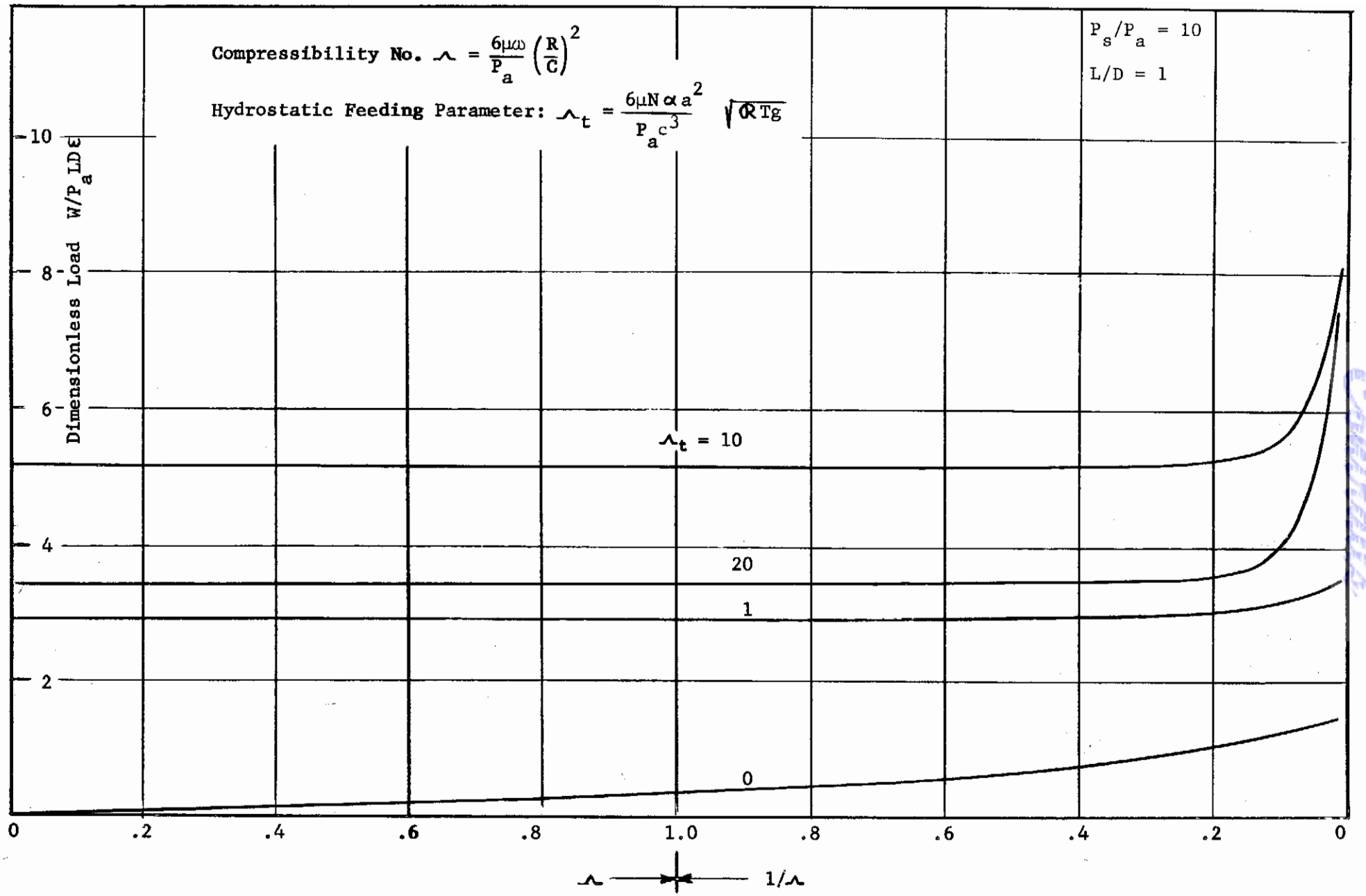

Figure 7. Load versus Speed of Rotation for the 360 Degree Hybrid Bearing

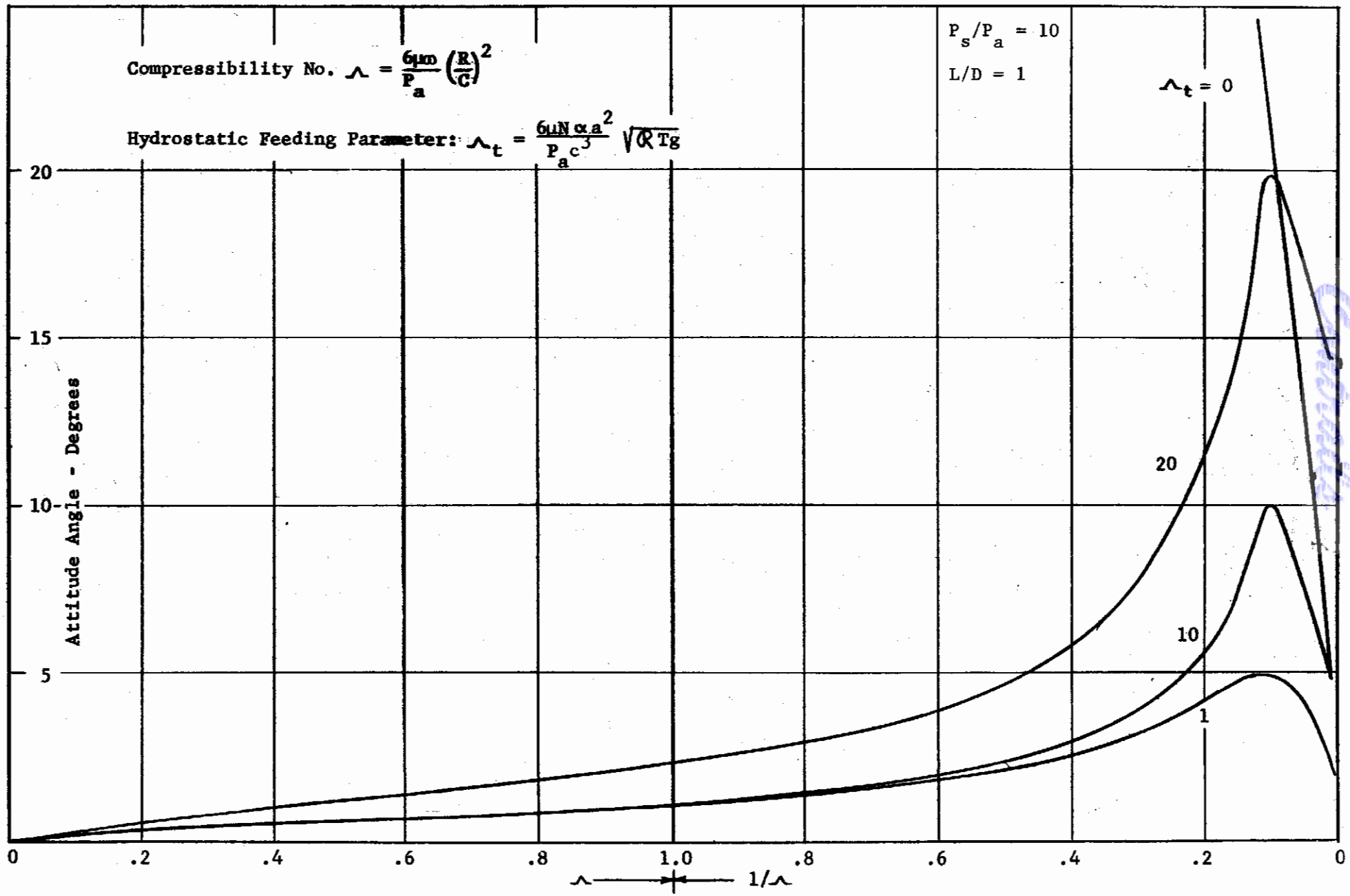

Figure 8. Attitude Angle versus Speed of Rotation for the 360 Degree Hybrid Bearing

TABLE 3

STEADY STATE PERFORMANCE

Type	Needed Data	Design Parameters
Externally Pressurized	Load-carrying capacity, Bearing or journal friction. Attitude angle. Minimum film thickness. Supply pressure, pressure ratio and flow requirement.	Bearing geometry (including effects of tolerance, centrifugal growth, thermal & mechanical distortions). Speed Fluid characteristics. Ambient pressure. Supply pressure. External flow resistance.

DYNAMIC PERFORMANCE

Externally Pressurized	Region of stable operation. Stiffness characterisitics. Damping Characteristics. Other film force characteristics. (Bearing influences on rotor criticals)	Bearing geometry (including effects of tolerance, centrifugal growth. Thermal & mechanical distortions). Speed. Fluid characteristics. Ambient pressure. Rotor flexibility. Time varying loads. Supply pressure. External flow impedance.

An analytical investigation of the instability threshold for the externally pressurized bearing due to shaft rotation was made (Reference 8). The analysis was based on two major assumptions: 1) the journal eccentricity is small compared to the radial clearance clearance, and 2) the pressurized air is supplied to the bearing through a sufficiently large number of orifices that they may be represented by a line source in the centerplane of the bearing. Experience has shown that these assumptions are, in general, valid when predicting the load-carrying capacity and the flow for the externally pressurized bearing. Therefore, it seems natural to employ the same assumptions in the instability investigation, thereby simplifying an otherwise very difficult analysis. With these simplifications, the basic equation for the gas film, Reynolds' equation, becomes linear and can be solved by numerical integration. Thus, the resultant forces on the journal can be obtained, first for the steady-state operating position, and then under the influence of a small disturbance with a prescribed frequency. Knowing the forces, the equations of motion for the rotor are established and the stability of the motion for the given frequency may be investigated. Scanning the frequency range, the inception of instability can be determined.

Numerical results are given in Reference 8 in the form of 24 graphs, spanning a wide range of design parameters, for both the speed of threshold of instability and the corresponding frequency. The following simple relationship is found to hold true in close approximation.

$$\frac{\text{(Speed at Instability Threshold)}}{\text{(Natural Frequency of purely hydrostatic bearing)}} = \frac{\text{(Operating Speed)}}{\text{(Frequency at Instability Threshold)}}$$

Since the ratio on the right hand side is equal to or greater than two, the result can also be formulated: instability sets in at twice (or more) of the natural frequency of the purely hydrostatic bearing. This relationship is confirmed by test results.

Apart from such qualitative agreements, discrepancies as large as 2:1 are found between calculated and measured threshold speeds. Whereas good correlation is indicated when the orifices are choked, deviations become serious in the unchoked region. Hence, it may be tentatively concluded that the gas film is properly treated and that the source of the problem is the orifice and feeder representation. The analysis could easily be modified to include different orifice characteristics and also a time depending effect, but for lack of any specific theory this has not been done. Even so, the analysis should be of value as a first step towards a more comprehensive study and, in addition, serve as a guide for conducting experiments and interpretation of data.

Thus, Figures 9 to 12 from Reference 8 show that for $\frac{\Lambda_s}{(\Lambda_s)_{opt}} < 1$, there exists a range where the threshold speed may be high or even infinite, depending on the corresponding value of Λ. The effect gets more pronounced with increased pressure ratio V and increased eccentricity ratio. This trend of improved threshold speed is qualitatively confirmed by test results as shown in Figure 13. It should be noted that all the tests have the conical mode as the lowest critical speed and, furthermore, that the data of Larson and Richardson (Reference 7) and most of the data of Sternlicht and Winn (Reference 5) is for the inherently

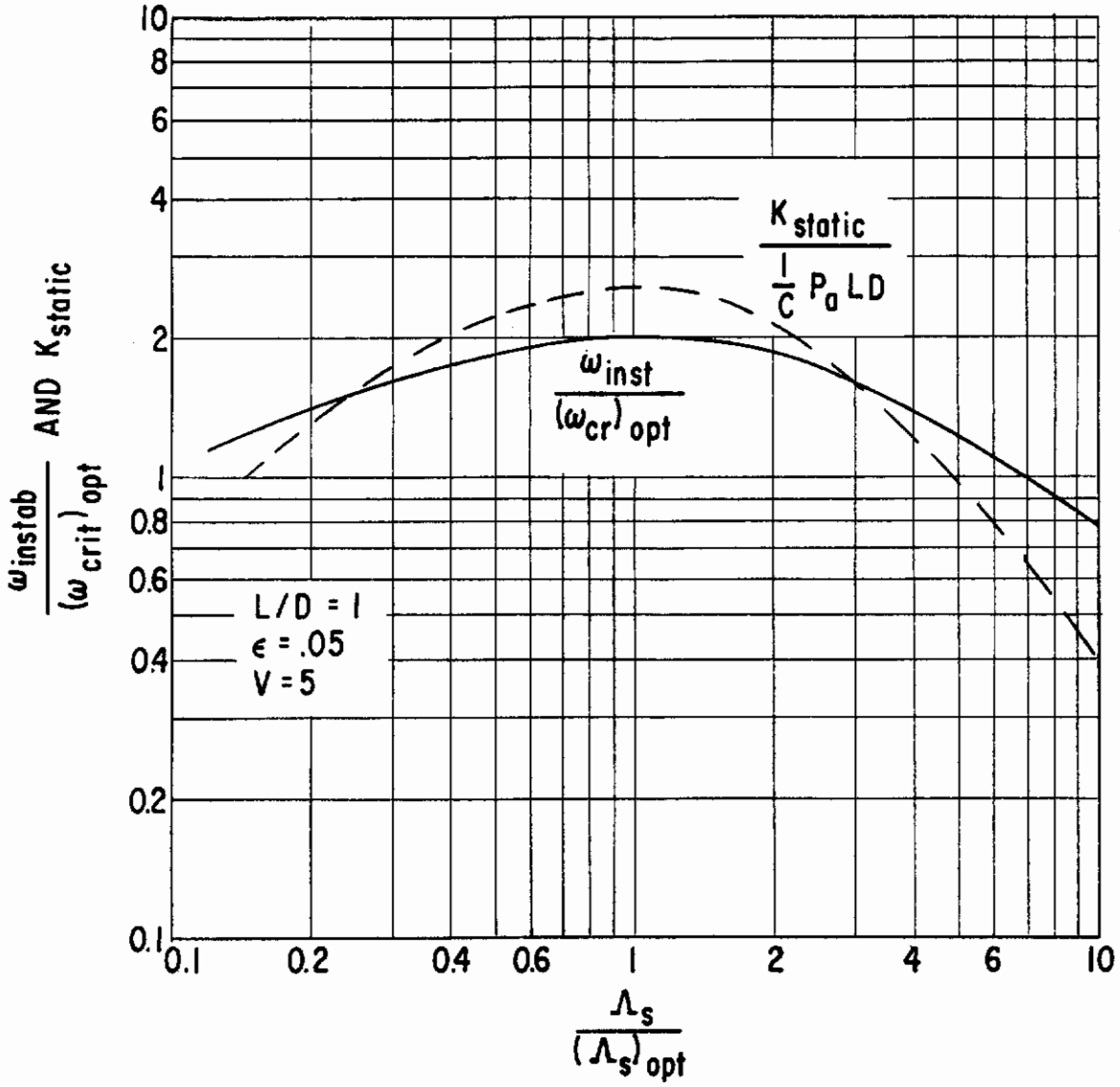

Figure 9. Speed Ratio versus Feeding Parameter Ratio for 360° Hybrid Bearing

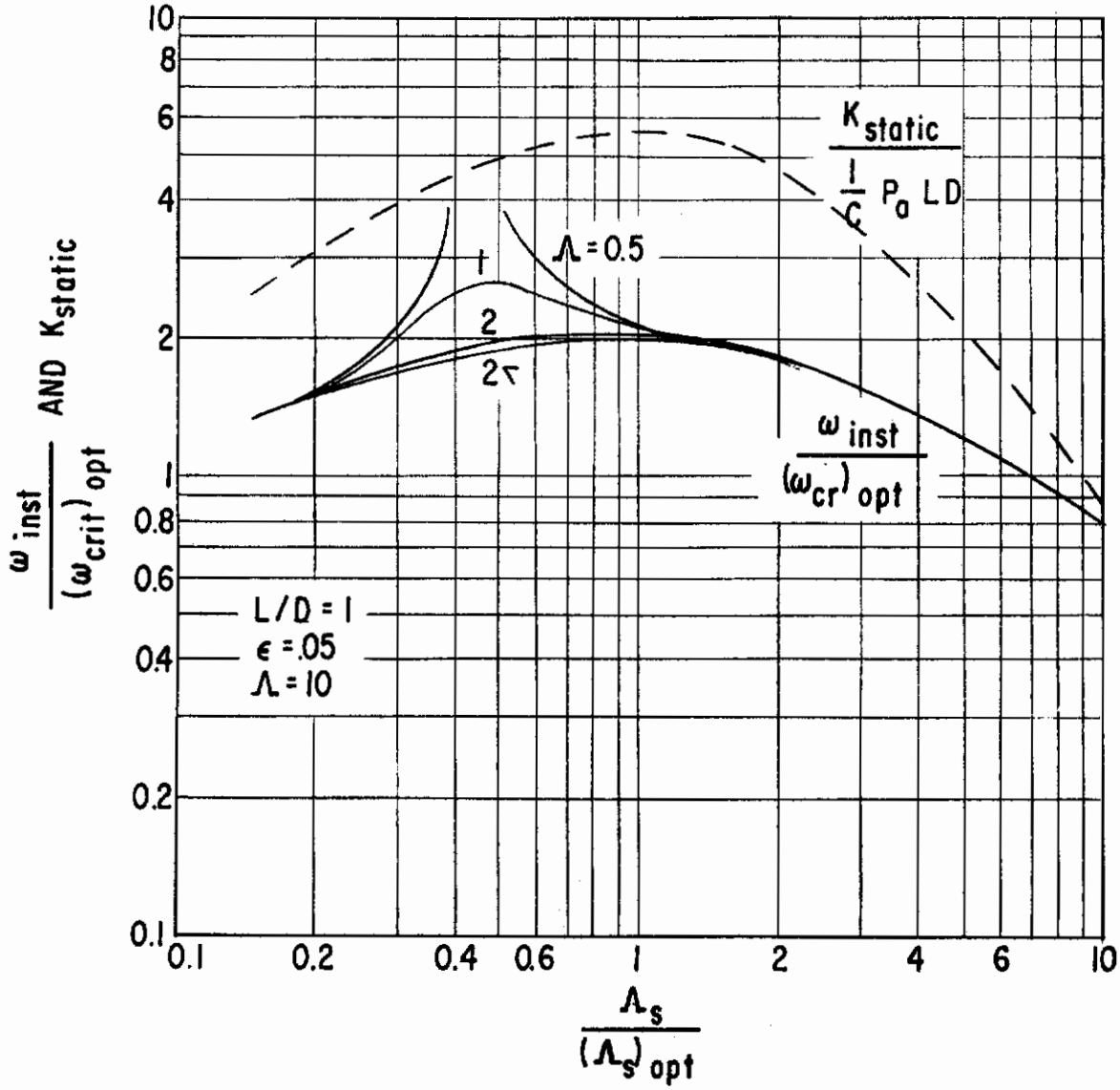

Figure 10. Speed Ratio versus Feeding Parameter Ratio for 360° Hybrid Bearing

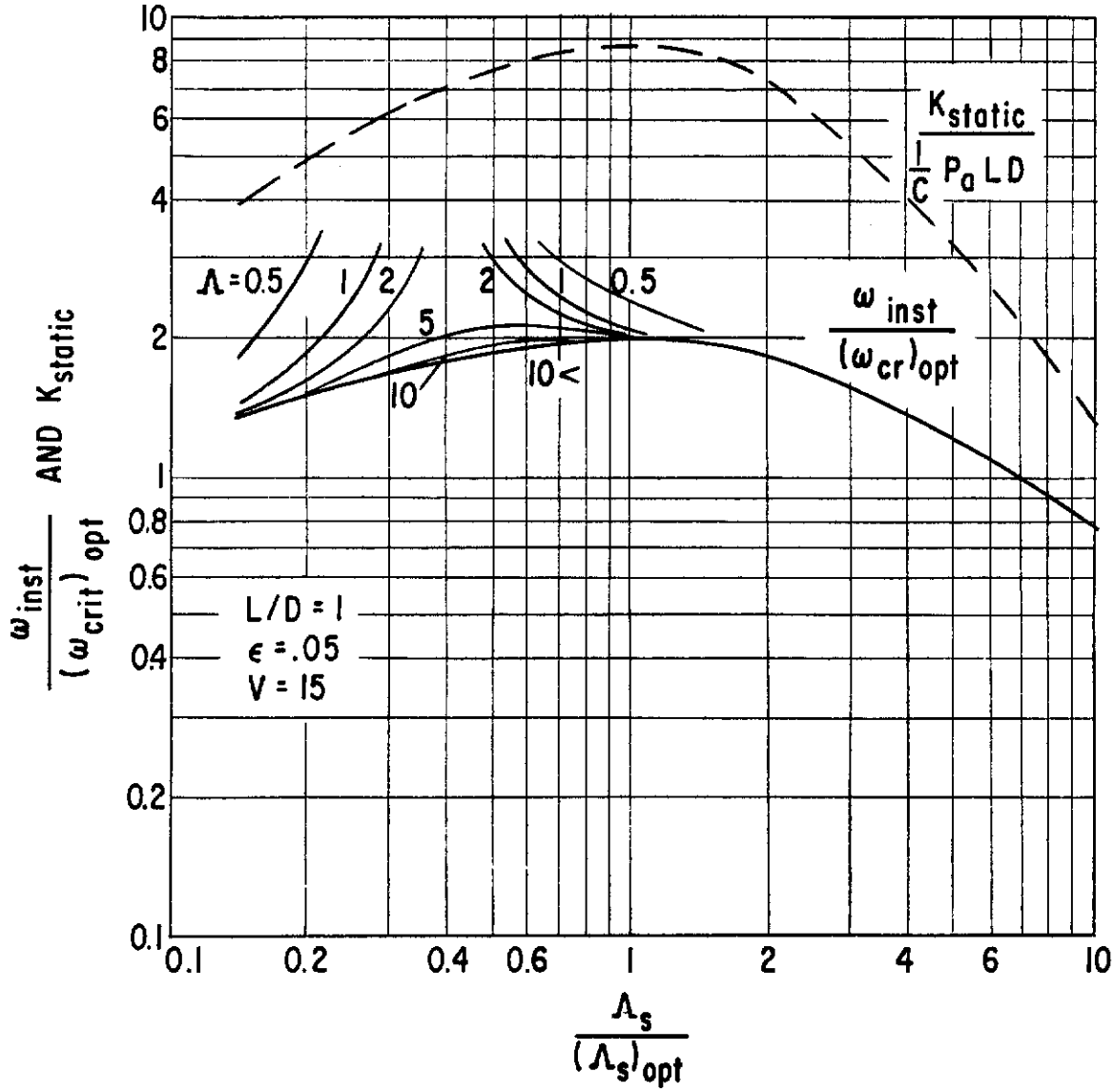

Figure 11. Speed Ratio versus Feeding Parameter Ratio for 360° Hybrid Bearing

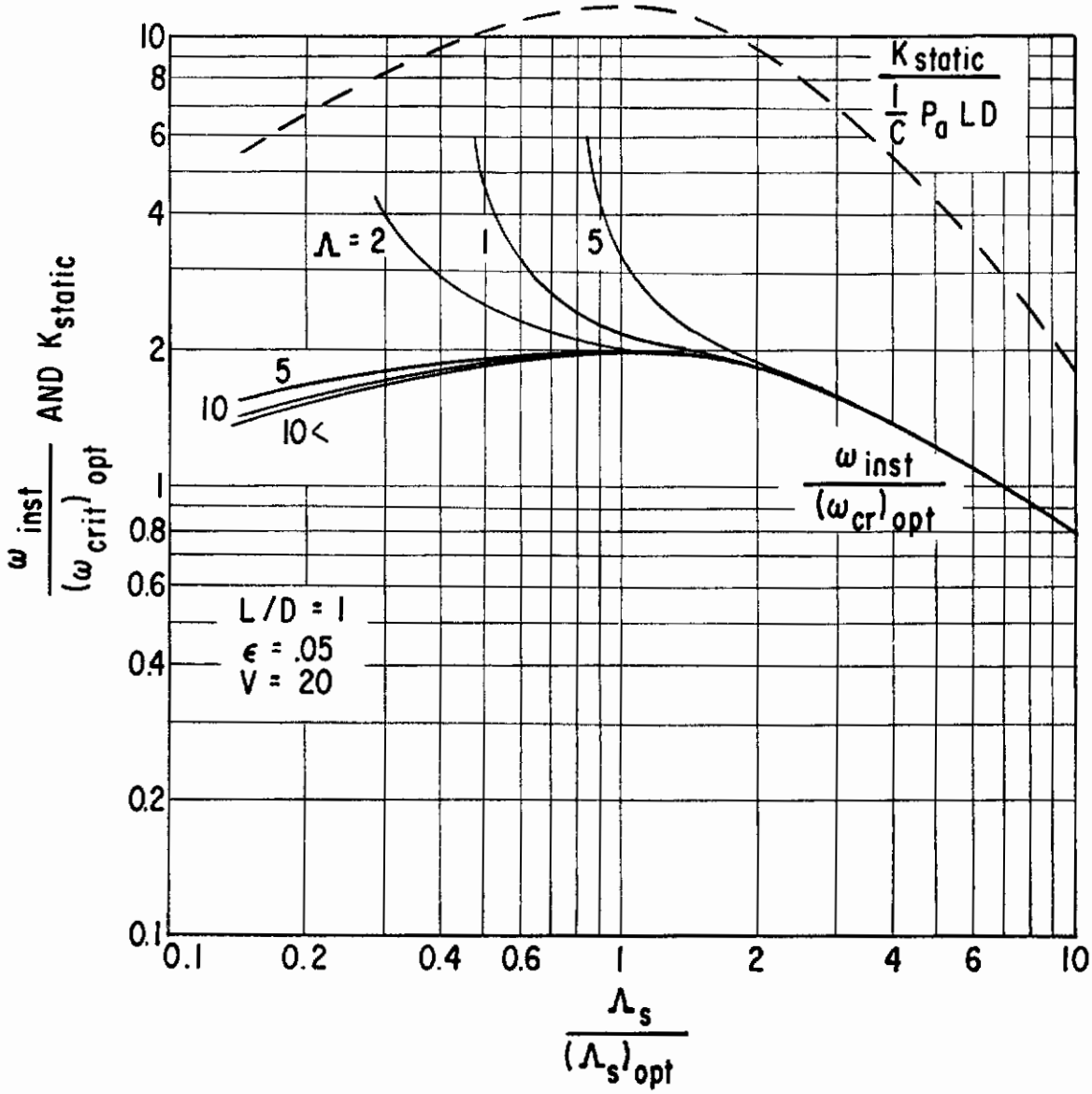

Figure 12. Speed Ratio versus Feeding Parameter Ratio for 360° Hybrid Bearings

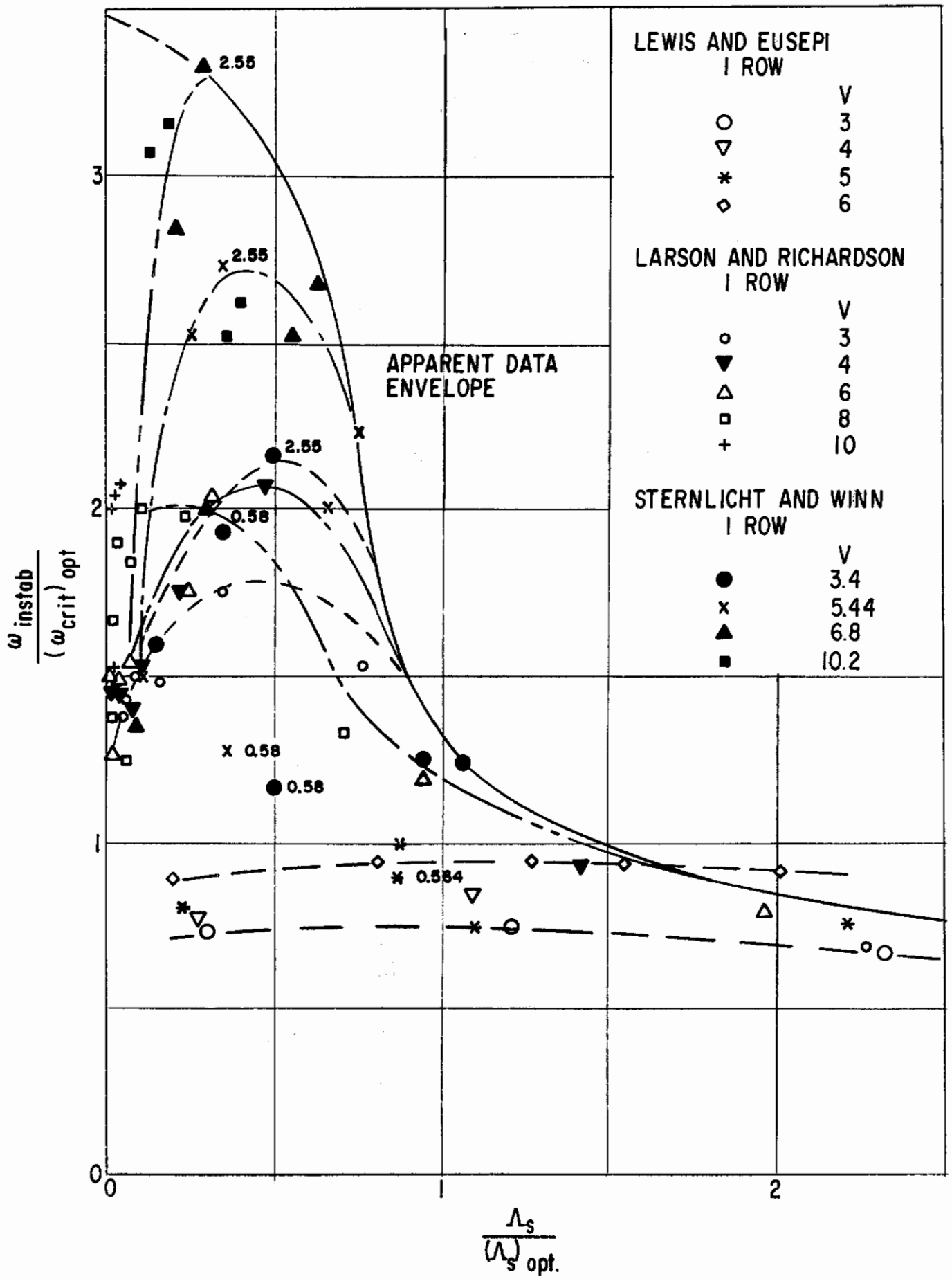

Figure 13. Speed Ratio versus Feeding Parameter Ratio for 360° Hybrid Bearings

compensated bearing for which the theoretical results should be somewhat modified.

Conclusions

1. Hybrid bearing instability, in general, sets in at twice the natural frequency of the hydrostatic bearing. The factor is never less than two and may be higher for an appropriate choice of bearing parameters; such as increased eccentricity ratio, increased supply pressure, small bearing number Λ and for the feeding parameter $\Lambda_s < \Lambda_s$ - optimum.

2. The qualitative agreement between theoretical and experimental results indicates that, in principle, the method of analysis is adequate for predicting the threshold of instability for the hybrid bearing.

3. The simple, thermodynamic orifice equation is not accurate enough for a stability analysis. Furthermore, the feeding hole geometry must be taken into account.

Design Considerations

Probably the most critical problem of high-temperature - high-speed equipment is that of geometry changes due to growth and distortion.

Growth and Changes in Geometry

It is evident that such a wide range of temperatures and speeds could result in dimensional changes and distortions. Many of these changes cannot be determined and, therefore, leave some area of uncertainty. It is imperative that those changes which can be predicted be included in the content of analysis and experiment.

A brief analysis was made to compare the centrifugal and thermal effects. The data are presented in Figures 14 and 15 in a form which permits easy comparison and selection of materials. Curves are presented for the selected rotor radius of 3/4 inch and also for 7/8 inch and 5/8 inch radii to show the effect of size variations.

From the figures, it can be seen that the centrifugal growth is small compared to the thermal growth. However, material should be selected to minimize centrifugal growth for two reasons. First, centrifugal growth affects only the rotor so that bearing clearance is reduced directly by the amount of growth. Second, the rotor will run somewhat hotter than the bearing which tends to further reduce bearing clearance. Furthermore, temperature gradients will be difficult to predict and control so that as much margin as possible should be provided to accommodate them.

Because the clearances in the bearings are small compared to the thermal expansion it will be necessary to fabricate high temperature bearings and rotor from the same material. The most favorable materials appear to be silicon carbide and the TZM alloy of molybdenum, (Mo-0.5 Ti- .08Zr). Both of these materials offer

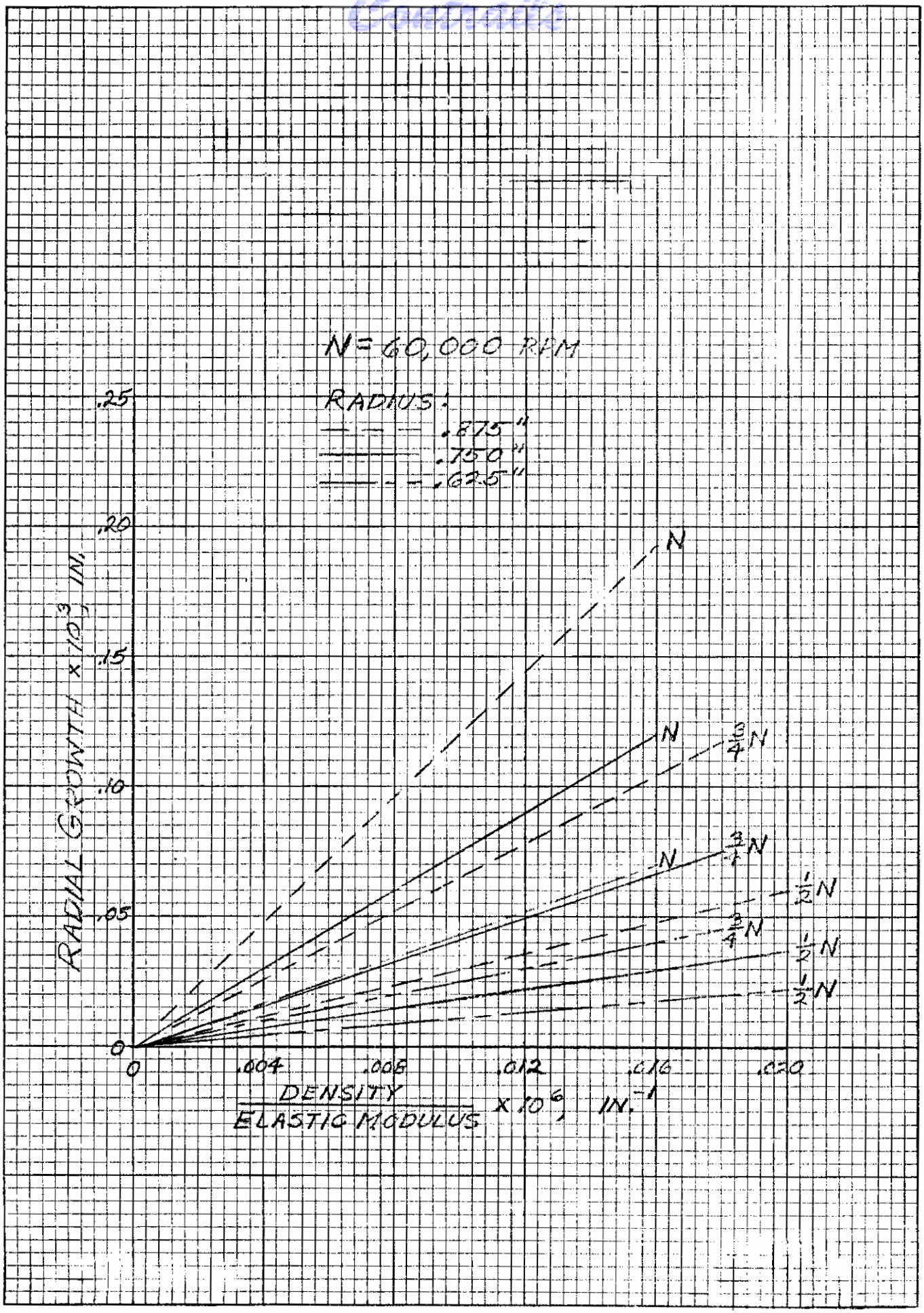

Figure 14. Centrifugal Growth of Solid Rotor

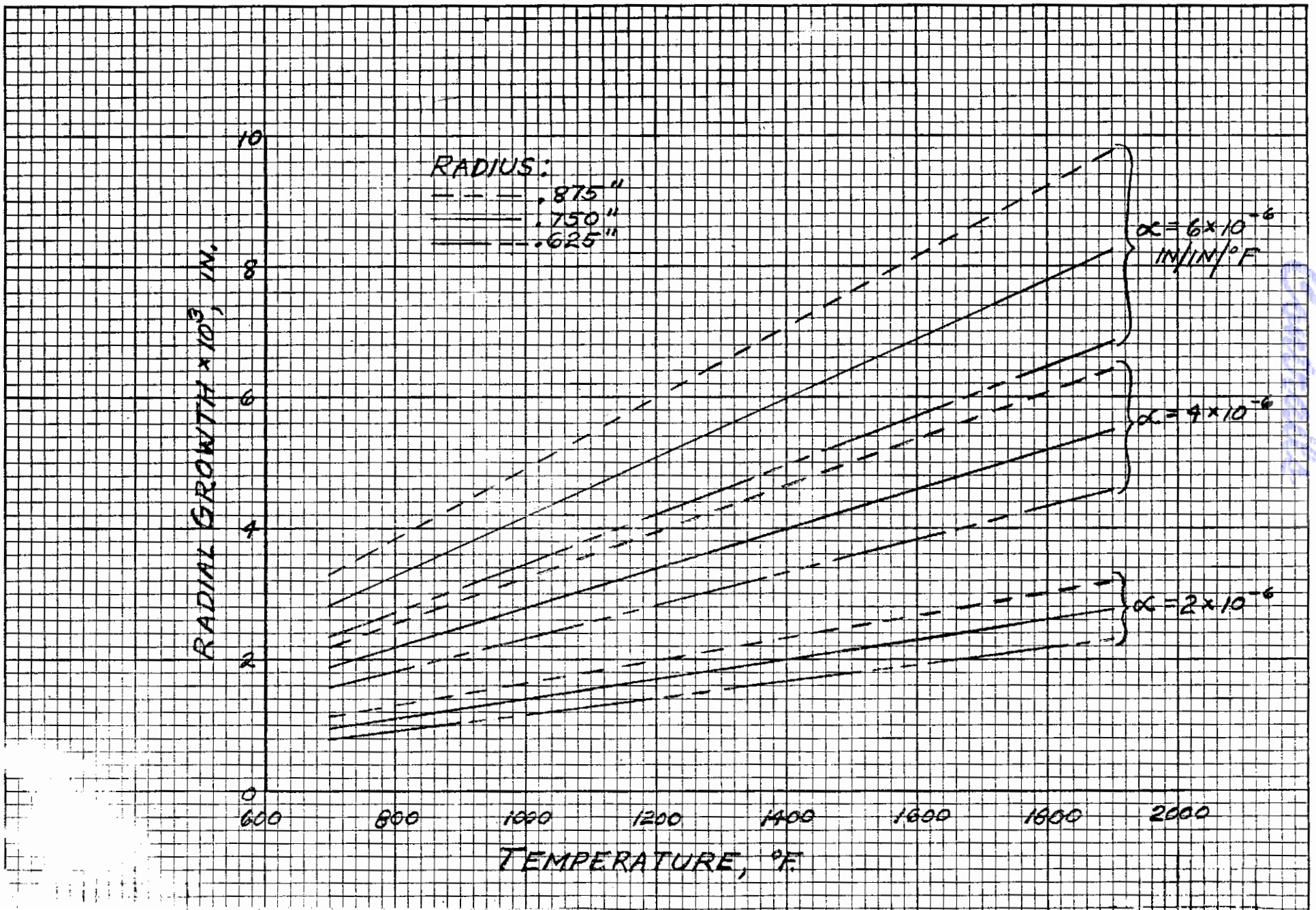

excellent strength at 1900 F and low thermal expansion coefficients (about 2 x 10^{-6} in/in/^{o}F for SIC and 3 x 10^{-6} in/in/^{o}F for TZM). The ratio of densities, about 1 to 3, will permit operation of the bearings with two significantly different loads (rotor masses).

It would be desirable to be able to use a design which would compensate for radial growth and axial gradients. If this were the only consideration, the designs shown in Figure 16 are typical of what would be selected. Note that this is most applicable to a partial arc-type of configuration.

However, if the lowest natural frequency criterion is taken to predict the maximum stable speed, then such mechanical flexibility cannot be tolerated. Figure 16d could be designed to incorporate a significant amount of damping. This would permit adjustment for slow, steady-state movements (such as growth) but would be extremely stiff with respect to transients. Because of the added complexity of sliding members, this technique will not be considered at this time.

A partial arc bearing with the sectors free to adjust angularly would give some tolerance to axial gradients as well as an increased inherent stability of the bearing itself.

Certainly, the pivoted shoe-type of bearing comes readily to mind in this respect. However, mechanical pivots like sliding members would be undesirable over the desired range of operation. If this action could be accomplished by elastic means, this approach looks very promising. Figure 2 shows a proposed design which uses a post to support the pad so that high radial stiffness is attained with low resistance to angular movement (bending). In order for the pad to "track" or follow the journal, the natural frequency of the pad on its mechanical and fluid film springs must be at least twice the rotational frequency. The mechanical spring must be soft compared with the fluid film spring in order that adjustment take place by bending of the support post. Additional considerations are:

1. Compressive stress in the post.
2. Bending stress in the post.
3. The pad be stiff enough to prevent unwrapping.
4. Extraneous resonances be avoided.

Although these are still being evaluated, it currently appears that obtaining a sufficiently low pad inertia and avoiding lateral resonances could be problems.

Flat Hydrostatic Pad Design

For engineering design purposes, the pads or partial arcs can be approximated by a flat pad. Therefore, an approximate analysis was made on a rectangular pad to provide a guide for the design of the hybrid pad bearing.

The solution was based on the assumption that the pocket pressure squared, reduced linearly to ambient pressure both in the x and z direction at the edges of the pad. Furthermore, the eccentricity ratio ϵ was assumed to be much smaller than unity.

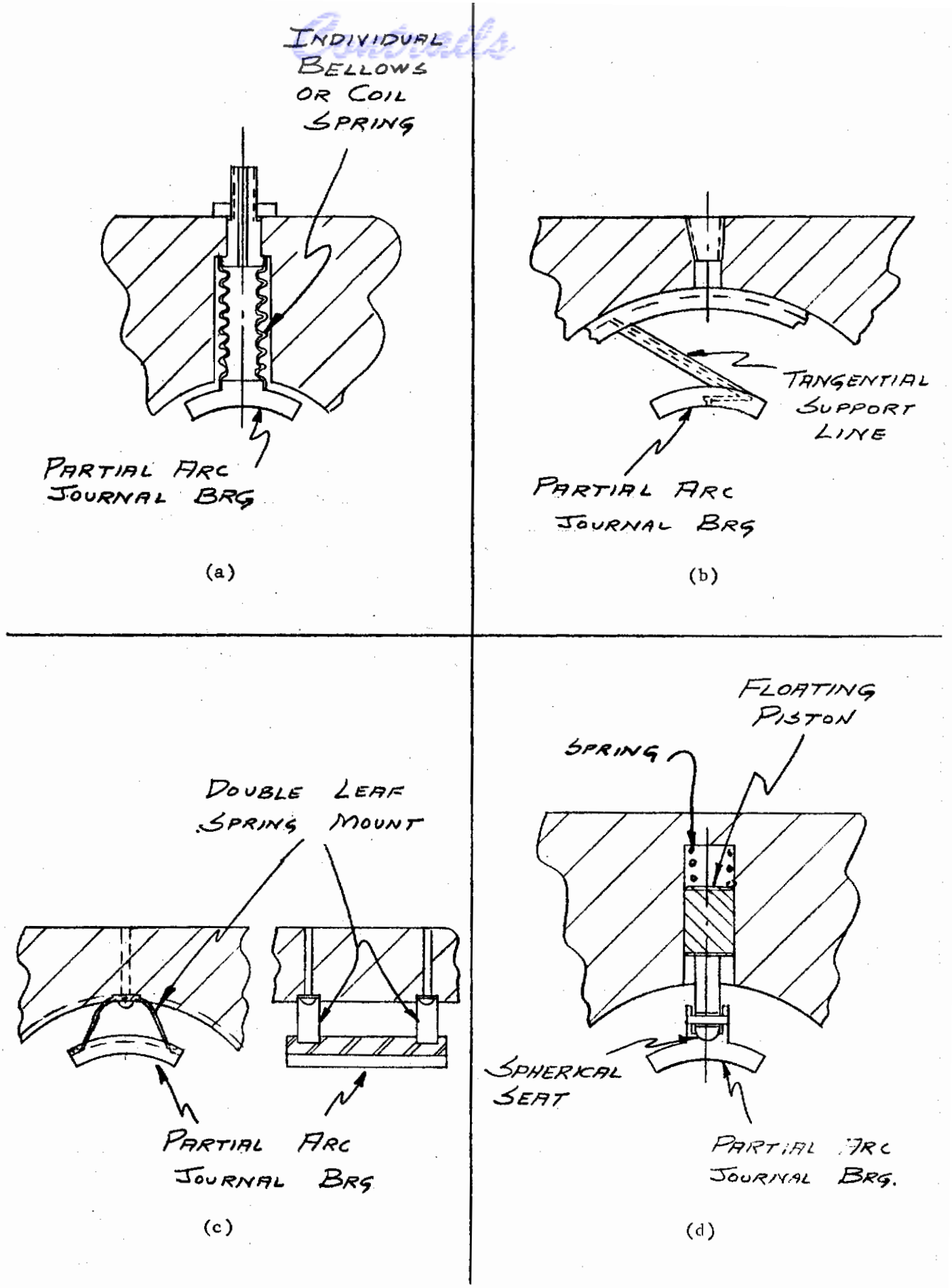

Figure 16. Flexibly Mounted Sectors

It is felt that the assumption made on the pressure distribution should hold very well in the region away from the corners of the pad. The local pressures close to the corners might be quite different from what was assumed. Since the area close to the corners is small compared with the total pad area, the error in the calculated result of load and stiffness should not be great. From the practical point of view, the orifices should not be located too close to the edges of the pad. The assumption of a constant pocket pressure may depend on the arrangement and size of the orifice. However, as will be shown, the analysis agrees with experimental results.

Figure a shows the rectangular pad bearing.

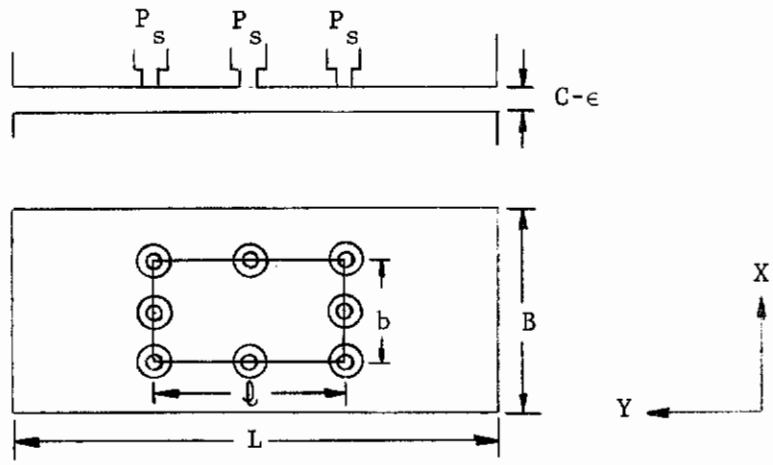

Fig. a

1. The pressure distribution:

Let the pocket pressure be a constant P_p. Then approximately, the local pressure in X and Z direction can be expressed, respectively, as shown in region of lower right corner.

$$p^2 = 1 + 2\frac{P_p^2 - 1}{B - b}X \text{ at } \frac{B-b}{2} \leq Z \leq \frac{B+b}{2} \quad \ldots\ldots(1)$$

$$p^2 = 1 + 2\frac{P_p^2 - 1}{B - b}Z \text{ at } \frac{L-\ell}{2} \leq X \leq \frac{B+\ell}{2} \quad \ldots\ldots(2)$$

To find P_p, let

$$P_p = P_o + \epsilon P_1 + \text{higher order terms} \quad \ldots\ldots(3)$$

then, for $\epsilon \ll 1$, one has

$$P_p^2 = P_o^2 + 2\epsilon P_o P_1 \quad \ldots\ldots(4)$$

The pressures in the other corners can be found by symmetry.

2. Flow through bearing:

The flow from one orifice can be approximated by:

$$M = \frac{\alpha \pi a^2}{RT} P_a \quad V^2 - P_o^2 - \epsilon \frac{P_o P_1}{V^2 - P_o^2} \quad \ldots\ldots(5)$$

where $V = P_s/P_a$

The total flow out of the bearing can be found as

$$M_t = (1 - 3\epsilon) \frac{C^3 P_a^2}{24 \mu RT} \frac{\partial P^2}{\partial X} (L + \ell) + \frac{\partial P^2}{\partial Z} (B + b) \quad \ldots\ldots(6)$$

From the continuity of flow for N orifices, one has

$$M_t = N \cdot M \quad \ldots\ldots(7)$$

Thus one obtains

$$P_o^2 - 1 = \Lambda_t \quad V^2 - P_o^2 = q \quad \ldots\ldots(8)$$

$$q = \frac{\Lambda_t^2}{2} - 1 + \sqrt{1 + \frac{4 (V^2 - 1)}{\Lambda_t^2}} \quad \ldots\ldots(9)$$

$$\Lambda_t = \frac{12\mu N\, \alpha\pi\, a^2}{C^3\, P_a} \frac{RT}{} \times \frac{1}{\frac{L+\ell}{B-b} + \frac{B+b}{L-\ell}} \quad \ldots\ldots(10)$$

Introduce:

$$\Lambda_s = \frac{\Lambda_t}{V} \quad \ldots\ldots(11)$$

$$\lambda = \frac{\Lambda_t}{V^2-1} \quad \ldots\ldots(12)$$

Thus the total flow can be expressed as

$$M_t = \frac{C^3\, P_a^{\,2}}{12\mu\, RT} \quad \frac{L+\ell}{B-b} + \frac{B+b}{L-\ell} \quad q \quad \ldots\ldots(13)$$

2. Load:

$$\frac{W}{P_a LB} \times \frac{1}{1 + \frac{\ell b}{LB} + \left(1 + \frac{\ell}{L}\right)\left(1 + \frac{b}{B}\right)} = \frac{1}{6} \quad 1 + q - 1$$

3. Stiffness:

$$\frac{k}{\frac{1}{C} LBP_a} \times \frac{1}{1 + \frac{\ell b}{LB} + \left(1 + \frac{\ell}{L}\right)\left(1 + \frac{b}{B}\right)} = \frac{1}{4} \times \frac{q}{1 + q \quad 1 + \frac{(\Lambda_s V)^2}{2q}}$$

The results of flow and stiffness are calculated and plotted in Figures 17 and 18. Figure 17 shows the plot of $\frac{q}{V^2-1}$ versus Λ.

Figure 18 shows the dimensionless stiffness versus parameter Λ_s.

The maximum obtainable stiffness from a pad bearing can be found from Figure 18 at a specific supply pressure ratio V. There is a corresponding Λ_s for the maximum stiffness. Thus, the designer must vary the dimensional parameters such as N, a, C, etc., as shown in Equation 10 in order to achieve the optimum Λ_s. The flow at the optimum Λ_s can be obtained from Figure 17 by calculating Λ_s and λ from Equations 11 and 12.

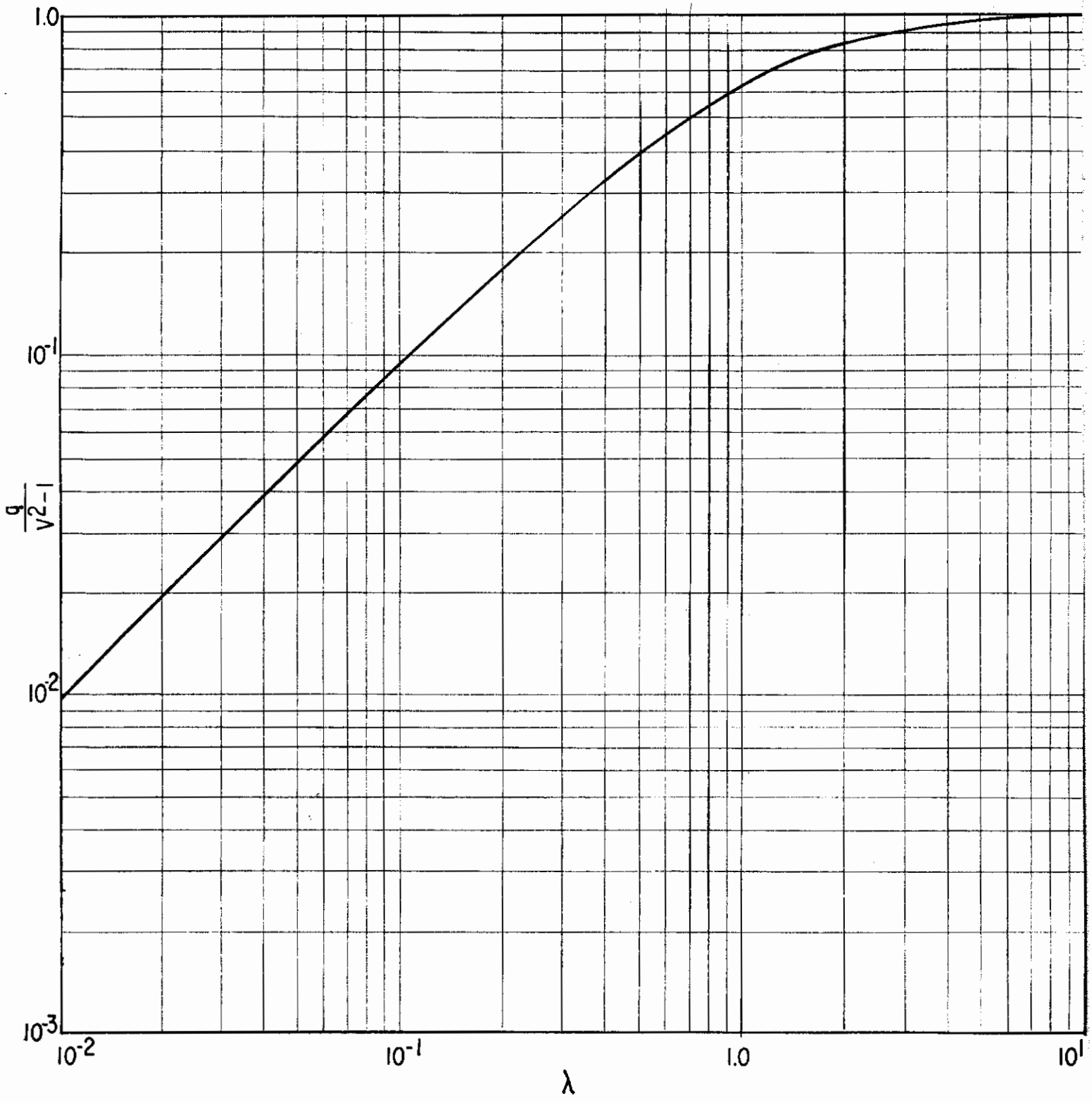

Figure 17. Dimensionless Flow vs. λ (Rectangular Pad)

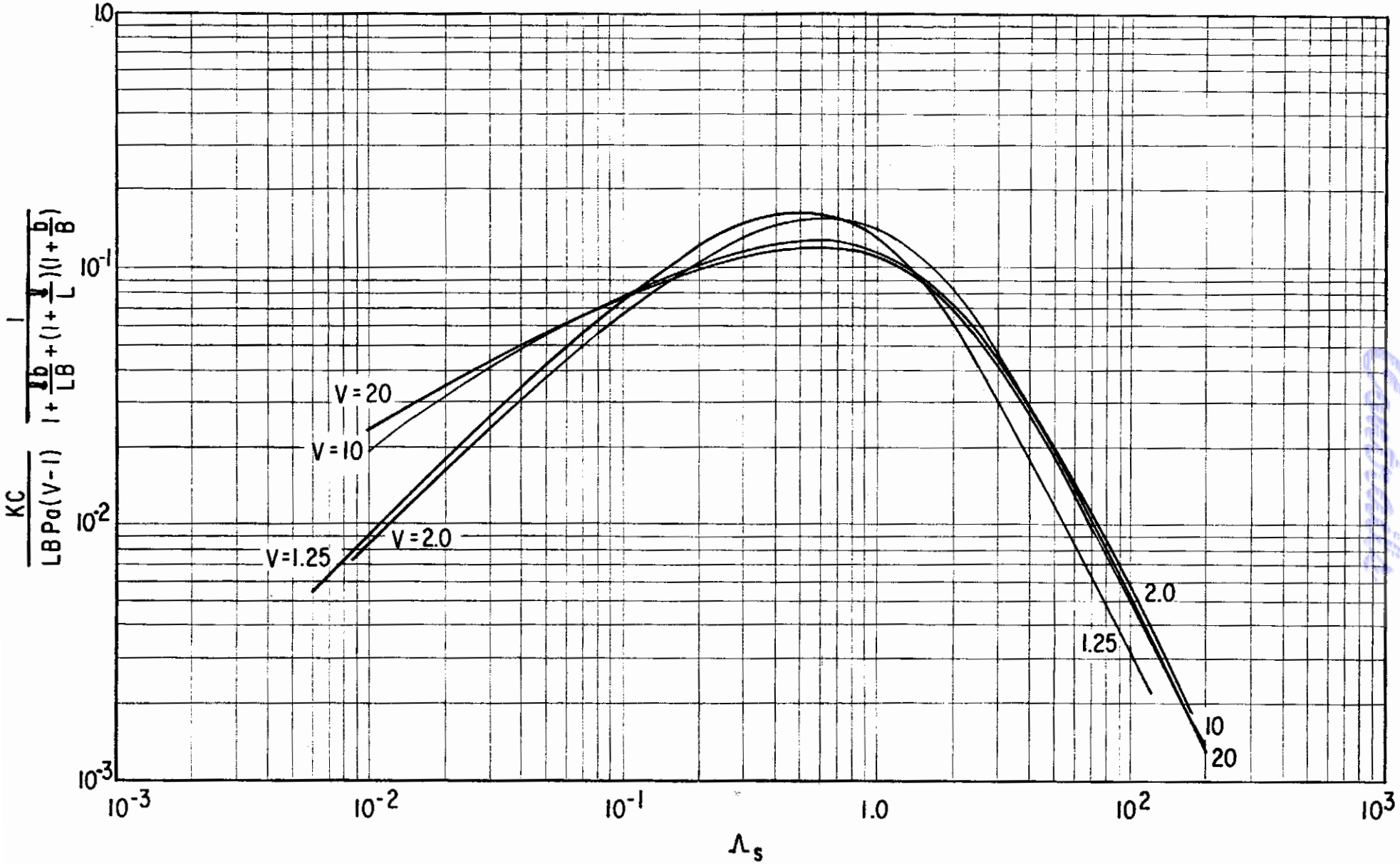

Figure 18. Dimensionless Stiffness vs. Λ_s (Rectangular Pad)

Design Procedure for Flexure Mounted Bearing Pad

A general outline and discussion was made on a flexure mounted hydrostatic, gas journal bearing, partial arc design procedure. The actual bearing is comprised of four such pads, mounted on individual hollow rods. The bearing design is a partial arc, with a number of discreet orifices in the surface. These orifices control the flow of gas, which is fed from a main supply through the tube-like flexure mount. The purpose of the flexure mount is to allow the bearing pad to follow, or "track", the shaft, and to align with the shaft, as well as to achieve the greater stability associated with the "adjustable", or pivoted pad type bearing.

The design procedure is basically comprised of three parts, which refer directly to the three parts of the bearing system design. They are the bearing surface, (size and configuration), the mass and mass-moment of inertia of the pad itself, and the flexure mount, (hollow rod cantilever).

The first step in the procedure is to size the bearing pad surface, based on the externally-applied load. A good approximation for a single pad is the full radial load plus loading from the diametrically opposite pad. A design configuration is chosen, and the particular bearing steady-state characteristics; namely fluid-film stiffness, load-carrying capacity and mass flow, are reviewed. For this case, a partial arc with discreet orifices is used. After once defining these characteristics, a good estimate of the bearing, fluid-film, angular stiffness must be obtained.

The second step is to make a preliminary design of the flexure mount. The length of this hollow rod is based primarily on physical spacing considerations, however, it also contributes to bending stiffness and stress level set up in this rod. The area required to pass the bearing total gas flow will help as a first guess for the inside diameter of the rod. The bending stiffness of this rod, acting as a cantilever with a mass on its end, must be much less than the angular fluid-film stiffness, no greater than one-half this bearing stiffness. Fulfilling this requirement will assure that a major portion of the misalignment will take place essentially by bending of the rod. It is wise at this point to check for the various stresses set up in the rod. The stresses that must be checked are the compressive, buckling, and bending. A good compressive working stress is around 15,000 psi. This check will help size the wall thickness of the hollow rod. The buckling load should be checked, and set at a minimum of four times the maximum applied load. The most important stress check is the bending stress. It should be remembered that a low stress level will also assure a flexible rod.

The third step is to set the "tracking" criteria; the combination of rod and film stiffness must be sufficient to make the pad "track" the journal. This condition requires that the natural frequency of the pad on the "springs" of the lubricant film and the rod must be at least twice the frequency, i.e., running speed, which is to be followed. (The rod radial, or compressive stiffness will be large — in the order of 10^{+7}). An estimate of the pad mass-moment of inertia may be obtained by satisfying this criteria. Finally, the bearing-rod system is analyzed as a two-degree of freedom system and the two critical speeds are checked. These speeds should be well above the maximum operating speed, or straddle the maximum operating speed, such that the lowest critical speed will be low in the operating speed range, and the highest critical speed much greater than the maximum operating speed. In reviewing these speeds, it is well to remember that a motor driven unit gives rise to a twice-per-rev disturbance.

These three steps must be tried, reviewed and revised until all criteria are satisfied.

The bearing pads are mounted on individual hollow rods as shown in Figure 2.

For this particular bearing design the bearing parameters used are:

$$\frac{q,\ RT}{A_o\ \alpha P_s},\ \frac{hK}{A\Delta P},\ \frac{W}{A\Delta P},\ \Lambda_s = \frac{1200\ \mu A_o\ L\alpha\ RT}{P_s\ h^3},\ P_s/P_a,\ P_i/P_a$$

where:

A = Bearing Pad, Projected Area, in^2

A_o = Total Orifice Area/inch of Axial Length, in^2/in

L = Bearing Pad, Circumferential Length, in.

K = Fluid-film Stiffness, lb/in

W = Applied Load, Lb.

P_a = Ambient pressure, psia

P_i = Orifice inlet pressure, psia

P_s = Manifold pressure, psia

$\Delta P = P_s - P_a$, psig

h = Fluid-film thickness, inc.

q = Mass flow per inch of Axial Length, $\frac{\text{lb-sec}}{\text{in}}/\text{in}$

R = Gas constant, $in^2/sec^2\ {}^oR$

T = Gas Temperature, ${}^oR$

μ = Gas Absolute Viscosity, $lb\text{-}sec/in^2$

α = Flow restrictor coefficient

These bearing characteristics are plotted in Figure 18. Figure 18 changes the parameters to some extent, but not the procedure.

A reasonable estimate of the bearing pad, angular, fluid-film stiffness is calculated as:

$$K_t = KL^2/16 \qquad \text{(lb-in/rad)}$$

The bending stiffness of the hollow rod is:

$$K_{rod} = EI/\ell \qquad \text{(lb-in/rad)}$$

where:

E = Modulus of Elasticity of Rod, psi

I = Cross-Section Moment of Inertia or rod, in^4

ℓ = Length of cantilever rod, in

Note: The rod compressive stiffness is: $A_R E/\ell \approx 10^7$

The following stress checks are made:

$$\sigma_c = \frac{W}{A_p} \quad \text{(Compressive Stress)}$$

$$\sigma_B = \frac{h}{D}\cdot\frac{d}{I}\cdot K_{rod} \quad \text{(Bending Stress)}$$

where:

W = Maximum load on Pad, lb.

A_p = Rod Cross-Section area, in^2

h = Fluid-film thickness, in.

D = Journal Diameter, in.

d = Rod, outside diameter, in.

Normally, the rod will act as a pure compression member; however, it is well to check the buckling load as follows:

$$P_{cr} \geq \frac{\pi^2}{\ell}\cdot K_{rod} \geq 4W$$

The following equations are used in the "tracking" criteria

$$f_{pp} \geq 2N$$

$$f_{pp} = \frac{1}{2\pi} \quad (K_t + K_{rod})/I_P$$

where:

N = Journal Speed, rps

$I_p = I_{cg} + M\left(\frac{\ell}{2}\right)^2$, $lb\text{-}sec^2$ in

I_{cg} = Mass Moment of inertia about pad center of gravity, $lb\text{-}sec^2$ in

M = Mass of pad, lb sec^2/in

f_{PP} = Frequency of Pad in Pitching motion, cps

Critical Speed Check:

$$\omega_{1,2}^2 = \frac{a+c}{2} \pm \frac{a\cdot c}{2}^2 + \frac{b^2 M}{I_{c\cdot g}} \quad (rad/sec)^2$$

where: $a = (K\cos^2\theta_R + \frac{12EI}{\ell^3})/M$

$$c = (KR^2_{cg} \cos^2\theta_R + \frac{4EI}{\ell})/I_{cg}$$

$$b = (KR_{cg}\cos^2\theta_R - \frac{6EI}{\ell^2})/M$$

$\theta = 70^\circ$ for 80° pad

R_{cg} = Radius measured from journal center to Pad c.g.

MATERIALS

The critical role which materials play in the operation of gas-lubricated bearings is a direct result of the fact that gases are very low viscosity fluids. Extremely close clearances are required between the bearing and the shaft, particularly in bearings of the self-acting type, in order to maintain as high a load carrying capacity as possible. The gas bearing is an ultra-precise component which demands the same degree of dimensional accuracy as the finest gyroscope and yet this bearing is expected to perform satisfactorily under much more stringent conditions. This is the crux of the problem insofar as materials are concerned.

For this type of application, the materials must meet certain criteria, particularly the following:

1. Dimensional stability to thermal effects and to centrifugal growth.
2. Resistance to corrosion and erosion in a nitrogen environment.
3. Matched coefficients of thermal expansion throughout the system.
4. Adequate strength at high temperature.

If these criteria were the only ones which had to be considered, many materials, particularly the ceramics and cermets, could satisfy the requirements easily. To eliminate the problem of differential thermal expansion, all that would apparently be necessary would be to build the entire test machine of one material. From a practical standpoint, however, it is essential to take one more step in order to select materials realistically. This step is to define what is to be accomplished as the primary goal of this work and to anticipate the materials problems which will be encountered as a result of this type of effort.

This is a program to study the major problem areas in high-temperature high-speed, externally-pressurized gas bearings by using both analytical and experimental techniques.

Certainly, one of the objectives of this work is to produce a final working model which can demonstrate the feasibility of various designs and experimental techniques. However, it is essential to be practical about the demands which will be made on the materials to be used in the test equipment. In a program of this sort, the materials will be subjected to a variety of unknown conditions:

changes will have to be made in finished parts, operation under very marginal conditions will be generally required, it may even be necessary to discard one set of bearings and replace these with a new set of a completely different design.

Ideally then, in order to satisfy these demands, the bearing materials should have all of the following characteristics:

1. Ease of fabrication and, even more important, susceptibility to alterations.

2. Good compatibility in case of a minor touch at high speed. In the event of a serious failure, no damage can be tolerated on the shaft.

3. All of the other characteristics which were listed previously including dimensional stability, corrosion and erosion resistance, etc.

(While major emphasis is being placed on the bearing and shaft materials, it must be borne in mind that there are other components, such as the housing and associated piping, which must also be matched up to make a compatible system.)

In the preliminary materials selection for this program, several high-temperature alloys were considered for use as shaft and bearing materials, but the dimensional stability of these materials was considered very questionable at 1500 F and above. These materials included:

Inconel X
Haselloy X
Rene 41
Inco 713

Nothing has been uncovered since that time which would change that opinion. Besides the problems of dimensional instability and nitriding at high temperatures, these nickel-base alloys also have very poor sliding characteristics, especially in a nitrogen environment.

Several cermets and carbides appeared to have promise, including:

(a) KT silicon carbide.

(b) LT 1-B (19% Al_2O_3, 59 CR, 20 Mo, 2 TiO)

(c) K 162B titanium carbide.

All of these materials have good thermal shock resistance, good stability, strength and hardness characteristics at high temperature and excellent compatibility, even when mated against themselves. In Table 4, some pertinent physical properties of the materials are given. These materials cover a wide range of thermal expansion characteristics.

TABLE 4

SOME PHYSICAL PROPERTY DATA ON MOST PROMISING MATERIALS

Material	Modulus of Elasticity	Temperature Limitation	Coeff. of (a) Thermal Exp.	Thermal (b) Conductivity	Hardness	Poisson's Ratio	Fabrication
KT Silicon carbide	68.5×10^6	4000 F	3.0×10^{-6}	800 BTU	8-9 on Moh's scale	0.18	Must be finished by diamond grinding
LT-1B metal bonded Al_2O_3		>2200 F	4.71×10^{-6}	300 BTU	hard	0.25-0.27 (flexure)	Slip cast, diamond ground
K162B	57×10^6	2200 F (in air)	5.3×10^{-6}	360 BTU	89 Rockwell		Diamond ground
TZM Alloy (Mo+0.5Ti .08 Zr)	46×10^6	2400 F(c) (inert atm.)	3.2×10^{-6}	970 BTU	About 250 Brinell. Can be nitrided to very hard case	.32 - .33	Machinable, preferably with carbive tooling

(a) in./in./^oF

(b) BTU/sq.ft./hr./in./^oF

(c) Recrystallization Temperature

It should also be noted that, even if their sliding compatibility is good, it is very doubtful if they could survive high-speed rubbing without any surface damage taking place.

For these reasons, further efforts were made to find a metallic alloy which could be used in this application. The TZM molybdenum alloy appears to have the greatest promise. This alloy has excellent strength at high temperature and, with a recrystallization temperature of 2400 F, should be stable in the required temperature range and it is readily machinable. The major problem with this alloy is corrosion. In air, at high temperature, the oxidation rate would be catastrophic, since MoO_3 sublimes about 1500 F. Even below 1000 F, the rate is extremely high. In nitrogen, there is a definite nitriding reaction which appears to start about 1500 - 1600 F. Actually, when TZM is to be used as a sliding member, it has been recommended that the surfaces be deliberately nitrided to produce a hard, wear-resistant surface. While nitriding, whether deliberate or by corrosion, does involve some dimensional changes, these changes are usually slight. Normally, when preparing materials for nitriding it is customary to finish grind to within a few tenths of a mil, nitride, and then lap to final finish. Therefore, while corrosion by nitrogen is definitely a factor, time-at-temperature must also be considered in determining how serious the problem really is. The rate of reaction will also be slower if the parts have been nitrided first.

As far as the oxidation of the outside of the bearing housing is concerned, several oxidation-resistant coatings for molybdenum were investigated with regard to their ability to provide satisfactory protection for several hundred hours even at 1950 F.

The TZM molybdenum alloy was selected as the best choice for the test rig in spite of its lack of corrosion-resistance. It was decided that all critical parts, particularly the shaft, would be deliberately nitrided before finishing, and all molybdenum parts to be exposed to the air were scheduled to be treated with an oxidation-resistant coating, pending a determination of that which would be most suitable.

Up to this point, the discussion of materials has been fairly general and directed primarily toward the shaft and housing. As far as the bearing surfaces are concerned, some pertinent comments are in order here.

Because of the expense, time and fabrication difficulties inherent in using ceramics or similar materials, a decision was made to select the best available material for the test shaft and to choose two classes of materials for the test bearings. One of these classes of bearing materials was chosen for expendability. The class of material, or materials, was selected based on the following criteria:

1. Readily obtainable
2. Reasonably economical to fabricate
3. Capable of use at 1900 F in nitrogen
4. Would do little or no damage to the shaft in the event of a failure.

The purpose of this class of materials is to allow the engineering group to evaluate design concepts as economically as possible.

The second class of bearing materials was chosen for use in the final configuration tests using proven design concepts.

Under the first category of "expendable" bearing materials, the impregnated carbon-graphites, and boron nitride appear to have promise. Impregnated carbon-graphites were evaluated in a dry nitrogen atmosphere both in laboratory sliding test equipment and in actual gas bearing tests. Good performance has been obtained. As long as a non-oxidizing environment is used, these materials should tolerate 1900 F operation for a period of hours without excessive oxidation. Normally, the low thermal expansion of the carbon-graphites has made their use highly questionable over such a wide temperature range. However, if cermets, ceramics or the TZM alloy are used for the shaft material, the thermal expansion problems become much less critical.

Boron nitride also has many interesting characteristics for use as an expendable bearing material. It is readily available, can be machined with standard high-speed steel tools and will take an excellent finish. In addition, the material is relatively soft. If a high-speed seizure takes place, the bearing surface should powder without damaging the shaft. Boron nitride is also an anisotropic material. Its thermal expansion coefficient varies from 5.0 to 0.4 microinches/in/in/^{o}F depending on the orientation of the material with respect to the direction of forming. This suggests that the coefficient of expansion can be adjusted by taking a solid block of boron nitride and machining-out a section at some angle to the direction of forming. The technique can be visualized as follows:

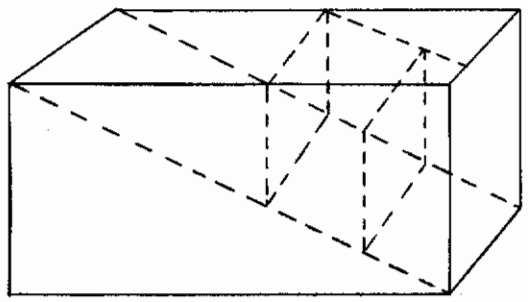

The thermal expansion characteristics of the center section can thus be adjusted to any value between 0.4 and 5.0 microinches by cutting at a suitable angle. The bearing can then be fabricated from this section.

To demonstrate that boron nitride is a suitable, sacrificial bearing material for this application, some sliding tests were run under various conditions. In the first series of tests, thrust washers of boron nitride were run under a stress of 6 psi at 1000 rpm (290 feet/min) and 3000 rpm (870 feet/min) at room

temperature. One set of washers was machined so that the sliding surface was perpendicular to the direction of pressing (the "A" direction), and the second set was machined to contact on the "B" face, parallel to the direction of pressing. A test was also run with P-303-C high temperature carbon-graphite for comparison. These specimens were rotated in contact with a flat plate of 304 stainless in contact with a flat plate of 304 stainless which was mounted on a ball thrust bearing to permit the torque to be measured. The stainless steel was chosen because it is a poor mating surface and should represent the worst case. The results of these tests are shown in Table 5. In every case, there was a definite smoothing action on the stainless surface which removed the polishing scratches. From the results of these tests, it appears that a harder surface than the 304 stainless is necessary.

An attempt was made to repeat this test at 1400 F in nitrogen, but the bearing which supported the stainless disc would not function at this temperature. However, visual observation of the stainless surface showed no increase in damage over the room temperature tests.

Tests were also run on these same materials in a high sliding velocity test machine. In this machine, a 3/8 inch diameter rod of the test material was loaded down against the periphery of a high-speed rotating metal disc. The surface of this disc had a hard, lapped chrome plate. The results are given in Table 6.

When the "A" direction specimen was used, isolated "rabbit tracks" of transferred boron nitride were observed on the chrome plate. This material could be scraped off with the fingernail and no damage could be observed under these spots. When the "B" direction specimen was used, no material transfer took place and no surface damage was observed. The wear rate of the boron nitride was very high in all tests. In air, the powder spewed out of the wear area in a shower of bright yellowish-green sparks. In nitrogen, the sparks were darker and more orange. At this time, we have no explanation for the fact that the friction was lower in nitrogen than in air. This is contrary to what one would expect, but this could have been due to the high sliding velocity cancelling out other effects.

The original premise - that boron nitride would powder and disintegrate without damaging the shaft material - appears to be borne out by the results of these tests. However, further checks on the ability to match expansions indicated that there would be a thermal expansion differential in one direction. To sum up the status of the materials selection:

1. The molybdenum alloy, TZM was selected from the standpoints of cost, machinability and possibility of making minor changes after finishing.

2. Boron nitride was selected as a possible sacrificial bearing material.

Because of the necessity for a series of low temperature evaluations, it was decided that a bronze bearing, hardened steel shaft combination be utilized. Therefore, the use of a sacrificial bearing material has been de-emphasized for the time being.

TABLE 5

EVALUATION OF SACRIFICIAL BEARING MATERIALS
SLIDING AGAINST 304 STAINLESS

Room Temperature. Air Environment
290 fpm and 870 fpm. Stress 6 psi
Test time - 30 seconds

Bearing Material	Friction		Remarks on Damage
	290 fpm	870 fpm	
P-303-C Carbon Graphite	.33 to .39	.39 to .56	Friction gradually increasing. Stainless surface polished except for a few scratches in the direction of sliding.
Boron nitride "A" direction	.39	.33 to .45	Stainless surface polished. Less damage than with carbon-graphite.
Boron nitride "B" direction	.33	.33	Same as "A" direction but seems slightly better.

TABLE 6

EVALUATION OF BORON NITRIDE
SLIDING AGAINST HARD CHROME PLATE

Sliding Velocity - 245 feet/second. Stress 20 psi

Test Time - 30 seconds. Environment- Air and N_2

Bearing Material	Friction		Remarks on Damage
	Air	Nitrogen	
Boron nitride "A" direction	.32	.28	Boron nitride transferred to chrome plate as isolated "rabbit tracks", but could be scraped off. No surface damage underneath.
"B" direction	.30	.23	Boron nitride did not transfer. No damage to chrome plate.

TEST FACILITY

Test Rig

The unit consists of a solid shaft supported on two journal bearings with a loading bearing sector at the mid-span of the two journal bearings. A thrust bearing and thrust load act on opposite ends of the shaft. The unit is turbine driven with turbine blades machined on one end of the shaft. The journal bearings are removable. The housing is a cylindrical block. All instrumentation is brought to the housing block.

Figure 19 is the assembly drawing for the test rig, showing the relationship between the major components. The thrust bearing on the left side and the thrust loader and turbine nozzle block on the right side are simply clamped against the housing ends by through-bolts. This assembly method is feasible, since the concentricity requirements of these separate plates are not critical. The journal bearing loader is machined as an integral part of the housing. The journal bearings are installed in close tolerance recesses in the housing, machined concentric to the journal loader. The bearings are clamped in place with spacer rings which support the axial force of the through bolts holding the thrust plates in place.

Figure 20 is the housing drawing. Diameters P and R (4.25 inch) locate the journal bearing axes, and surfaces L and M are the reference planes for determining squareness between the bearing axes and the thrust surfaces. At the inboard end of each journal bearing, provision is made for mounting three non-contacting capacitance probes. Two probes with 90 degree separation allow definition of the shaft orbit and the third probe at 180 degrees will allow measurement of shaft centrifugal growth. Another probe mounting location is provided in the relieved portion of the journal loader. This was added, together with two small steps in the shaft surface at this plane, to provide an additional speed sensing system. The change to inert atmosphere blanketing around the rig and the consequent need for a relatively gas-tight liner in the oven would make the external light beam and photo-cell speed sensing system difficult to apply.

Figure 21 is the turbine nozzle box drawing. This was made as a separate piece to simplify machining. An annular pressure manifold is provided, which is sealed by the thrust loader plate. Three nozzles of .094 inch diameter drive the shaft. A radial clearance of .005 inch is provided between this piece and the shaft; therefore, concentricity is not critical. The two faces must be parallel, as the thrust loader squareness is dependent on this requirement.

Figure 22 is the thrust loader drawing. The load cell is similar to that developed in previous portions of this work, and should be satisfactory for small axial clearances. The turbine discharge ports were made as simple, drilled holes to minimize machining complexity.

The thrust bearing is shown in Figure 23. This is an annular bearing with twelve feeding-orifices. Orifice compensation is ensured by terminating each orifice in a pocket or recess. The orifice gas flow is supplied from a pressurized annulus machined in the bearing and sealed with a cover plate. Provision is made for

installing a clearance probe in the central unpressurized zone of the bearing. This will allow accurate clearance measurements without disturbing the pressure or flow patterns in the lubricant film. Consideration was given to the installation of separate orifice inserts, but the design and machining complexity outweighed the advantages to be gained. The same situation was found to be true of self-aligning, thrust bearing designs.

The shaft is shown in Figure 24. The turbine blade design had proved satisfactory during previous testing. The two slots for the light beam speed sensing system were retained for low temperature tests. The TZM shaft is nitrided to provide a harder surface less prone to galling and seizure. The end faces must be square to the shaft axis, to ensure parallelism of the rotating and stationary faces of the thrust bearing, since the thrust bearing is not self-aligning. Shafts of different diameters are used to vary the bearing clearance. In addition to the shaft shown in Figure 24, shafts having diameters of 1.4960 inches and 1.4968 inches will be used to provide diametral clearances of .0040 in. and .0032 in., respectively.

As discussed in the materials section, it was planned originally that all external surfaces of the housing would be coated with an oxidation resistant surface, molybdenum disilicide. However, it was later decided that the molybdenum disilicide coating be deleted from all components. The unit is to be blanketed with an inert atmosphere during high temperature tests. This decision was based on the experience of the vendor selected for manufacture of the rig, and tests performed at MTI.

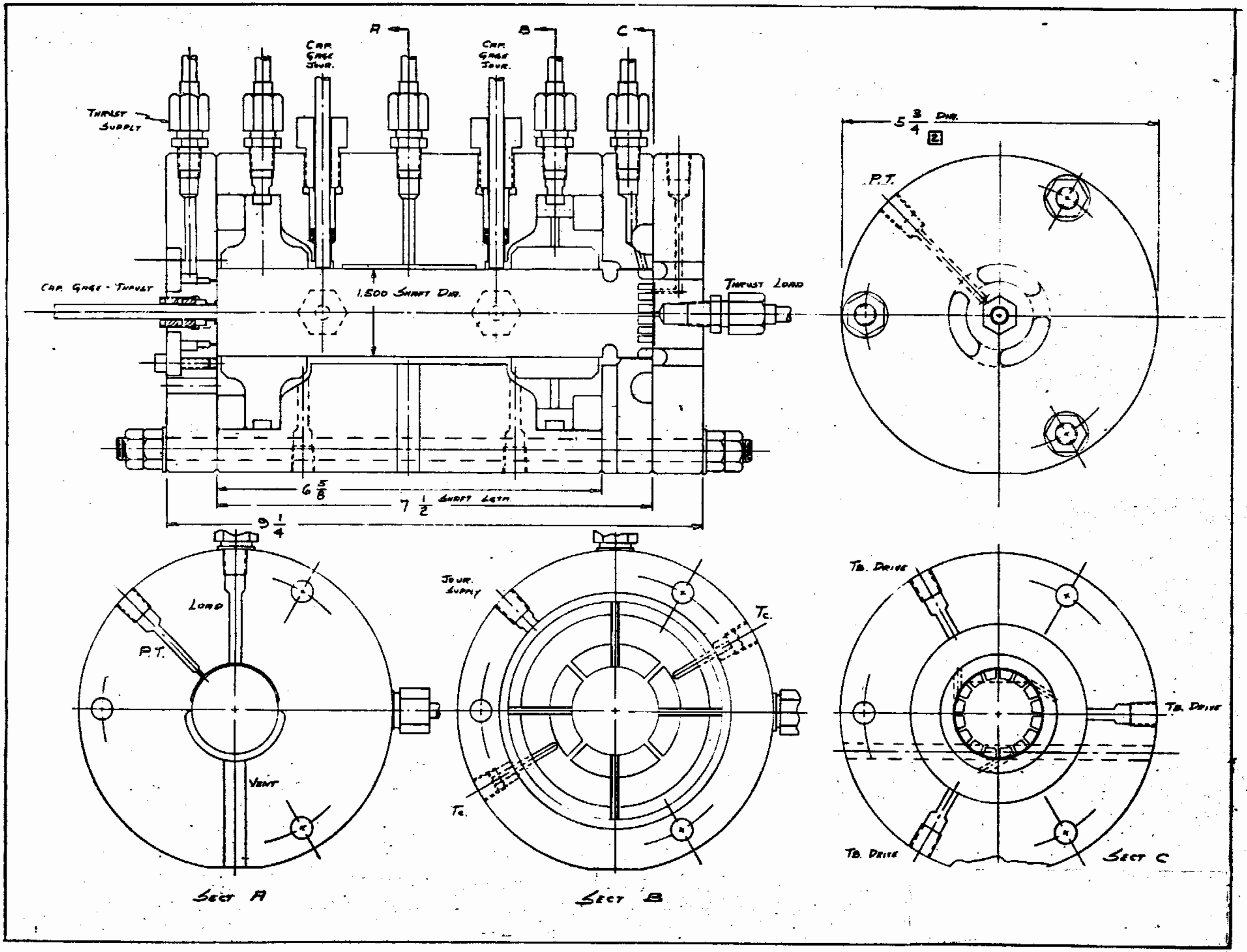

Figure 19. Assembly Drawing of Test Rig

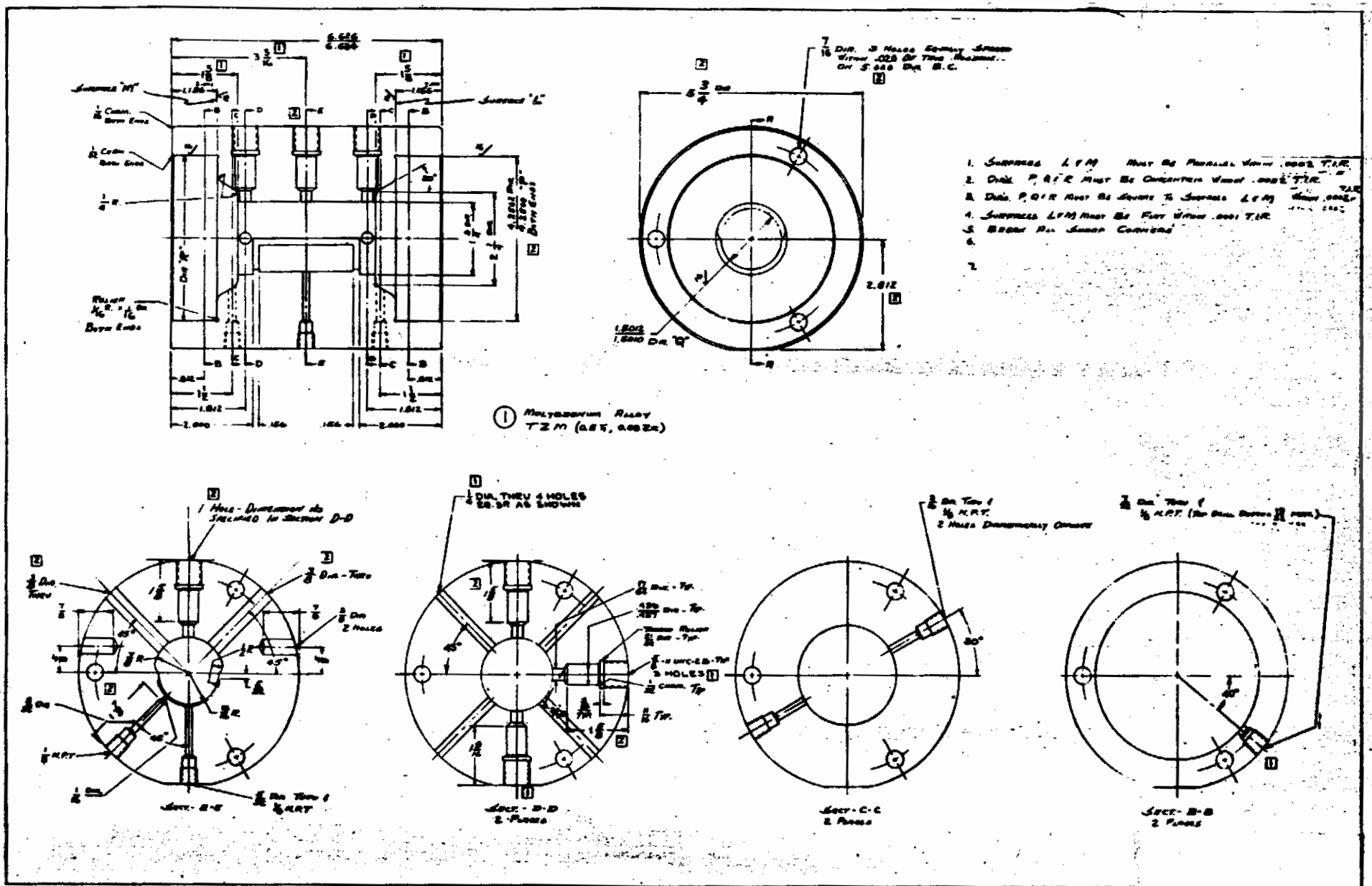

Figure 20: Housing Detail of Test Rig

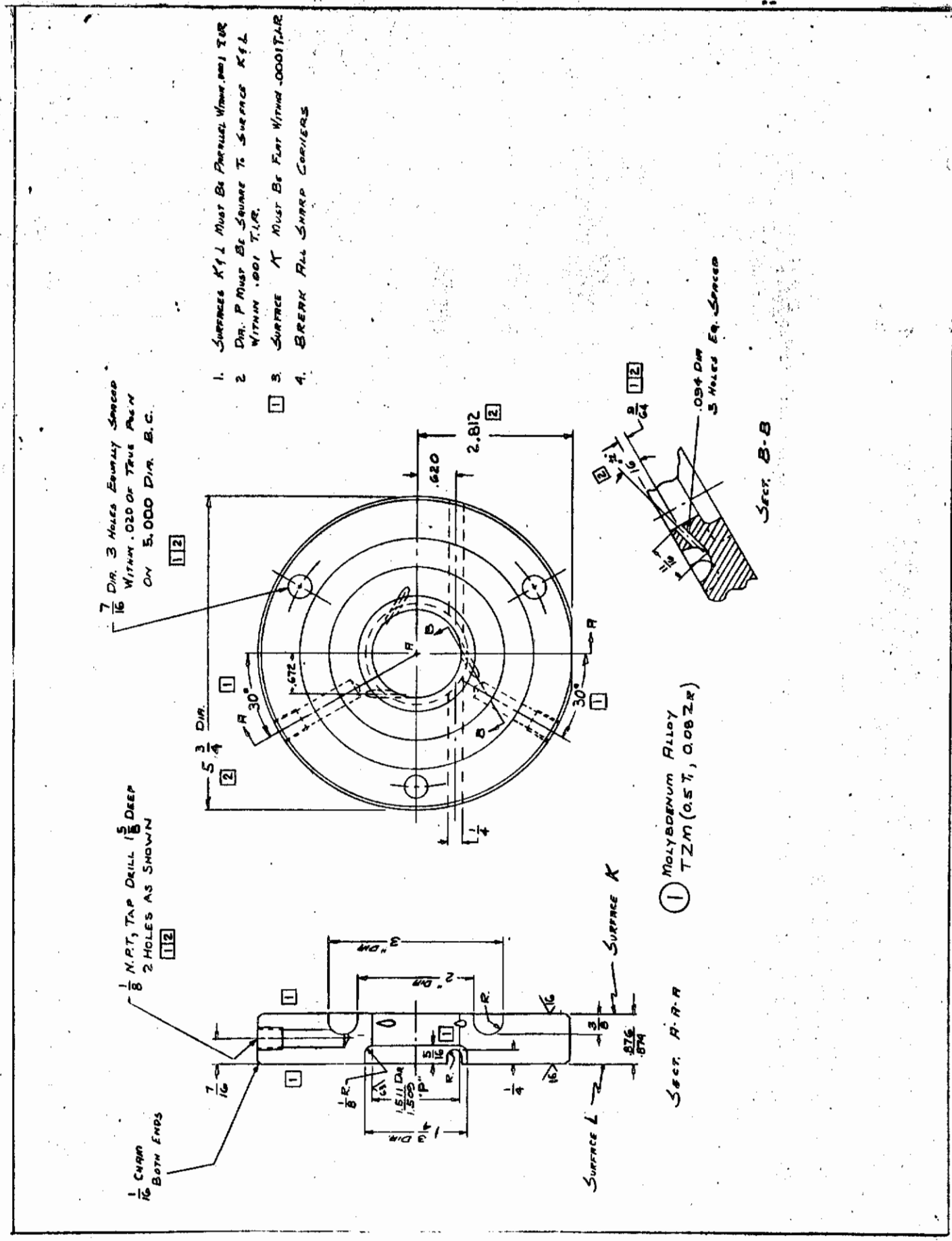

Figure 21. Turbine Nozzle Box Detail

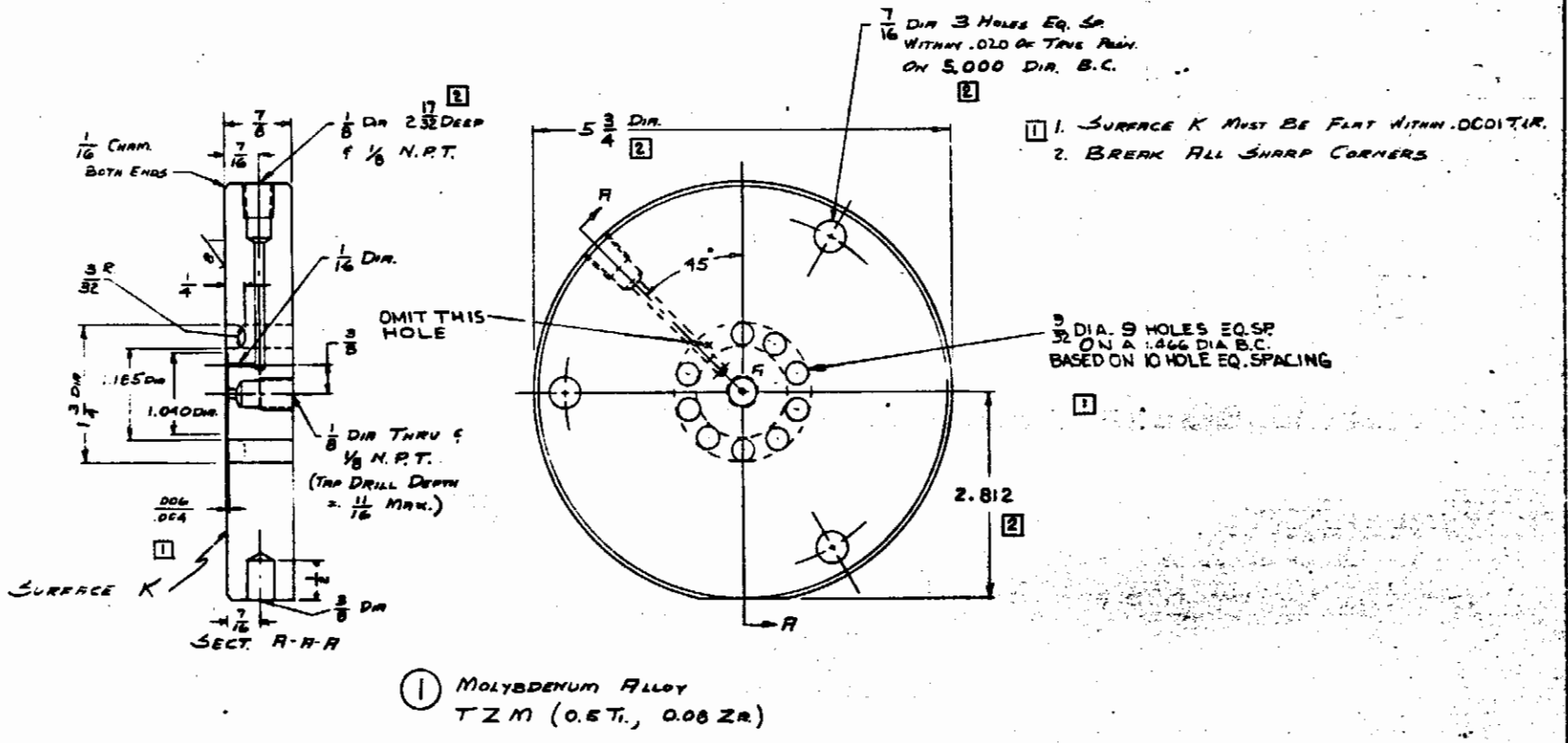

(1) MOLYBDENUM ALLOY TZM (0.5 Ti., 0.08 Zr.)

Figure 22. Thrust Loader Detail

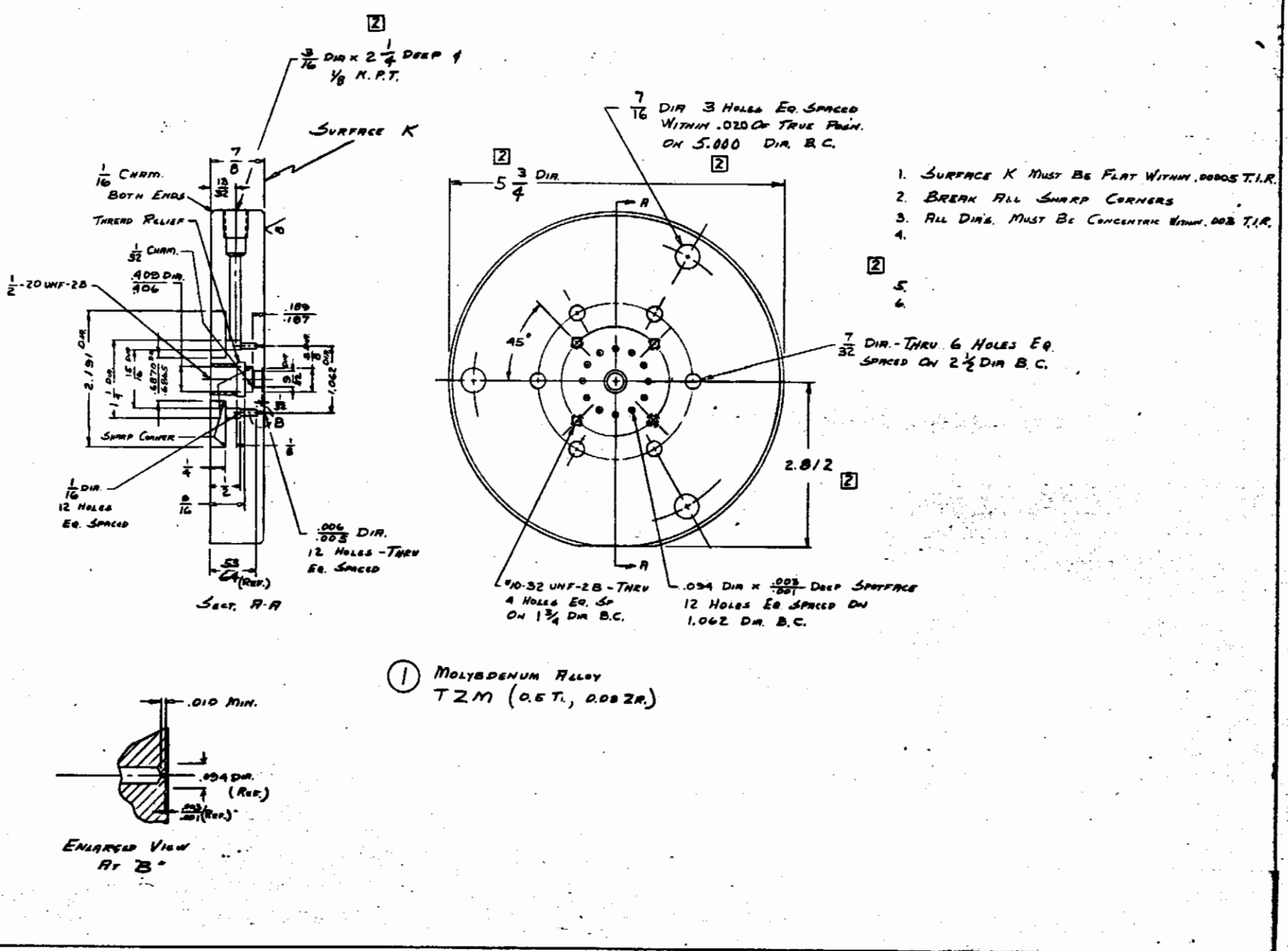

Figure 23. Thrust Bearing Detail

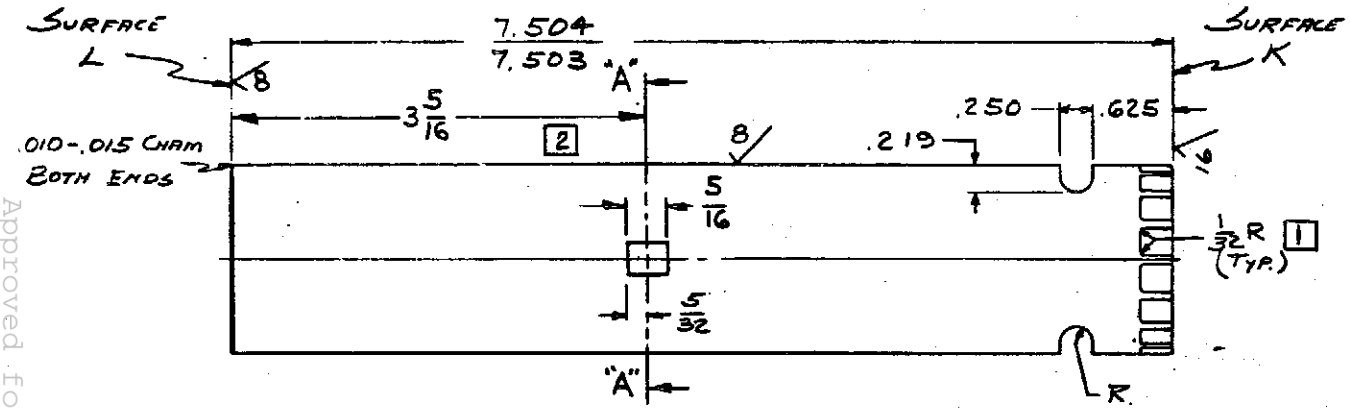

1 MOLYBDENUM ALLOY TZM (0.5 Ti., 0.08 Zr)

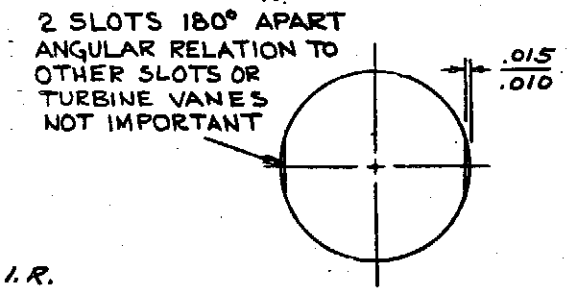

SECTION "A"-"A"
2

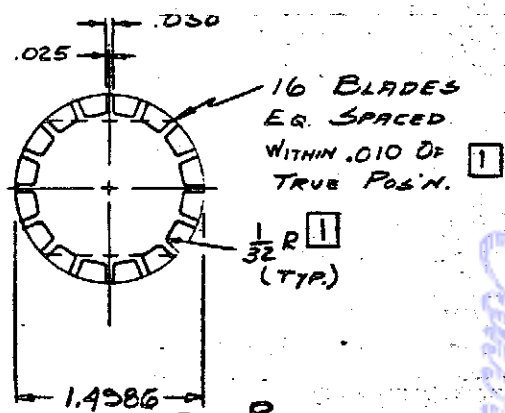

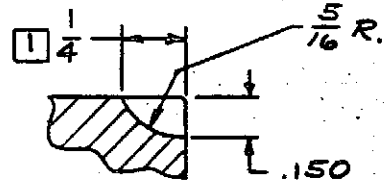

ENLARGED VIEW OF BLADE

1. CENTERS NOT ALLOWED ON FINISHED PIECE 1
2. BREAK ALL SHARP CORNERS
3. SURFACES K & L MUST BE PARALLEL WITHIN .0001 T.I.R.
4. SURFACES K & L MUST BE SQUARE TO DIA P WITHIN .0001 T.I.R.
5. DIA P MUST BE ROUND WITHIN .000025 T.I.R.
6. DIA P MUST NOT TAPER MORE THAN .000025 T.I.R.
7. CLEARANCE BETWEEN SHAFT & BEARING (116B30P1) MUST BE .0014 - .0015 DIAMETRAL 1
8. NITRIDE ALL OVER - HARDNESS 1200-1800 V.P.N. (THERMIONICS PRODUCTS CO. - PLAINFIELD N.J.)

Figure 24. Test Shaft

TEST BEARINGS

360 Degree Hybrid

Figure 25 shows the mounting or support ring for the 360 degree test bearing. The outside diameter (O.D.) of this ring locates the bearing in the housing and also forms a secondary annular gas supply manifold. The inside diameter (I.D.) of the ring locates the bearing insert and also seals the primary gas supply manifold. Radial holes feed gas from the secondary to the primary gas manifold. Axial holes through the web of this ring allow equalization of the ambient pressure at the two ends of the bearing.

The 360 degree bearing insert is shown in Figure 26. Two rows of sixteen orifices are provided at the quarter length axial stations. The orifice configuration is such that interchangeable orifice inserts can be installed with retaining screws. By varying the size of the drilled orifice holes and using various orifice insert plates, any degree of inherent or orifice compensation can be achieved. All orifices receive gas flow from the primary manifold formed between the bearing insert and the mounting ring.

Detailed drawings from a flexibly mounted, self-aligning, 360 degree bearing were completed and submitted for manufacturing quotations. However, the success of the design hinged on several very close tolerances and difficult machining operations. It was decided that the cost and complexity outweighed the advantages to be gained, at least in the light of the present test objectives.

The initial 360 degree bearing design had also included a "sacrificial" boron nitride bearing insert. This concept was deleted due to difficulties arising from the difference in thermal expansion, in one direction, between boron nitride and TZM.

Additional 360 degree bearing inserts of the same configuration have been made of leaded bronze, together with hardened steel shafts, for preliminary room temperature evaluations.

Flexure Mounted Hybrid Pad

A review of the fabrication procedure for the initial design (Figure 2) indicated that there would be a great deal of difficulty in maintaining the accuracies. Therefore, further design effort was placed on this bearing type.

The assembly drawing of the design shown in Figure 27 is the final result which will be used for initial evaluations of this bearing type. The unit shown in Figure 27 has the mounting ring and flexure rods as an integral unit. An annular groove in the mounting ring acts as a gas manifold which supplies gas through the hollow flexure rods. The gas passage in the rod communicates with a countersink on the outside diameter of the pad, and then to two axial holes in the pad which supply the orifices. The one-piece assembly for mounting ring and flexure rod was necessary for accuracy and strength.

Figures 28 and 29 show details of this design. Figure 28 shows the fastening means and other manufacturing information, while Figure 29 shows the pad construction. This bearing can be installed in the test rig housing in place of the 360 degree bearing described previously. The test pieces ordered for initial room temperature evaluation consist of steel flexure supports and bronze pads. The final configuration for high temperature tests is to be made of TZM.

Oven

Some modification to the oven was necessitated by the decision to use an inert atmosphere blanket to prevent oxidation of the test rig. Consideration was given to the design of a sheet metal "can" fitted over the test rig enclosing a minimum volume. However, the multitude of connections for gas supply lines and instrumentation (which would have to pass through the wall of such a can at various points) made this approach impractical. Installing a pressure tight jacket around the outside of the oven would allow the use of low temperature materials, but would enclose within the inert area all of the air in the oven insulation. It was therefore decided to modify the liner inside the oven chamber to create a relatively, gas-tight chamber inside the oven insulation, but enclosing the oven heater elements as well as the test rig.

Inconel sheet metal end covers for the liner were fabricated with simple baffle-type joints. Minimum clearance holes are provided for the bundle of gas supply tubes and the bundle of instrumentation leads. The resulting enclosure is not completely gas tight, but the inert blanket will be ensured by injecting sufficient nitrogen into the enclosure to maintain a slight positive pressure.

The oven has been used several times for high temperature probe calibration and has operated satisfactorily.

Preheater

The gas preheater design places the heating elements outside the gas flow path. Since the gas flow path is completely enclosed in the Inconel tube coil from the room temperature filters to the test bearing, the possibility of dirt or grit being introduced into the bearing via the lubricant gases is minimized. Figure 30 shows the completed unit with the oven in position for testing. Preliminary flow, pressure, and gas heating tests have been performed.

The configuration of one of the six gas-heating circuits is shown in Figure 31. The heater gas flow-path for each circuit consists of about seventy feet of one quarter inch, O.D. Inconel tubing with a .025 square feet of heat transfer surface. The tubing is formed into two helical coils about nineteen inches long with an inside diameter of 1-1/2 inch, connected in series. A silicon carbide, resistance heater rod passes through the center of each coil, and the two rods are connected in series electrically. The heater bars have the following

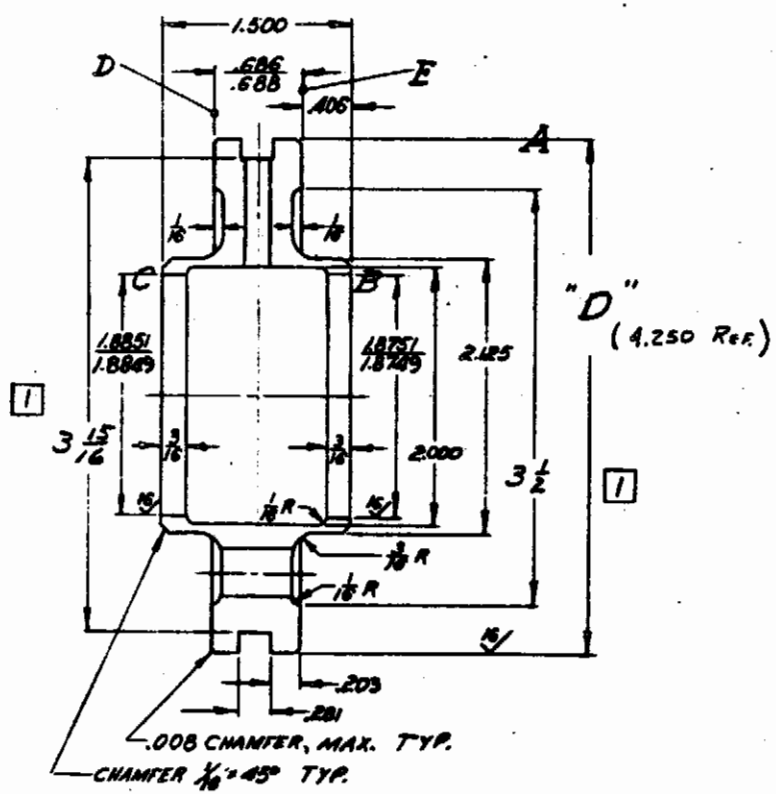

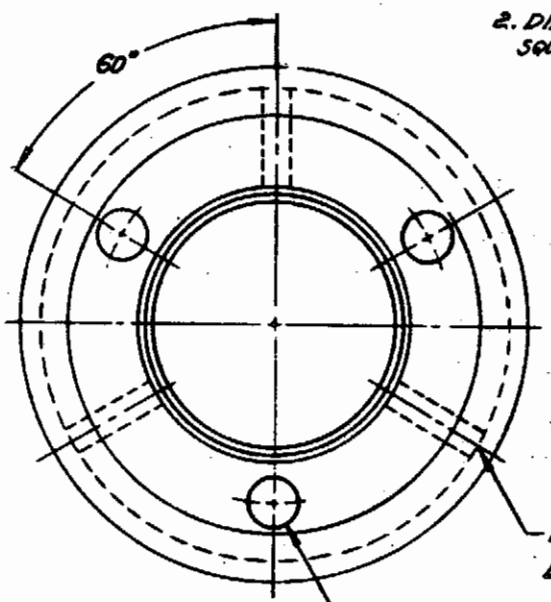

1. DIAMETERS A, B, & C TO BE CONCENTRIC WITHIN .0001 F.I.R.

2. DIAMETERS A, B, & C TO BE SQUARE TO SURFACES D & E WITHIN .0001 F.I.R.

DRILL THRU 7/32 DIA, 3 HOLES EQUALLY SPACED AS SHOWN

DRILL THRU 3/16 DIA, 3 HOLES EQUALLY SPACED AS SHOWN, ON 2 3/4" B.C.

MATL.: MOLYBDENUM ALLOY TZM (.5 Ti, .08 Zr.)

[1] PART 1 - 1 REQ'D - DIA "D" TO GIVE .0001-.0003 DIA. CLEARANCE WITH DIA. "P" OF HOUSING

PART 2 - 1 REQ'D. - SAME AS PART 1 EXCEPT DIA "D" TO GIVE .0001-.0003 DIA CLEARANCE WITH DIA "R" OF HOUSING

Figure 25. Bearing Support Ring

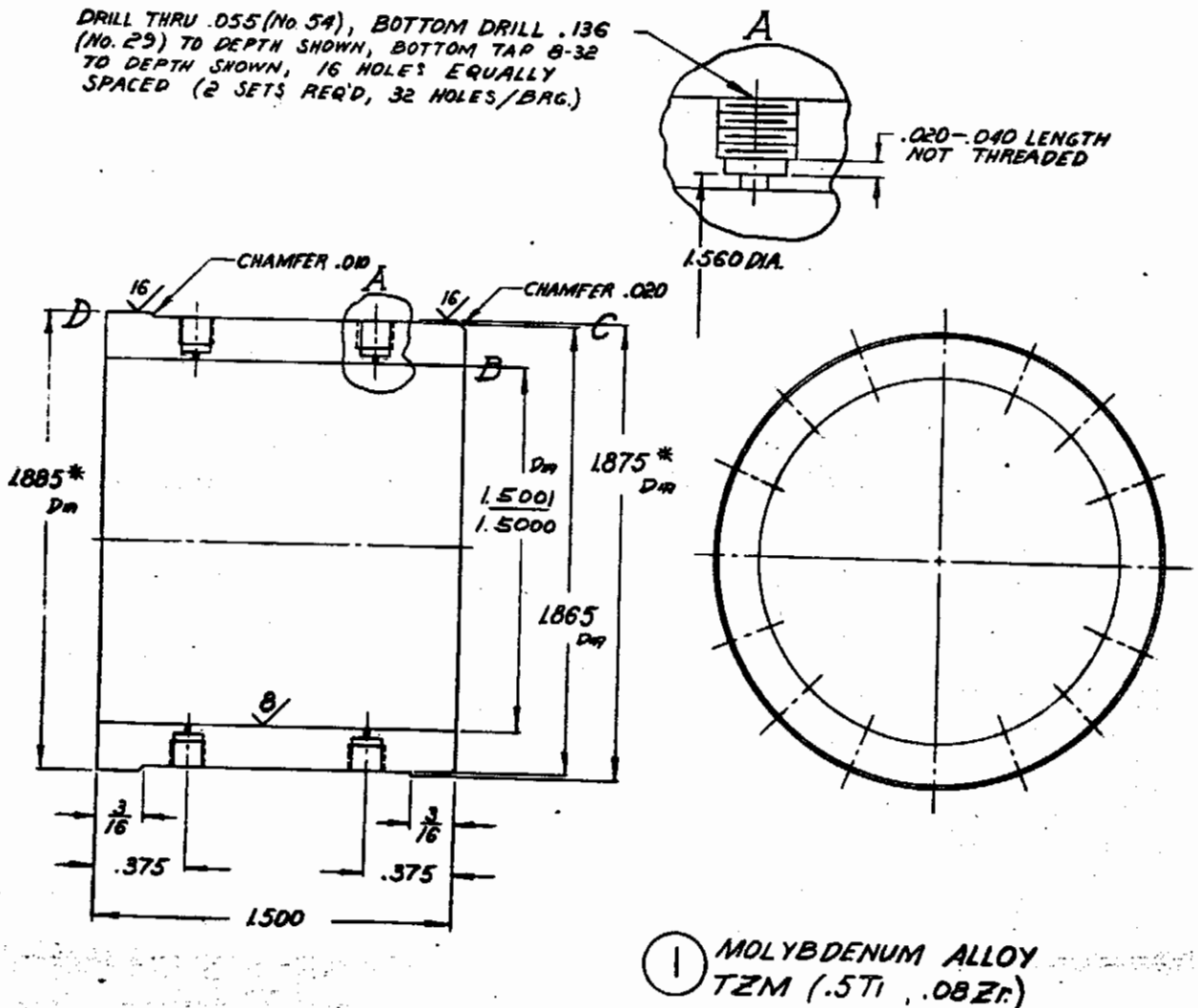

1. DIAMETERS B, C, & D TO BE CONCENTRIC WITHIN .0001 F.I.R.
2. DIAMETERS C & D (*) TO BE .0001 INTERFERENCE FIT WITH CORRESPONDING DIAMETERS OF BEARING RING 116B29 P-1
3. DIAMETER B TO BE ROUND & FREE OF TAPER WITHIN .000025

(1) MOLYBDENUM ALLOY TZM (.5Ti, .08Zr)

Figure 26. 360 Degree Test Bearing

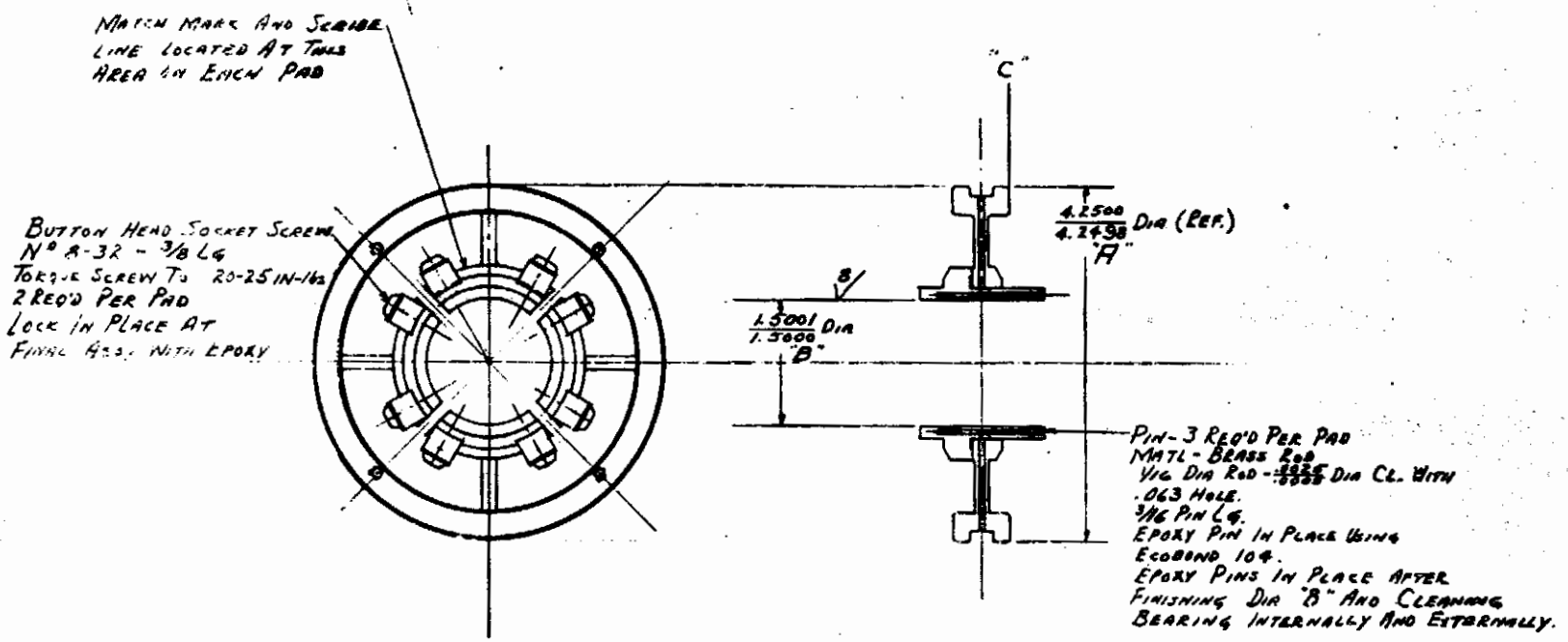

NOTES:

1. ASSEMBLE PAD (116833) AND SUPPORT (116832) AND POT IN LOW TEMPERATURE METAL. MASK HOLES TO ASSURE METAL DOES NOT ENTER THE HOLES. MACHINE DIA. "B".
2. DIA. "B" TO BE ROUND AND STRAIGHT WITHIN .00005 T.I.R.
3. DIA "B" TO BE CONC. WITH DIA. "A" WITHIN .0001 T.I.R.
4. DIA "B" TO BE SQUARE TO SURFACE "C" WITHIN .0001 T.I.R.
5. MATCH MARK BEARING PAD TO SUPPORT AND PROVIDE SCRIBE MARK FOR ALIGNMENT.

Figure 27. Assembly of Flexure Mounted Hybrid Pad Bearings

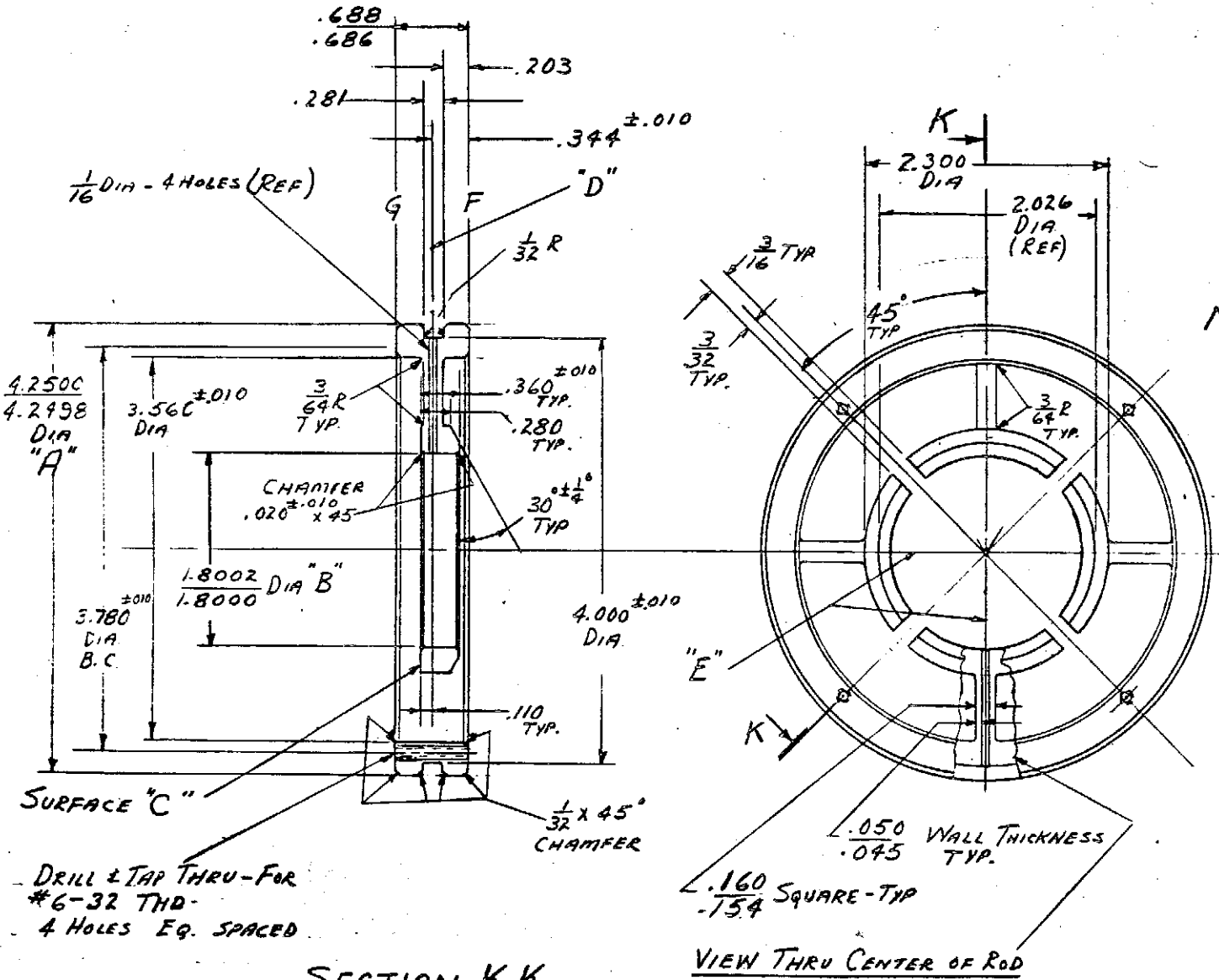

NOTES:

1. MATL. - A151 4340 - BN 220 - 250 ANNEALED CONDITION
2. FINISH - ZINC PHOSPHATE COAT AND TREAT WITH CORROSION INHIBITING OIL ON ALL EXTERNAL SURFACES.
3. ℄ "D" OF FOUR RODS TO BE "⊥" TO DIA "B" WITHIN .001 T.I.R.
4. ℄ "E" OF FOUR RODS TO BE RADIAL AND PASS THRU CENTER OF DIA "B" WITHIN .001 T.I.R. ℄ "E" OF FOUR RODS TO BE EQUALLY SPACED AND LOCATED WITHIN .010 T.I.R.
5. DIA "A" TO BE ROUND WITHIN .0002 T.I.R
6. DIA. "B" TO BE CONC. TO DIA. "A" WITHIN .0002 T.I.R
7. SURFACE "C" TO BE "⊥" TO DIA. "B" WITHIN .0002 T.I.R.
8. SURFACE "F" TO BE "⊥" TO DIA "A" AND PARALLEL TO SURFACE "G" WITHIN .0002 T.I.R.
9. UNSPECIFIED CONC., SQUARENESS, AND PARALLELISM TO BE WITHIN .005 T.I.R.
10. STRESS RELIEVE AS REQ'D. TO INSURE ASSEMBLY IS DIMENSIONALLY STABLE WITHIN THE TOLERANCES SPECIFIED.
11. BREAK SHARP CORNERS AND REMOVE BURRS.

Figure 28. Flexure Detail

2 Req

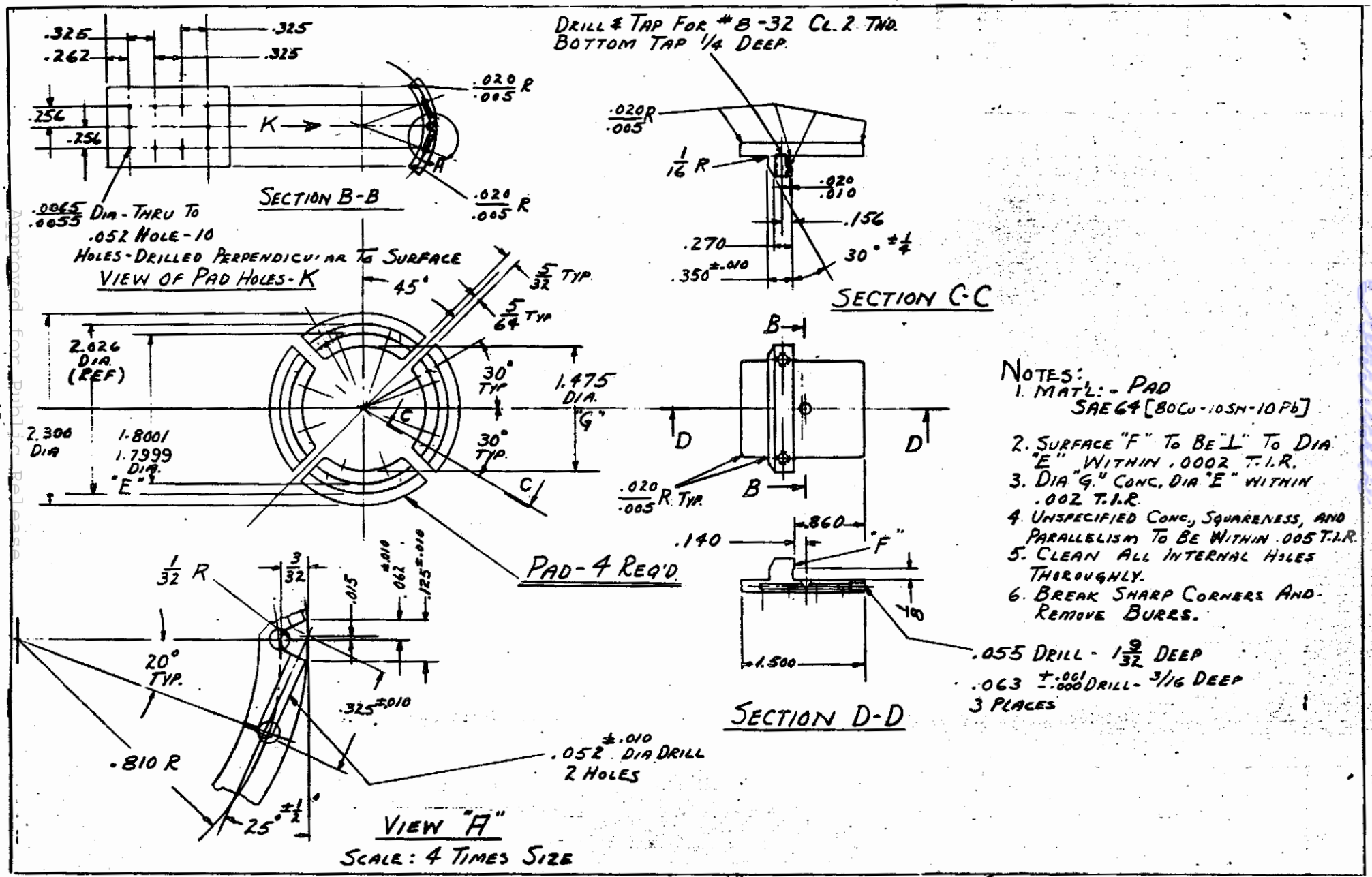

Figure 29. Pad Design

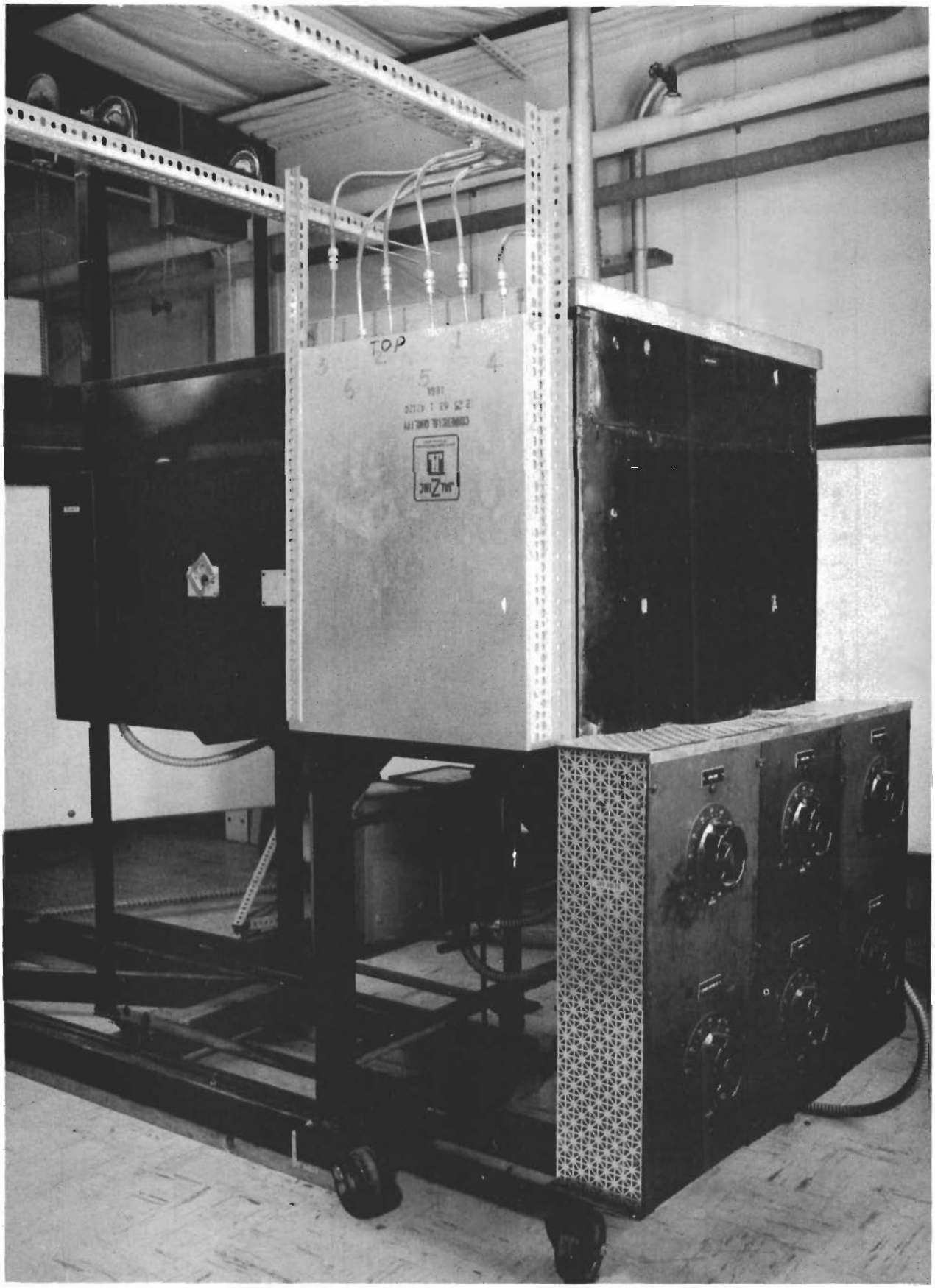

Figure 30. Heating Facility for Gas Bearing Tests

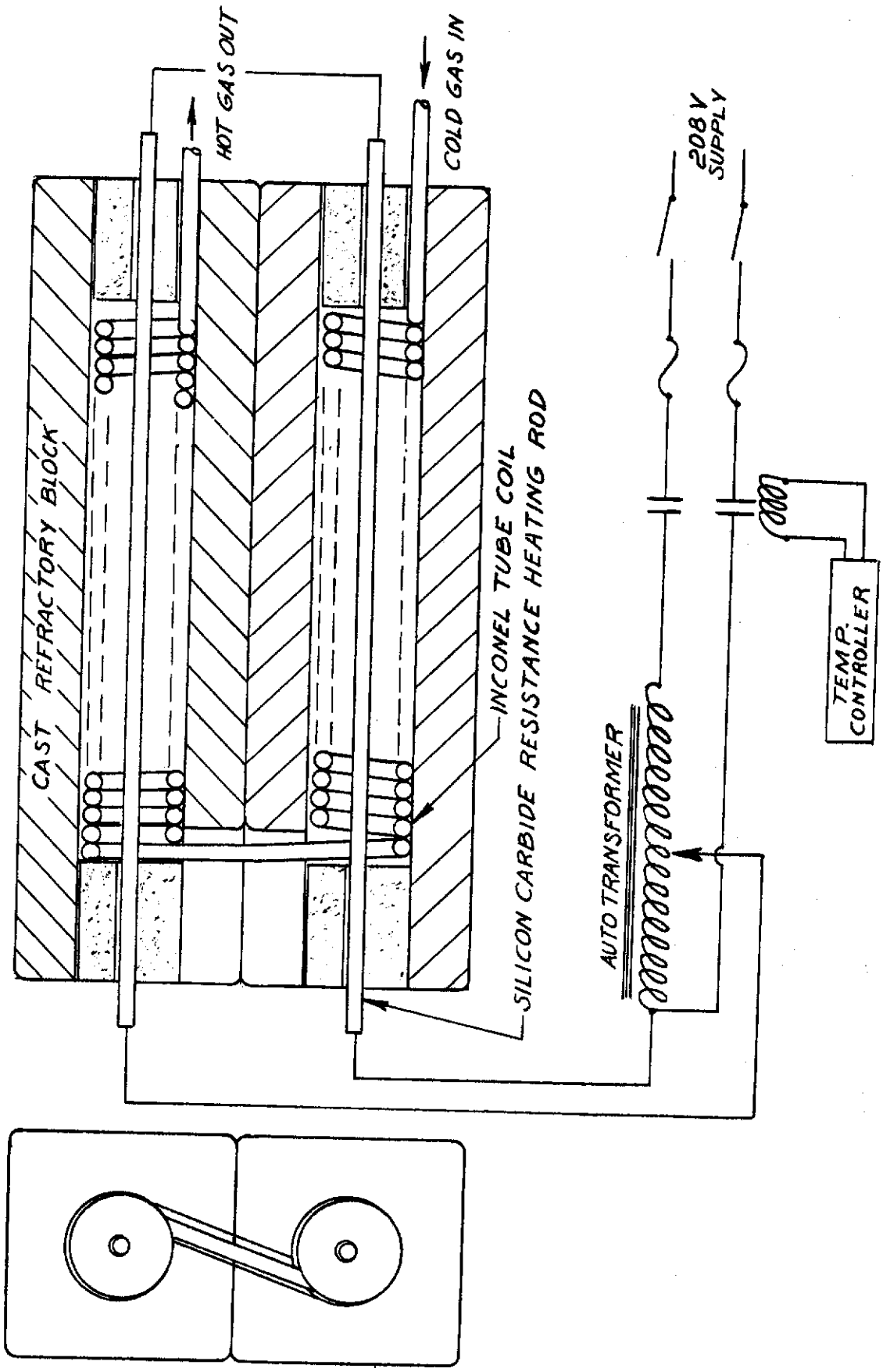

Figure 31. Schematic of Gas Preheater

characteristics:

Over all length	39 inches
Heating length	20 inches
Diameter	1/2 inch
Resistance (each)	4.14 ohms
Power delivered by series - connected pair	4.15 kilowatt
Voltage at above power	185 volts
Current for above power	22.5 amperes
Watt density at heater rod surface	66.7 watts/inch^2

The heater rods have the capacity to operate at a maximum watt-density of 90 watts/inch^2 at a furnace temperature of 2100 F. The maximum voltage available at the heater bars is 208 volts which will allow operation at a power level of 5.2 kilowatts with a current draw of 25 amperes.

A 7.8 KVA, 240 volt autotransformer is installed in each circuit to regulate the power circuit level. (Actually the autotransformer will make available voltages greater than the 208 volt line voltage.) This allows continuous variation of the applied voltage and power to each circuit between zero and maximum power level. Fine control of temperature is achieved by a temperature controller operating a magnetic contactor in the power line.

The outlet connections from the preheater are made at right angles to the axis of the tube coils. This is necessary to keep the electrical connections at both ends of the heater bars out of the high-temperature test oven.

The maximum design gas pressure of 300 psig will produce a stress of 1200 psi in the tubing material. This is a negligible stress at moderate temperatures. At 1900 F, this stress represents about one third of the yield strength of Inconel, giving a safety factor of three. Extended use at maximum pressure at high temperature will lead to creep fracture of the tubing material. The estimated life of the inconel tubing coils under continuous exposure to 1600 F temperature and 1200 psi stress is 100,000 hours. Continuous exposure to 2000 F and 1200 psi would result in an estimated life of slightly more than hundred hours. It is anticipated that the total test time at the combined maximum temperature-maximum pressure conditions will not reach one hundred hours. A reduction in pressure to 150 psig results in a reduction in stress to 600 psi and an increase in estimated life at 2000 F to 10,000 hours. These estimates are based on creep fracture data for Inconel presented in International Nickel Company Technical Bulletin, T-7.

The six separate heater units are all contained within an insulated housing thirty-seven inches long, twenty-five inches wide, and thirty-two inches high. The autotransformers, magnetic contactors, fuse boxes, and associated wiring are all mounted on the housing support stand, as shown in Figure 30.

Control Panels

Figure 32 is a schematic diagram of the gas supply control panel. The panel provides independent flow and pressure control of six separate gas circuits. All six separate circuits receive gas from a single manifold made from one and one-half inch diameter, Schedule 40 pipe. The manifold is supplied with nitrogen from high pressure cylinders. A constant manifold pressure of 325 psi is maintained by a gas pressure regulator in series with a standard gas-cylinder pressure reducing valve. A five micron filter is installed in each circuit just downstream from the manifold.

The turbine supply, journal loader, and thrust loader systems consist of shut-off valve, pressure regulator, and pressure gage. The two-journal bearing and the thrust bearing supply systems also incorporate flow measurements stations. The valving arrangement allows anyone of three flow meters to be put on line in either journal bearing supply circuit without interrupting the gas flow. A flow meter can be switched from one bearing circuit to the other without interrupting the flow to either bearing. The flowmeter with the lowest range (.05 to .5 pounds/hour) is shared between the journal bearing and thrust bearing systems. Figure 33 is a photograph of the control panel.

Flow tests of the system, in conjunction with the gas preheater, have indicated negligible pressure drops through the circuits, except at the pressure regulators. These are small-volume regulators and are satisfactory for low-flow requirements.

High Temperature Displacement Probe

Without some means to monitor high-temperature performance, merely running at high temperature would yield only a "go" or "no-go" indication. This was not felt to be satisfactory, and considerable effort was allocated to the determination of feasibility of high-temperature displacement measurement. The effort was directed to capacitive type displacement probes, since the electronics and readout equipment have achieved an advanced status in our laboratory.

One of the initial concerns was that it might not be possible to utilize these over the entire temperature range because of the change in resistivity of the gas at elevated temperatures.

This was checked qualitatively using the expressions for high temperature gases. The electron concentration for a singly ionized gas is given by:

$$N_e = 1.5 \times 10^{15} \frac{C}{P} \epsilon T^{5/4} e^{-\frac{5800V}{T}}$$

where P = total pressure

V = ionization potential

ϵ = degree of ionization of the gas

C = % concentration of the ionizing gas

T = absolute temperature (^{o}K)

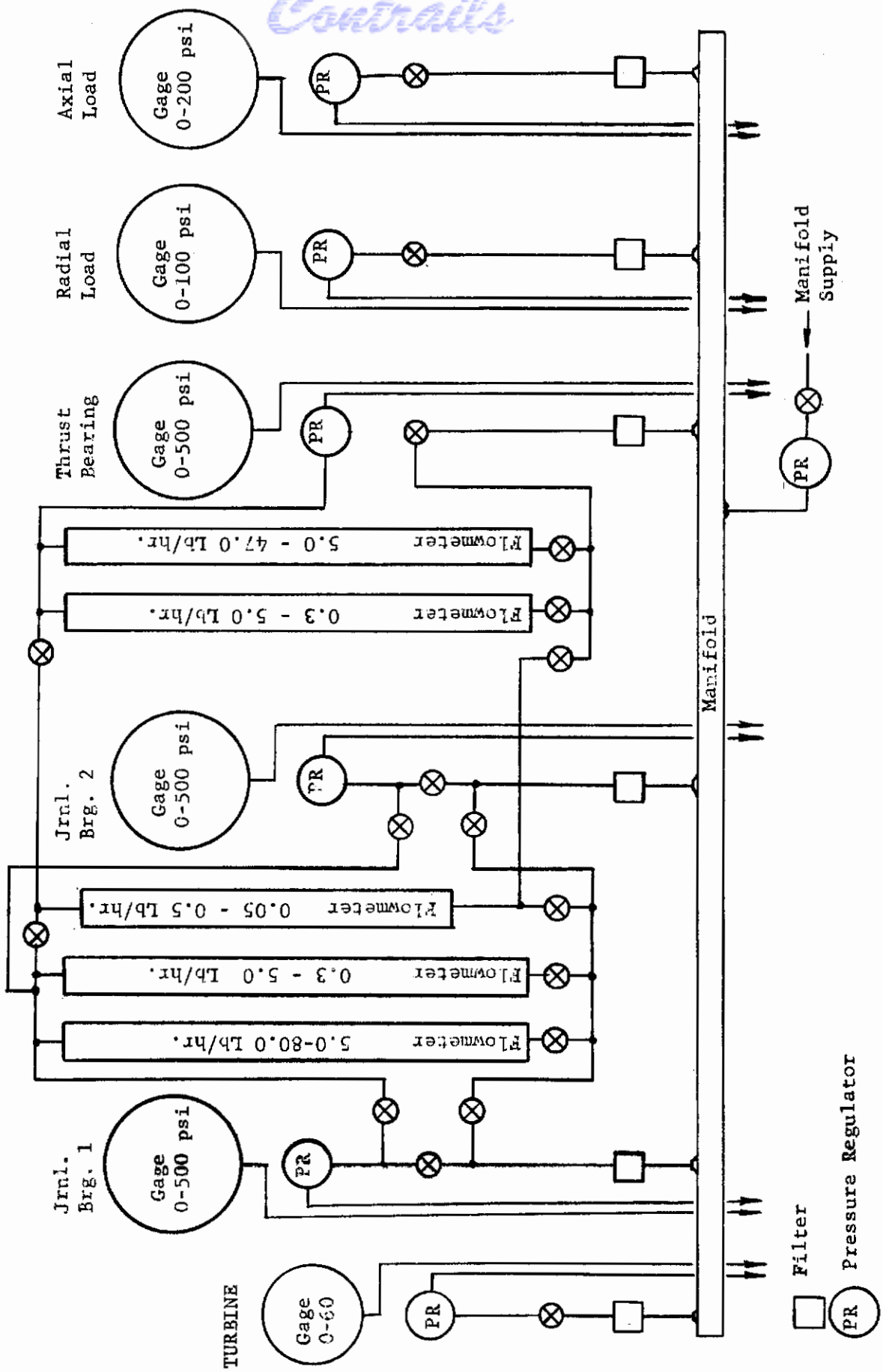

Figure 32. Schematic of Gas Control Panel

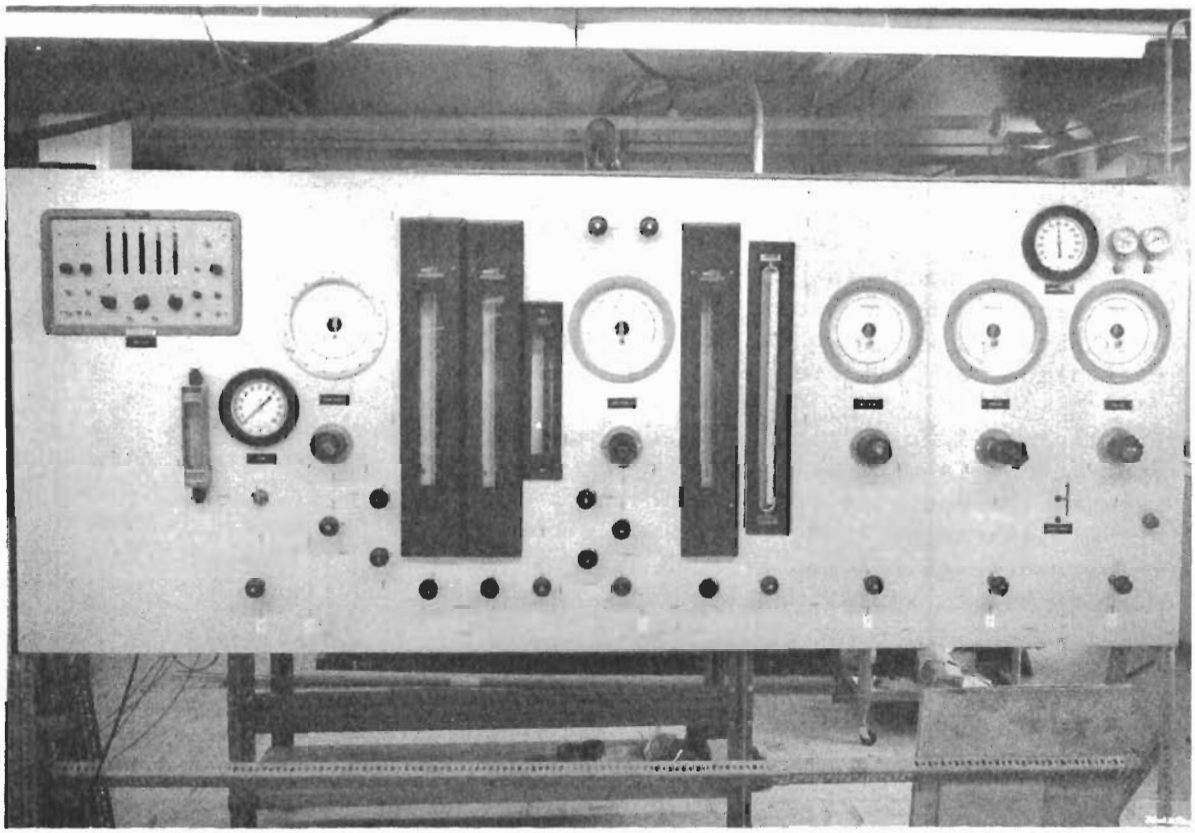

Figure 33. Control Panel

The resistivity is given by:

$$R_o = 3 \times 10^{13} \frac{T}{N_e} \epsilon$$

The previous equations can be combined to give:

$$R_o = \frac{2 \times 10^{-2} T^{-3/4} P}{C} \quad \frac{5800V}{T}$$

Comparing the resistivities at 20 C (29 K) and 1038 C (1311 K) for V of one volt, indicates a change in resistivity by a factor of 10^7. How this will affect the operation of the measuring system was not known at the time. The general concensus was that this would not be the limiting item. Therefore, probe construction and evaluation was initiated.

For the metallic portion, a high-temperature nickel base alloy was selected. Four materials were selected for the insulating or dielectric material. These were of the castable ceramic category. For discussion, the dielectric materials are designated as A, B, C, and D. Probes of each type were tested in the high temperature calibration fixture shown in Figure 34. It should be noted that this fixture brings approximately one inch of the probe tip to the test temperature.

The tests on probes with dielectric A were of short duration since the resistivity of the probe decreased sufficiently with temperature to make the probe inoperative at 700 F.

More success was achieved with dielectric material B. Figure 35 shows how the high temperature calibrations compared with a normal room temperature calibration. Figure 36 illustrates the way in which the output of this probe varied with temperature. The maximum range of usefulness for this probe was 1350 F.

Material C extended the range to 1450 F. Although this material did not deteriorate at higher temperatures, a loss in linearity would preclude its use above 1450 F. Figure 37 shows typical calibration curves for this material and illustrates the loss in linearity with a 1600 F calibration.

Material D gave, by far, the best performance with predictable behavior to 1800 F. Calibration at 1900 F indicated some loss in sensitivity. However, the calibration was generally linear and could be used at the higher temperature. Figure 38 shows the calibration curves for this material.

Although further work remained to be done to demonstrate the durability and applicability of the previously described probes, it was necessary to consider what was to be used as the high-temperature lead wire. A sample piece of coax wire was evaluated to determine how the center conductor-to-sheath resistance varied with temperature. These data are summarized below:

T	Resistance Center to sheath
400	∞
500	∞
700	∞
800	∞
1000	∞
1200	7.5 meg Ω
1400	3.0 meg Ω
1500	2 meg Ω
1600	.7 meg Ω
1800	.12 meg Ω

The center conductor resistance remained constant at 1.7 Ω, the sheath resistance at 0.2 Ω.

A test was subsequently performed on this same co-axial lead wire in conjunction with a high temperature probe. The entire assembly, including a four foot length of lead-wire, was mounted in the oven chamber. Calibrations at increasing temperatures indicated that the sensitivity of the probe-lead wire combination remained essentially constant up to 1400 F. Above this temperature a rapid decrease in sensitivity occurred, until at 1600 F the output signal did not vary with clearance.

Subsequent to the above tests some room temperature calibrations were made. These indicated that variations in lead-wire, center conductor-to-sheath resistance and capacitance would affect the probe output in the manner shown. Therefore subsequent tests utilized larger diameter lead wire so as to reduce the lead wire capacitance and increase the initial resistance. No real gain was realized over the smaller diameter lead wire. The data for the 3/16 diameter lead wire is shown in Figure 39. Although the probe is operative above 1400 F, the output becomes highly non-linear. These evaluations are not as yet complete. However, unless some of the other lead-wire candidates show greater improvement, accurate determinations of shaft motions will be restricted to 1400 F and below. Above 1400 F, the motions will be determined on a relative basis.

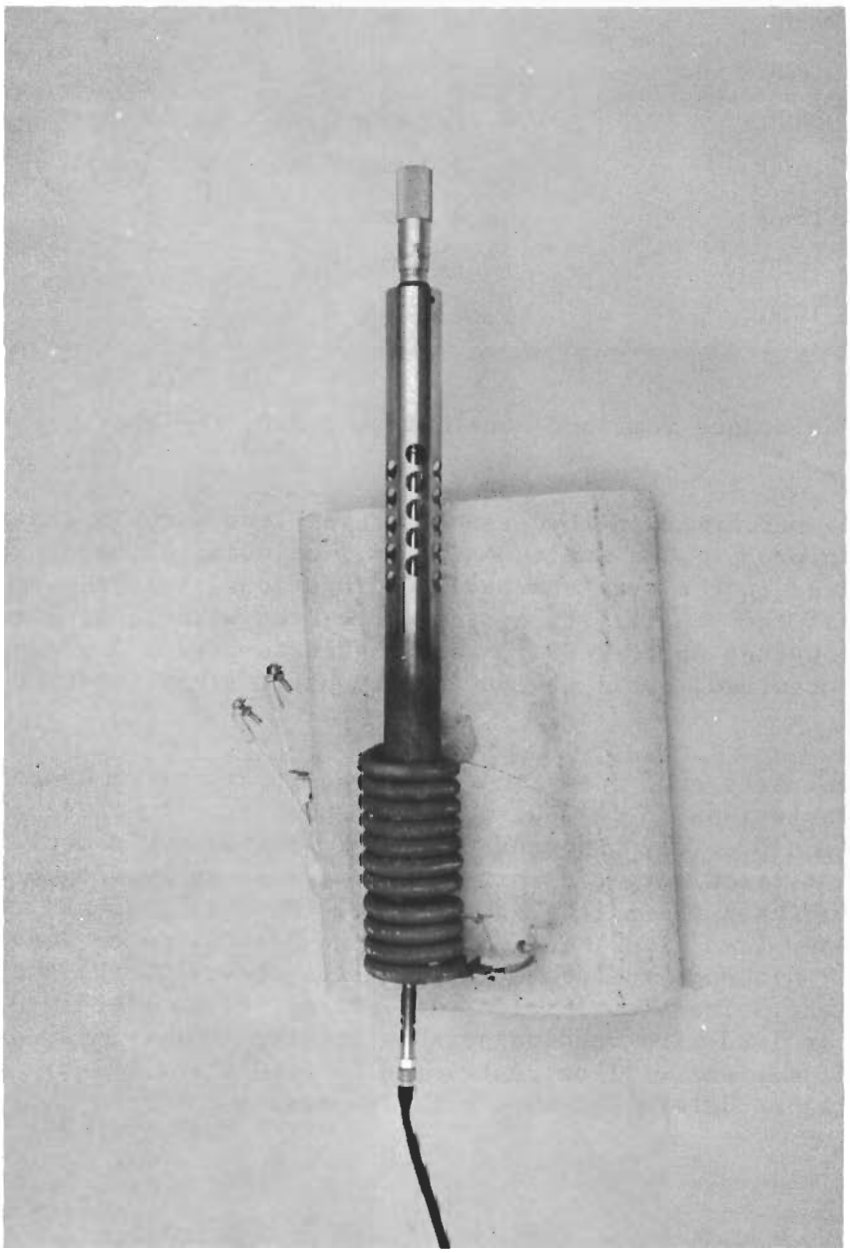

Figure 34. Probe Calculation

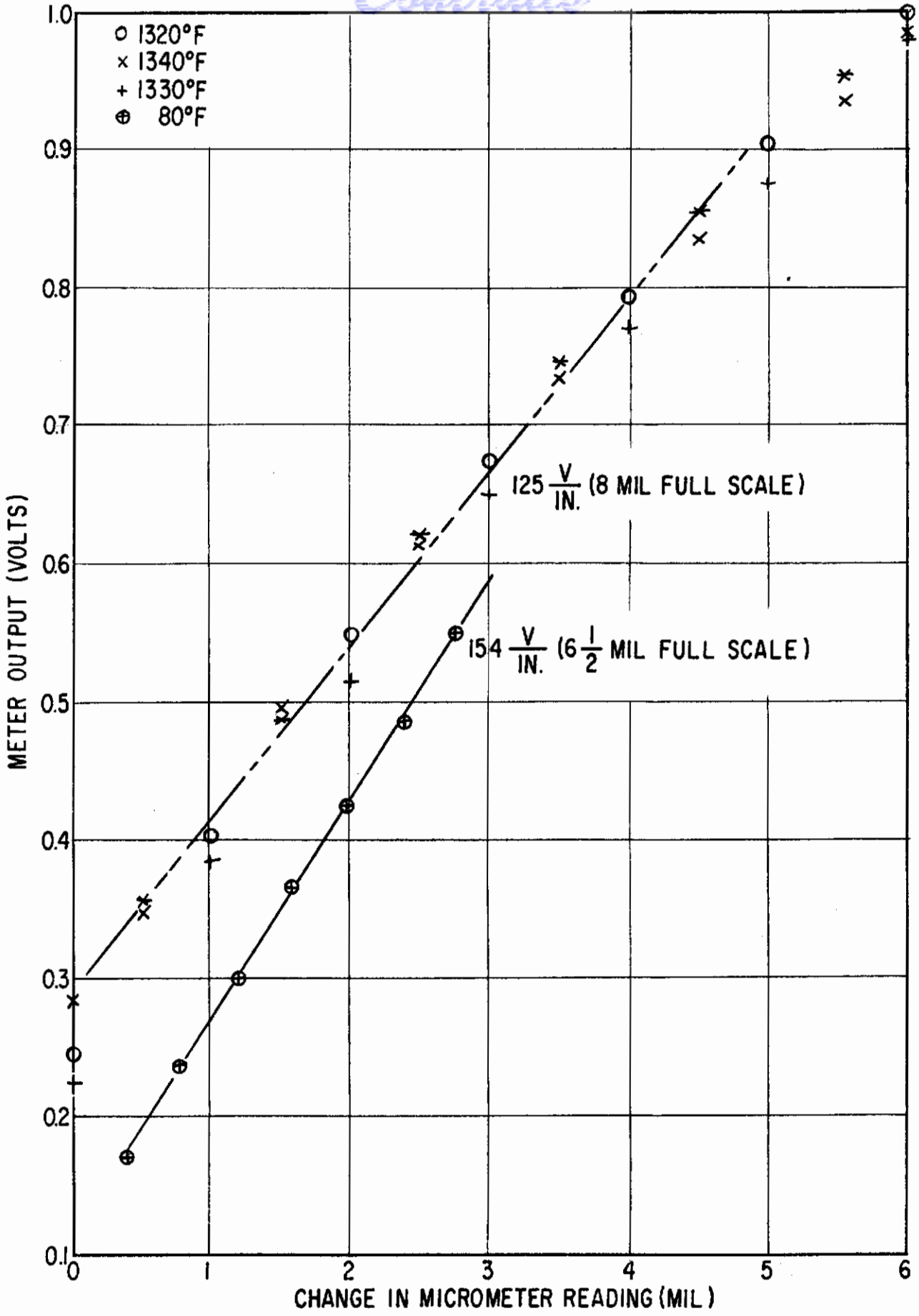

Figure 35. Probe Calibration - Dielectric Material B

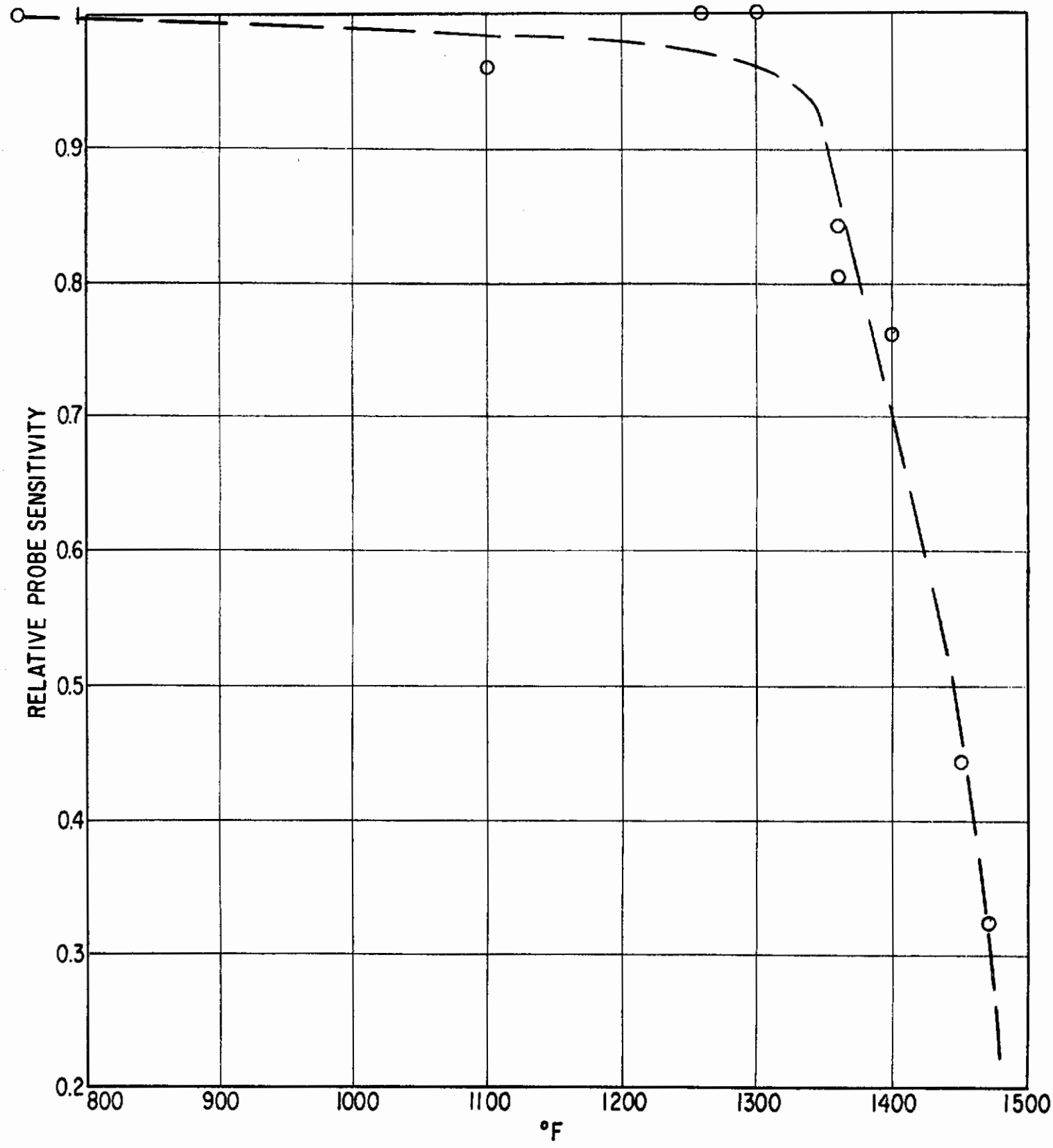

Figure 36. Probe Sensitivity versus Temperature - Dielectric Material B

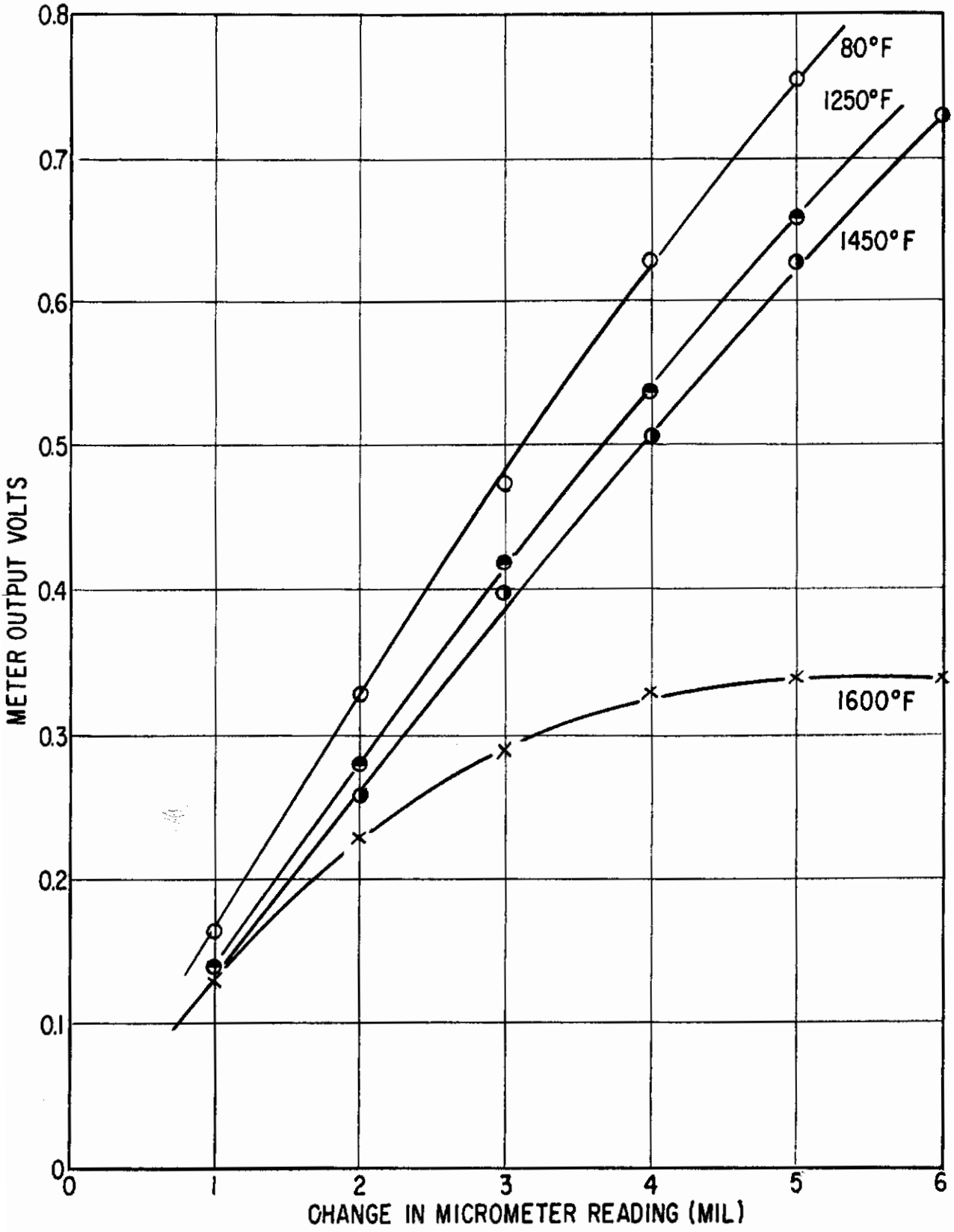

Figure 37. Probe Calibration - Dielectric Material C

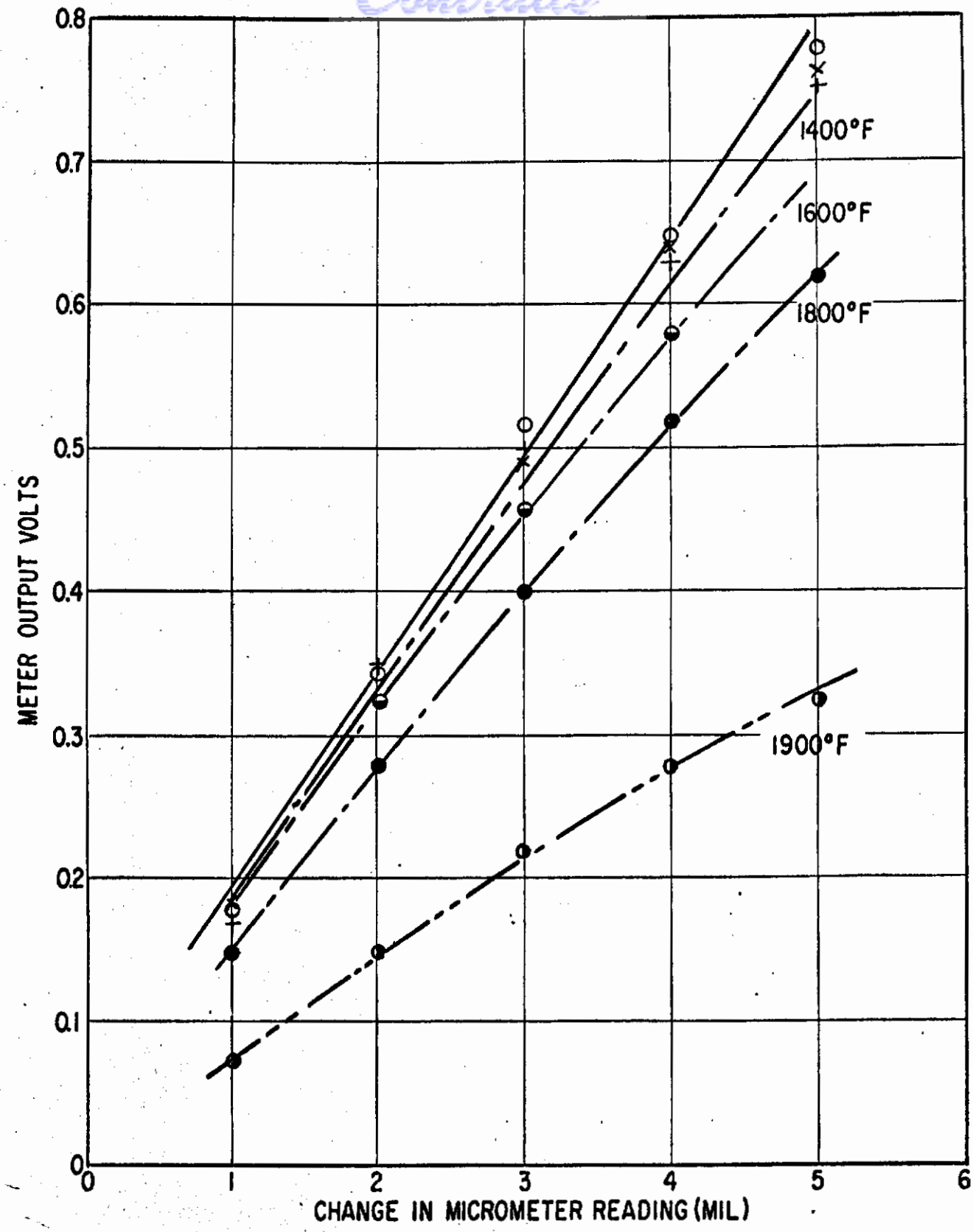

Figure 38. Probe Calibration - Dielectric Material D

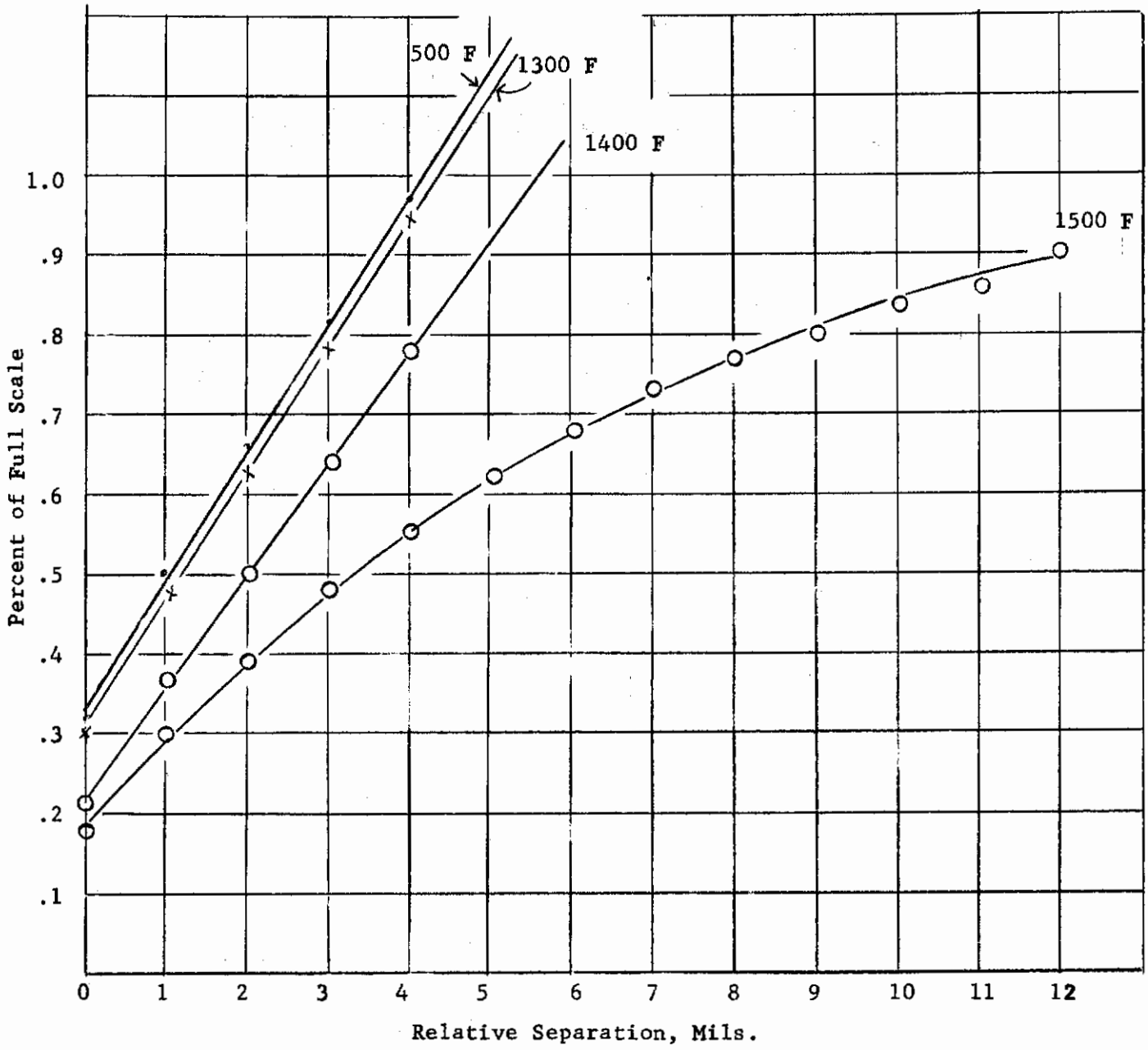

Figure 39 Probe Calibration
Insulation D and 3/16 Coaxial Cable

EXPERIMENTAL WORK

Several evaluations, other than the running of the equipment designed for this program, were made in order to make certain judgements and guide the decisions made to date. These, and the program equipment runs, are described in this section.

Flat Hydrostatic Pad - Experimental Check

As mentioned in a previous section, the flat pad analysis was made in order to guide the design of partial arc (hybrid pad) bearings. A brief experimental effort was devoted to verification of the analysis.

The test bearing is shown in Figure 40. The ten orifices were drilled .0135 inch diameter, relatively high loads were required to reach the maximum stiffness point. The surface of the bearing was lapped flat, as was the mating member, a 3-1/8 inch diameter by 3/16 inch thick stainless steel disk.

The bearing was mounted in a bench vise and leveled with a machinist's level. During the first series of tests, a load was applied by stacking metal billets directly on top of the mating disk. During the final series of tests, the loading billets were mounted on a platform suspended by chains from a pivot point on the mating disk as shown in Figure 41. The weights of the loading billets were determined to within $\pm$ 1 gram (.002 lb).

Three adjustable screws were mounted on the test bearing to control the position of the mating disk and load C.G. with respect to the bearing center.

Oil-free shop air was used as lubricant gas. The air supply and measurement system is shown schematically in Figure 42. Rotometer pressure was maintained constant within $\pm$ .5 psi when taking data in order that a constant calibration factor could be applied to the rotometer readings. The bearing supply pressure was adjusted to within $\pm$ .2 psi of the desired value when taking data. This required adjustment of the supply pressure regulator whenever the shop-air compressor came on the line. Supply pressure was measured at a tee in the line about six inches upstream from the bearing manifold. No thermocouple was installed in the bearing supply line; it was assumed that the supply gas temperature was approximately equal to room ambient temperature.

The bearing clearance was measured at two points across the narrow dimension of the bearing with capacitance probes. The output voltage of the probes were displayed on a dual beam, cathode ray oscilloscope (c.r.o.) During the first test, the C.R.O. sensitivity was set at 100 mv/cm, giving probe sensitivities of 0.90 and 0.85 mill/cm. The mating disk position was adjusted after each loading billet was added to produce C.R.O. displacements differing by the ratio of probe sensitivities, and consequently equal gaps at the two probe locations. There was no means installed for detecting difference in clearance across the long dimension of the bearing.

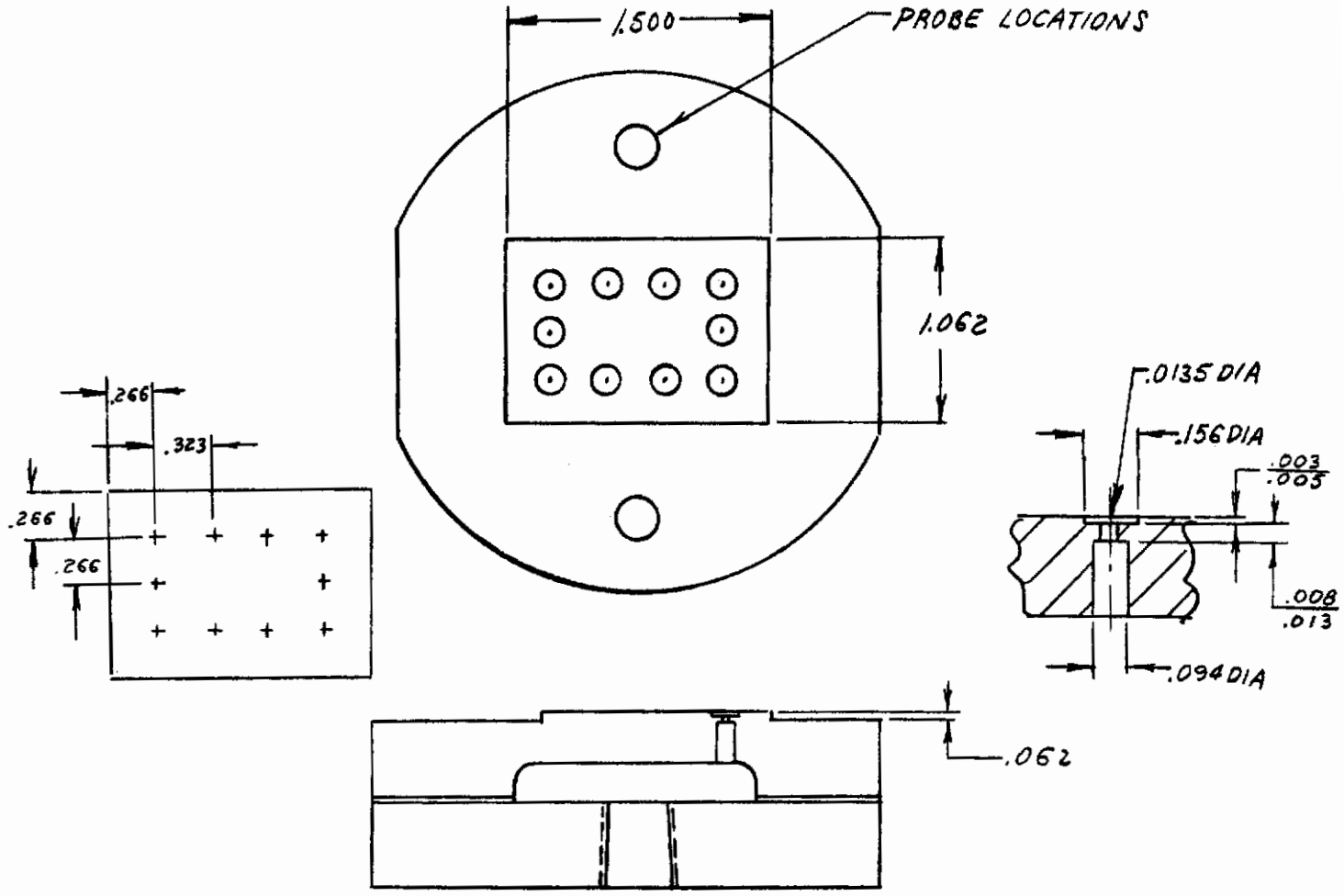

Figure 40. Rectangular Pad Test Bearing

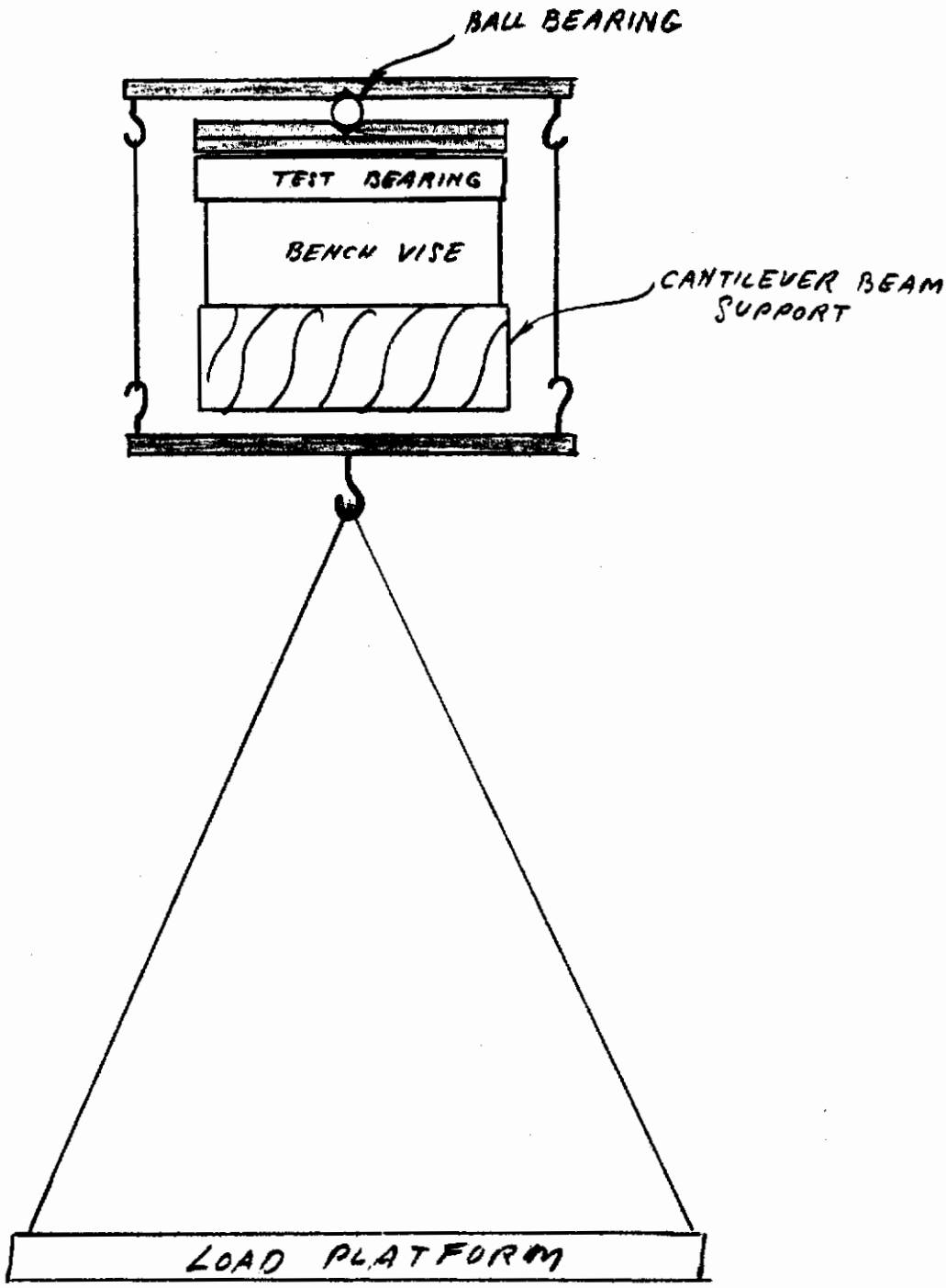

Figure 41. Schematic of Test Set Up for Rectangular Pad

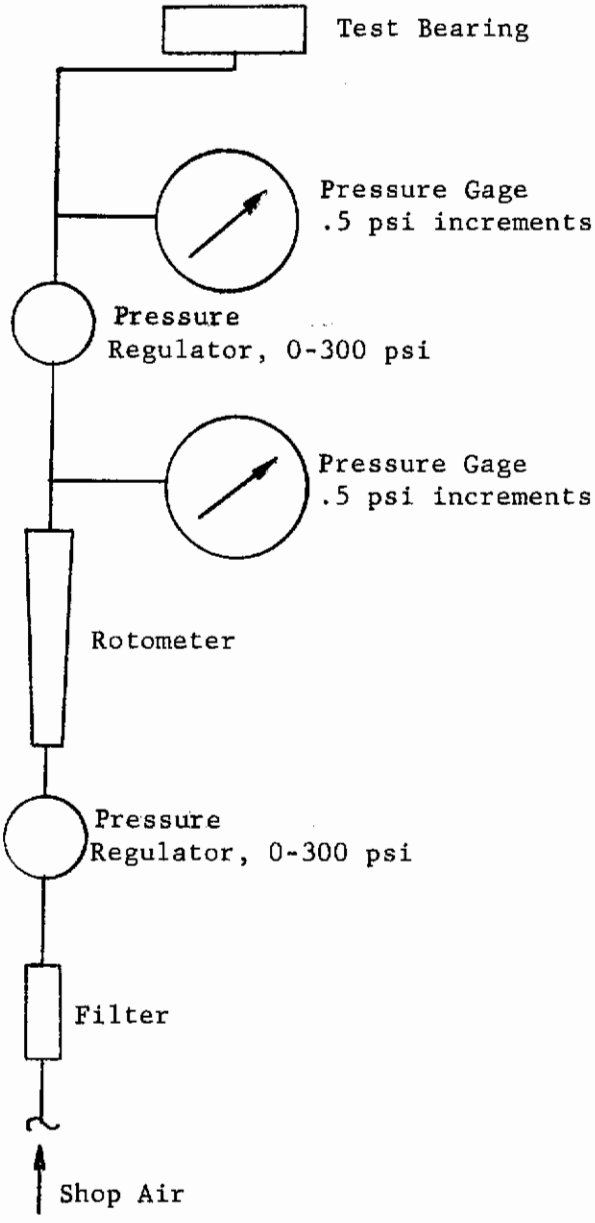

Figure 42. Air Supply and Measurement for A Rectangular Pad

Test Data

Figure 43 shows the measured air flow and load-deflection data for a P_s/P_a ratio of 2 (P_s = supply pressure = 14.7 psig, P_a = ambient pressure = 14.7 psia). Figure 44 shows similar data for $P_s/P_a = 4$, supply pressure = 44.1 psig. The discontinuity in the flow and load-deflection curves for $P_s/P_a = 4$ occurred when the loading arrangement was changed to the chain-suspended platform. Probably a shift in clearance probe position relative to the bearing contributed to this discrepancy, although the C.R.O. was readjusted after this change was made. The clearance values plotted are the average of the two measured gaps.

The rotometer used for these tests indicated percentage of full-scale, 10 to 100 percent with 100 % = 46.3 lb./hr. calibrated with N_2 gas at 300 psig, 70 F. The rotometer is essentially a variable area orifice maintained at a constant ΔP by the weight of the float, neglecting buoyant and drag forces. A calibration correction factor can then be approximated by considering the flow through an orifice operating at a ΔP less than one percent of the initial pressure.

$$W = \rho A v$$

$$v = \frac{2g\ RT\ \Delta P}{P}$$

$$\rho = \frac{P}{RT}$$

$$W = A\ \frac{P}{RT}\ \frac{2g\ RT\ \Delta P}{P} = A\ \frac{2g\ P\ \Delta P}{RT}$$

For a given rotometer operating at a given scale reading, A 2g ΔP is a constant, and the flow is proportional to the factor

$$\frac{P}{RT}$$

Substituting the values for P, R, and T for calibration and for actual use:

	Calibration	Usage
P, psia	347.7	94.7
R, ft/^{o}R	55.16 (N_2)	53.34 (air)
T, ^{o}R	530	535

the roto correction factor is then

$$\frac{94.7}{314.7}\ \frac{55.16}{53.34}\ \frac{530}{535} = 0.548$$

and full-scale flow is then

$$0.548 \times 46.3 = 25.40 \text{ lb/hr}$$

In Figure 45, the experimental data is compared with the analytical prediction for a pressure ratio of two (V=2). The agreement is very good, differing only at high values of Λ_s.

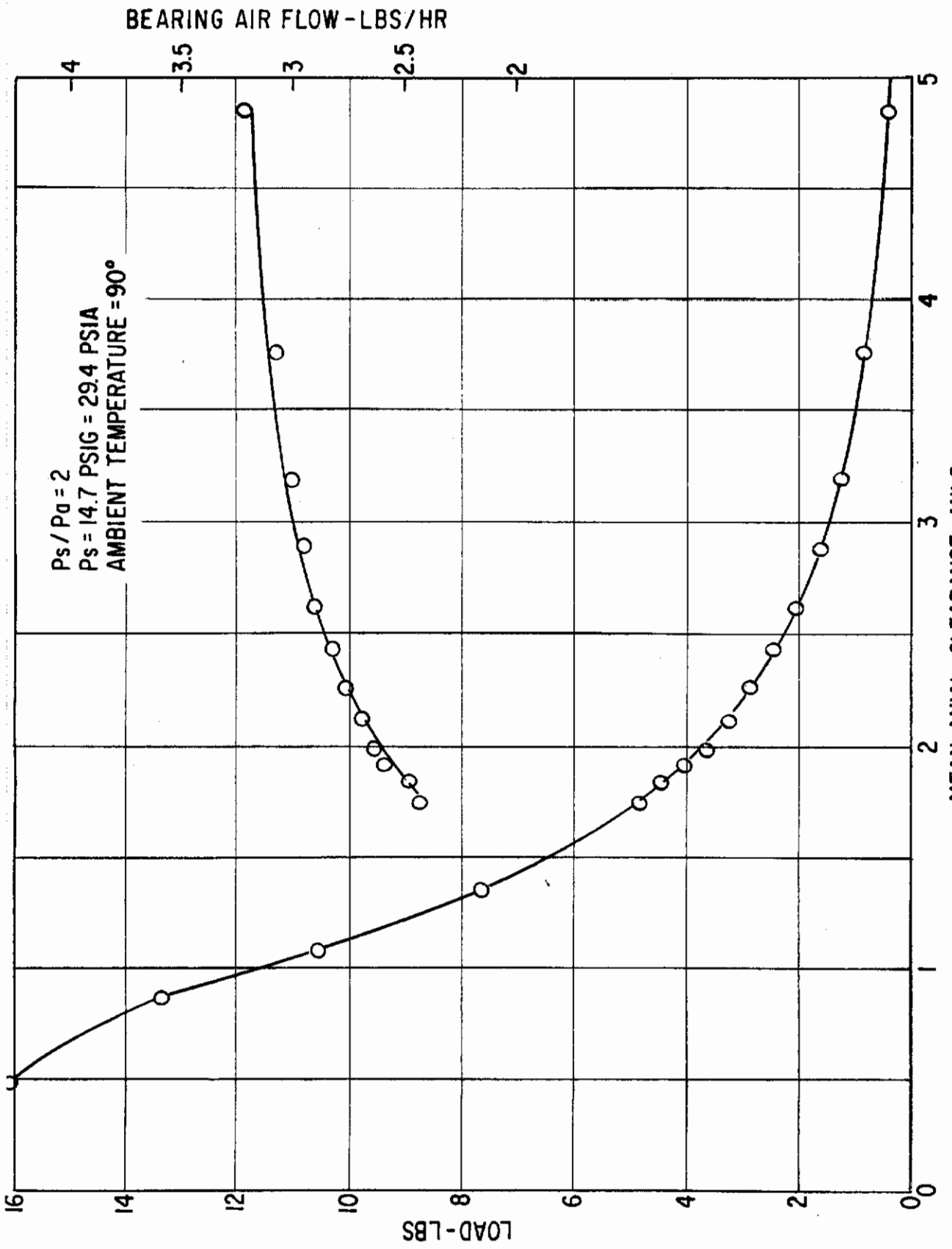

Figure 43. Data P_s/P_a = 2 (Rectangular Pad)

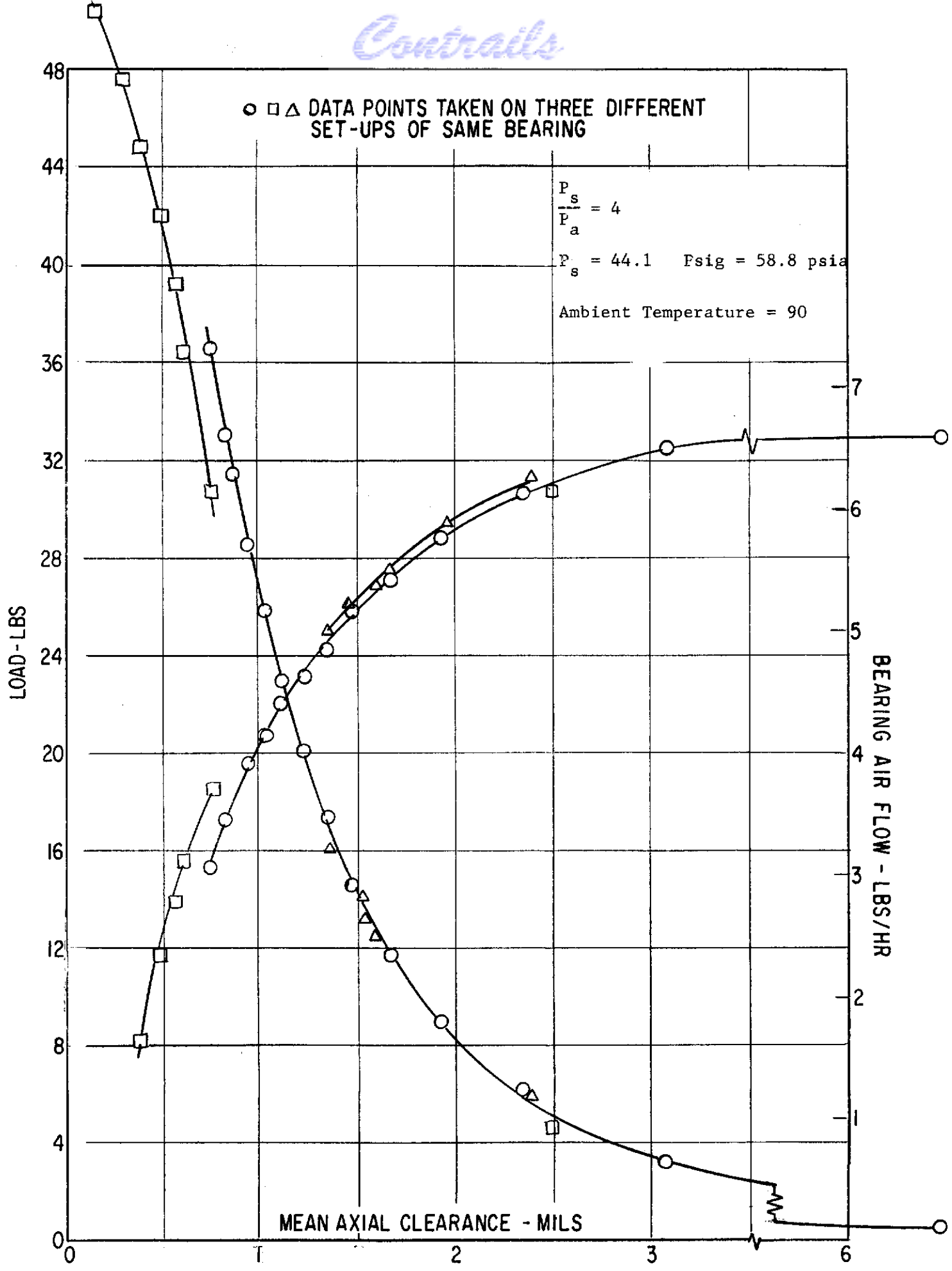

Figure 44. Data P_s/P_a = 4 (Rectangular Pad)

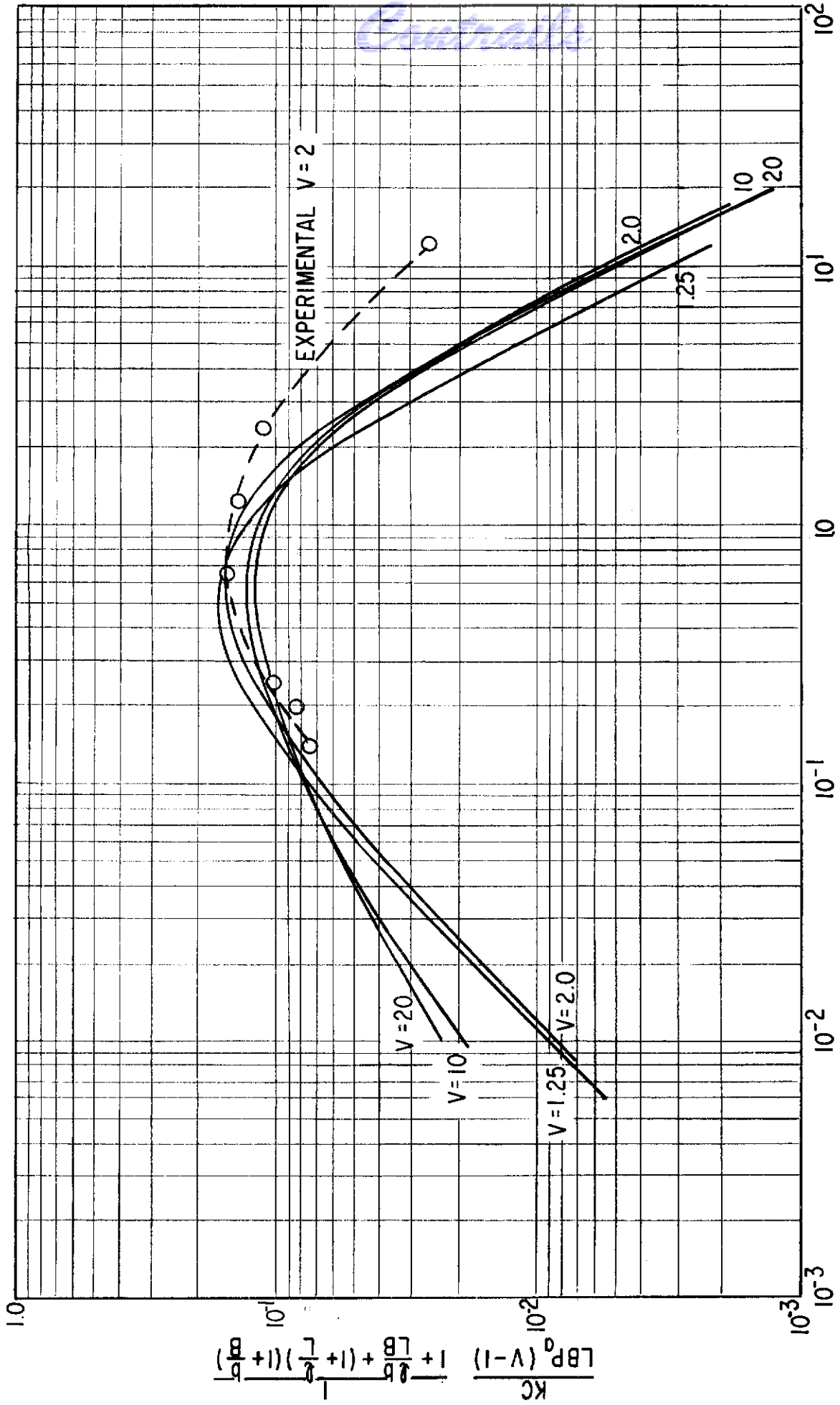

Figure 45. Dimensionless Stiffness vs Λ_s
(Rectangular Pad)

Preliminary Hybrid Bearing Tests

Prior to the assembly of the test equipment for this program, a few selected experiments were performed on an existing test stand. These data were for the following:

L/D = 1.5 inches

D = 2.0 inches

Rotor Weight = 13.5 pounds

This was done in order to collect a few check points for another configuration as well as to get some guidance for establishing the experimental procedures for this program.

The test rig consisted of a housing incorporating two journal bearings, the length of which can be changed up to three inches maximum. The shaft is two inches in diameter and accommodates Terry-type impulse drive turbines on each end. The turbine employs full-arc admission to minimize aerodynamic forces on the rotor. One of the turbine wheels serves also as a speed signal generating device.

The bearings (leaded-bronze) are externally fed through a total of eight orifices per bearing, with all connections extending to a common manifold for each individual bearing. The orifice holder includes a removable insert to facilitate rapid orifice changes. In addition to the replaceable orifices, fixed orifices (.050 inch diameter) are permanently incorporated in the journal bearing. This series orifice combination provides a means for changing the feeding system from orifice compensation to a combination of orifice-inherent compensation, or pure-inherent compensation through changes in replaceable orifice diameter and clearance.

One journal bearing is fed via a flow metering manifold. The flow meter circuit is designed to measure flow to any one of eight individual orifices and covers a range from 0 - 1.9×10^{-4} lb/sec with accuracy within six percent of measured flow. Pressure gages, calibrated to indicate gage pressure with accuracy of $\pm$ .15 psi, are used to register supply pressure levels.

Each bearing end is supplied with two capacitive probes placed 90 degrees apart with the output of each fed directly through proximity meters to a cathode-ray oscilloscope (CRO). Calibration of the CRO screen with the probe input permits determination of shaft position with a minimum accuracy of $\pm$ 8×10^{-6} inches. The same probe outputs are also used to determine frequency of oscillation, criticals and phase relationships between rotor ends.

Two thrust plates externally pressurized through six 0.020 inch diameter orifices are used to contain the rotor in the axial direction. Total axial play amounts to 0.004 inch.

Several of the parameters involved in the bearing design include: the number, N, and radius, a, of the feeding orifices; the bearing supply pressure P_s; the radial clearance c; and the bearing length to diameter ratio L/D. In the test results described below two parameters were varied — the orifice radius and the bearing supply pressure.

A useful factor for determining bearing performance is its stiffness. A typical procedure for experimentally determining this quantity is by obtaining the slope of a load-deflection curve. Examples of this type of data, obtained at a pressure ratio (P_s/P_a) of 6, for two different sets of orifices is given in Figures 46 and 47. When sufficient stiffness data is collected calculation of the two rigid body critical speeds (translatory and conical) as a function of supply pressure are made. A similar set of critical speed calculations are also made based on theoretically determined stiffnesses. The results of these two calculations are then plotted with experimentally determined critical speeds obtained by direct observation of the operating rotor-bearing system.

Results of calculations and experimental observations over a pressure range of P_s/P_a = 3 to 6 for two orifice sizes are shown in Figures 48 and 49. The only critical speeds observed were when the rotor became unstable and went into fractional frequency whirl. None of the rigid body critical speeds were observed. This was to be expected since the bearings under the conditions tested were critically damped.

Oxidation Coating for TZM

During a combustion chamber development program, the vendor had found molybdenum disilicide coatings prone to faults and cracks, especially on edges and corners. At temperatures above 2600 F, the coating becomes plastic and such faults are "self-healing" would not occur and oxidation would result at any fault.

A test was performed at MTI to verify the likelihood of difficulties arising from the coating. A sample of TZM one-half inch in diameter by two and one-half inches long was prepared with representative machining, including a tapped hole and steps on the outside diameter. After coating, the piece was examined under a microscope. The coating presented a smooth, unbroken surface except at edges, corners, and on the crests of threads. In these areas, the coating was rough and appeared to have faults or small cracks. The piece was then put in an air-atmosphere oven at 800 F for one hour. Examination after cooling revealed no change. The process was repeated at 1000 F with similar results. After one hour at 1200 F, a powdery white substance was seen in all faults and cracks previously noted on edges and corners. No new faults had appeared. After an hour at 1400 F, the white oxide was not apparent, but cavities had developed in the base metal under each fault in the coating.

Although the occurrence of faults can be minimized by modifications in the machined surfaces, the complexity of the test rig made this difficult to achieve. It was concluded that the coating would probably have defects at edges and corners, which would undoubtedly lead to oxidation and degradation of the component. A study of the test rig drawings indicated that it would be virtually impossible to eliminate all sharp corners. In addition, the dimensional requirements of the test rig would necessitate grinding the coating after deposition. No background of experience or knowledge of machining techniques or coating effectiveness after machining could be found. An additional factor for consideration was the difficulty of modifying a coated piece after initial manufacture. The above considerations led to the decision to rely on an inert atmosphere, rather than a coating, for oxidation protection.

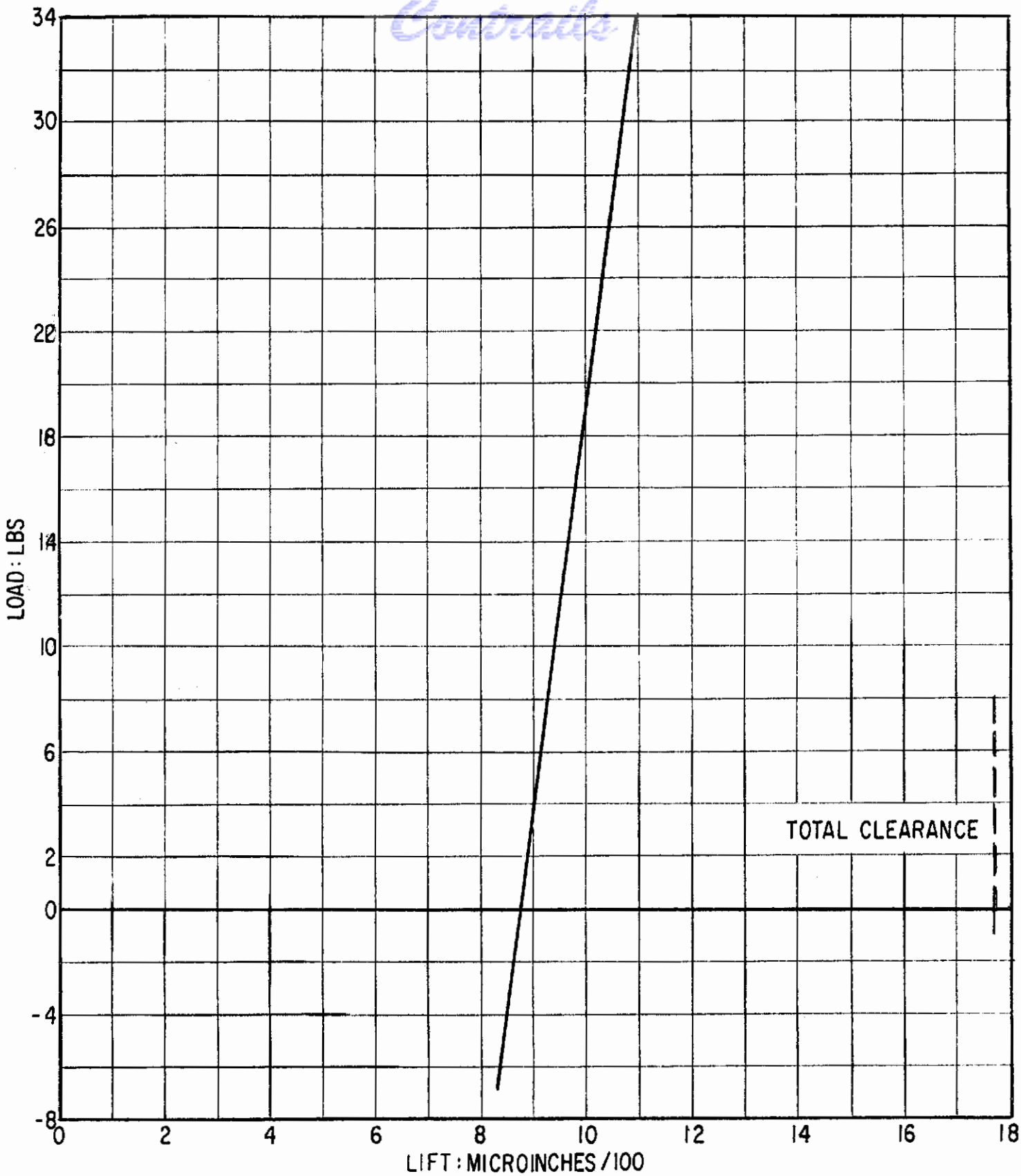

Figure 46. Externally Pressurized Bearing
Load Deflection Characteristics

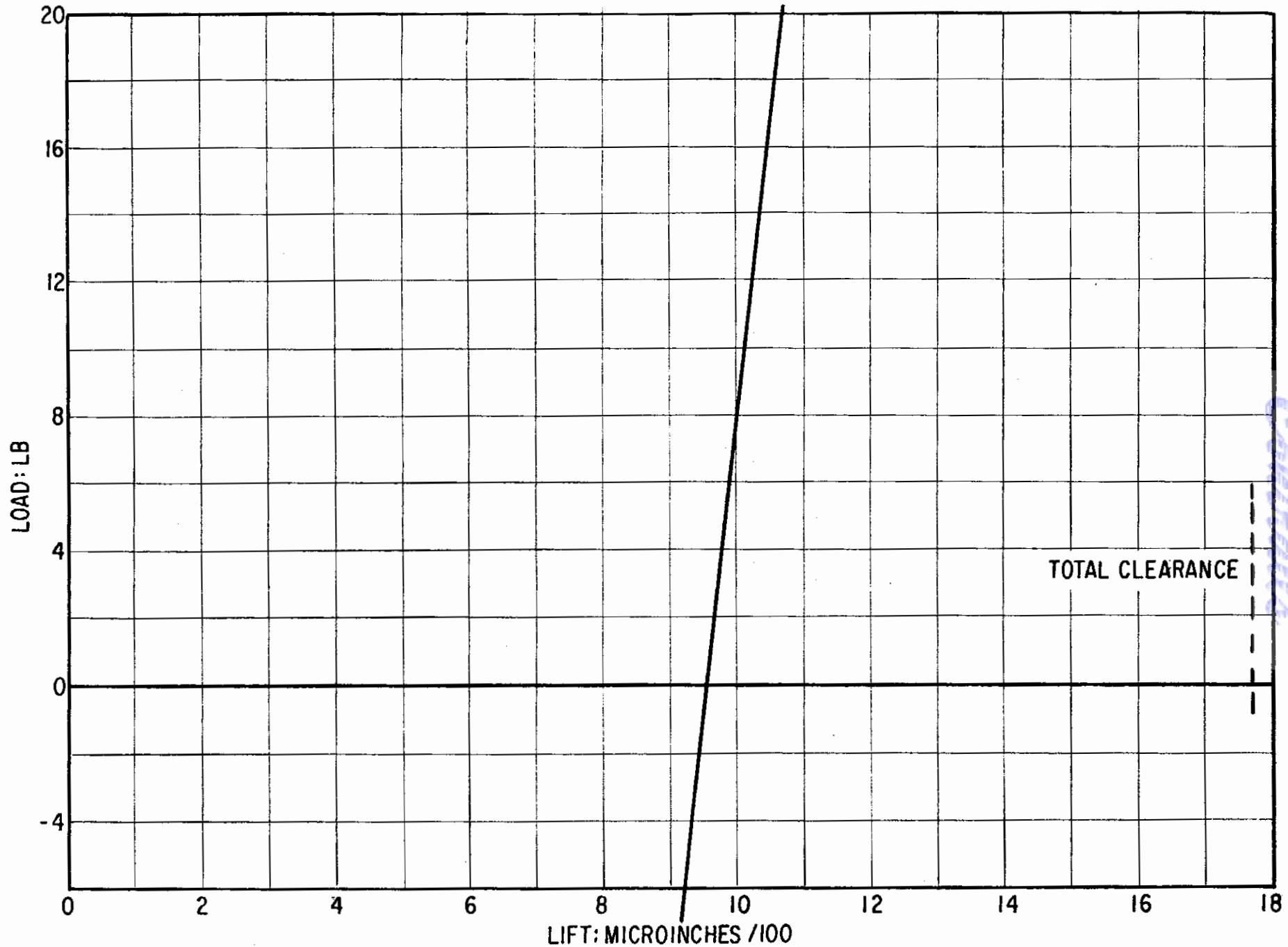

Figure 47. Externally Pressurized Bearing
Load Deflection Characteristics

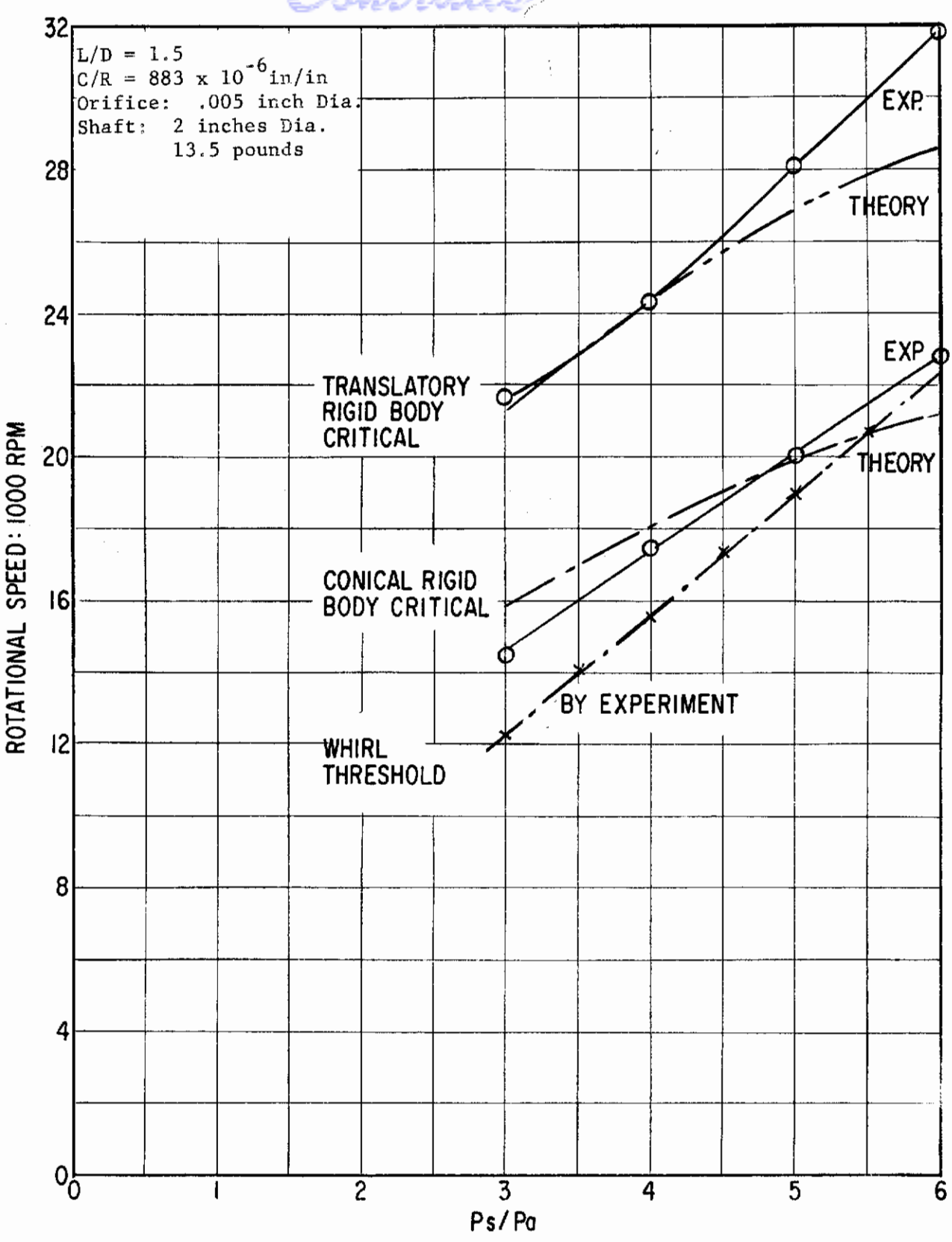

Figure 48. Stability Data for 360 Degree Hybrid Bearing

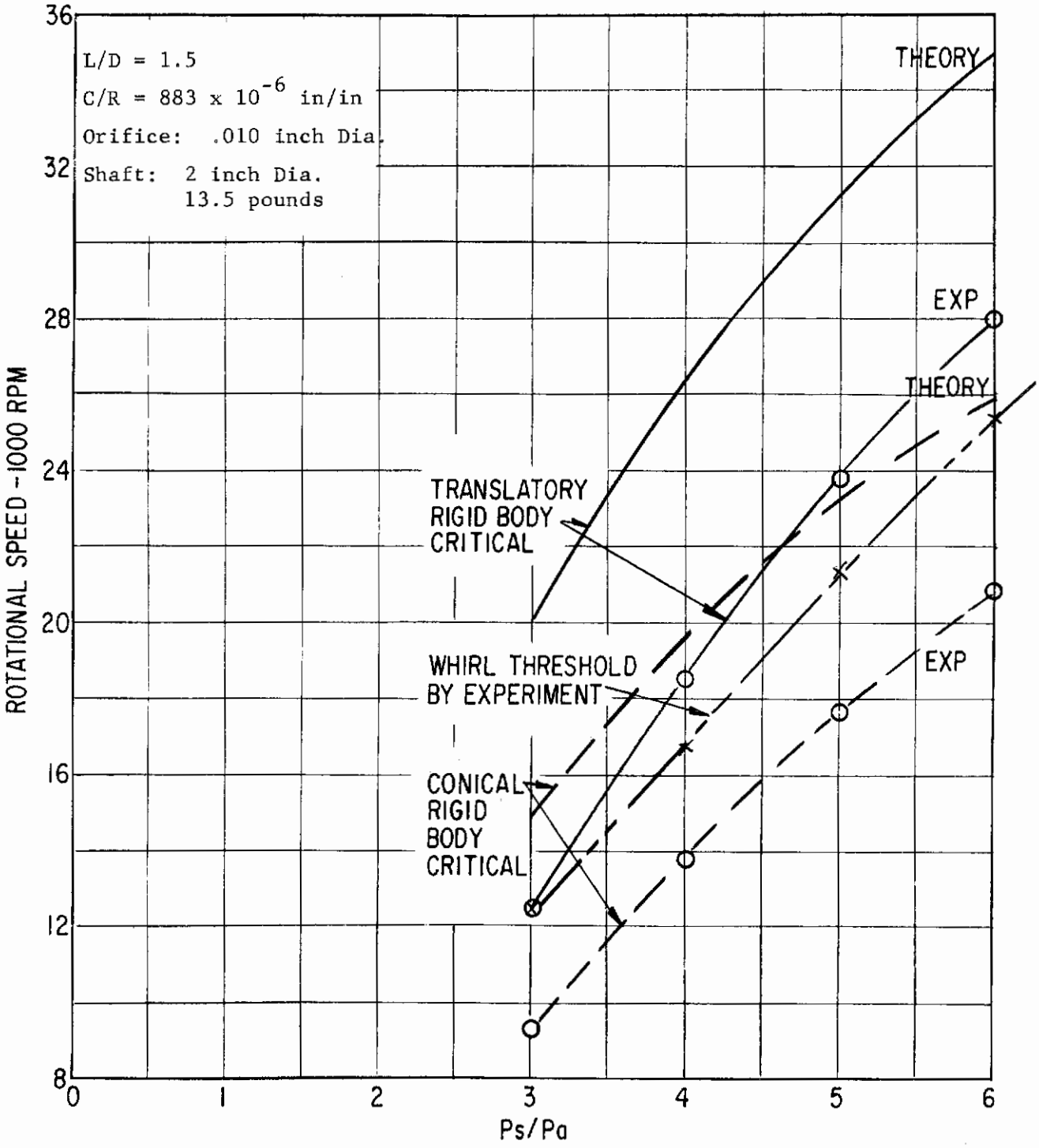

Figure 49. Stability Data for 360 Degree Hybrid Bearing

Erosion and Impingement Tests

Although an extensive evaluation of erosion effects would be beyond the scope of this program, some indication was felt to be necessary in order to be better able to interpret future high-temperature results and to anticipate test rig difficulties.

The object of the tests were:

1. To determine whether the flow of an inert, high temperature gas through a TZM aperture (orifice plate) causes significant erosion with resulting enlargement of the orifice.

2. To determine whether the impingement of a small, high velocity, high temperature inert gas jet would erode a closely positioned flat TZM plate.

A simple fixture was made which would evaluate a single orifice. The test fixture consisted of:

1. A TZM aperture .248 in. diameter, .004 in. thick with a centrally located 0.006 in. diameter hole.

2. A TZM impingement piece.

3. A TZM holder for positioning the impingement piece to within 0.005 in. of aperture.

4. A stainless steel can to provide an inert gas atmosphere for Item 3.

A coil of stainless steel tubing is used to supply high-temperature gas to the fixture. Figure 50 shows a print of the fixture. Figure 51 is a photograph showing the system in the furnace. It was first determined whether the addition of the impingement plate would affect the flow. Figure 52 shows that the flows are the same. Therefore, it was decided that a single series of tests could be used to determine deterioration of both orifice and impingement plate.

The flow was calibrated at room temperature to indicate mass flow at room temperature to indicate mass flow as a function of supply pressure. The fixture was installed in a furnace and gas line attached. Heating and gas flow are started. When the run was completed, the unit was allowed to cool, and a room temperature flow check was made. The thought was that should changes occur, the unit would be dismantled and examined under a microscope.

1. Re-calibration of test aperture after -
   5 hours at 1950°F, 1 hour at 1800°F, and
   2 hours at 1400°F showed absolutely no change in flow characteristic and therefore no change in effective aperture area.
2. Visual (microscopic) observation of the aperture and the impingement piece showed no effects of temperature or gas flow.
3. Re-calibration of test aperture after an additional 15 hours at 1950°F indicated no change in effective aperture area (Figure 53).

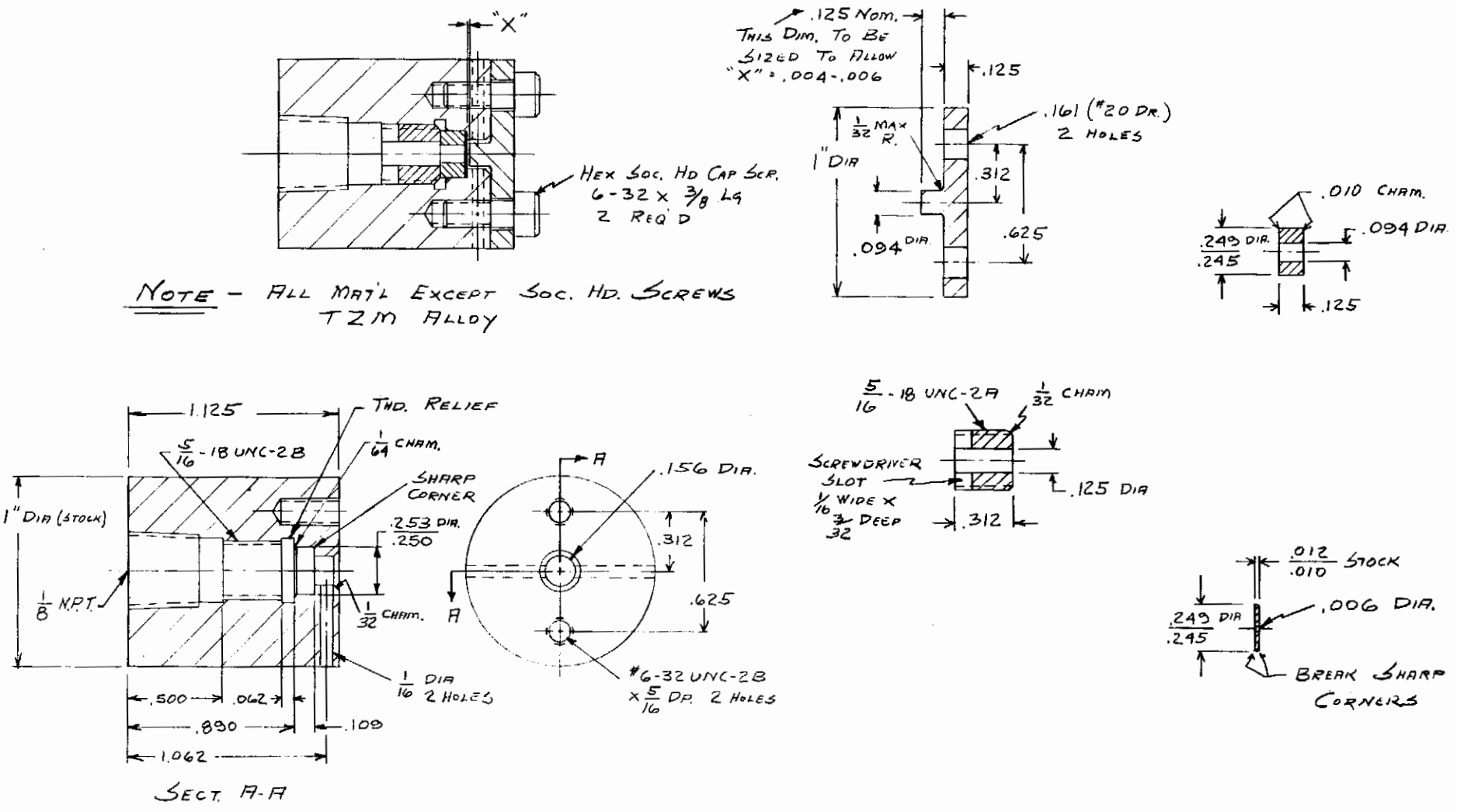

Figure 50. Erosion and Impingement Test Fixture

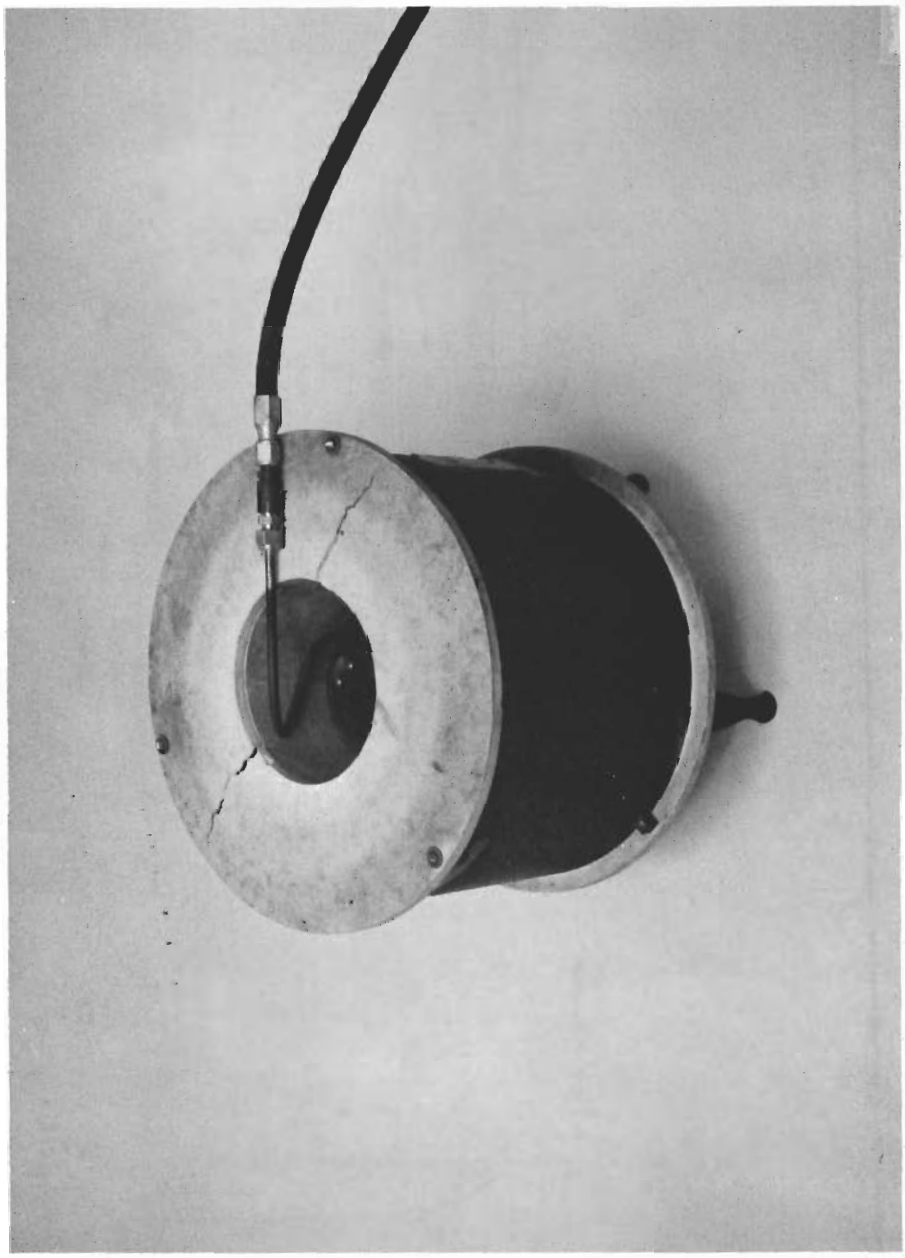

Figure 51. Erosion Test in Furnace

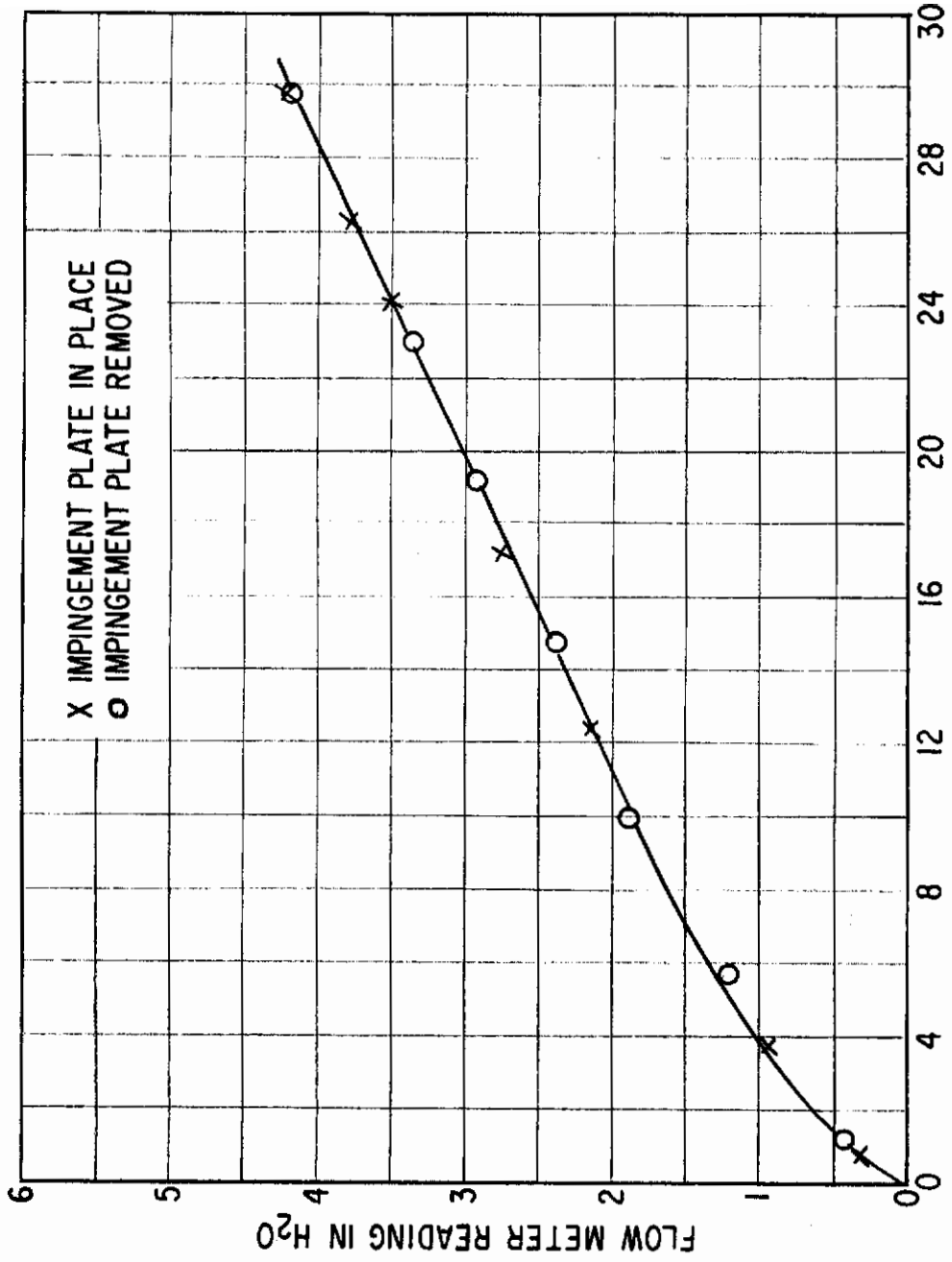

Figure 52. Flow Calibration Curve-Erosion Test

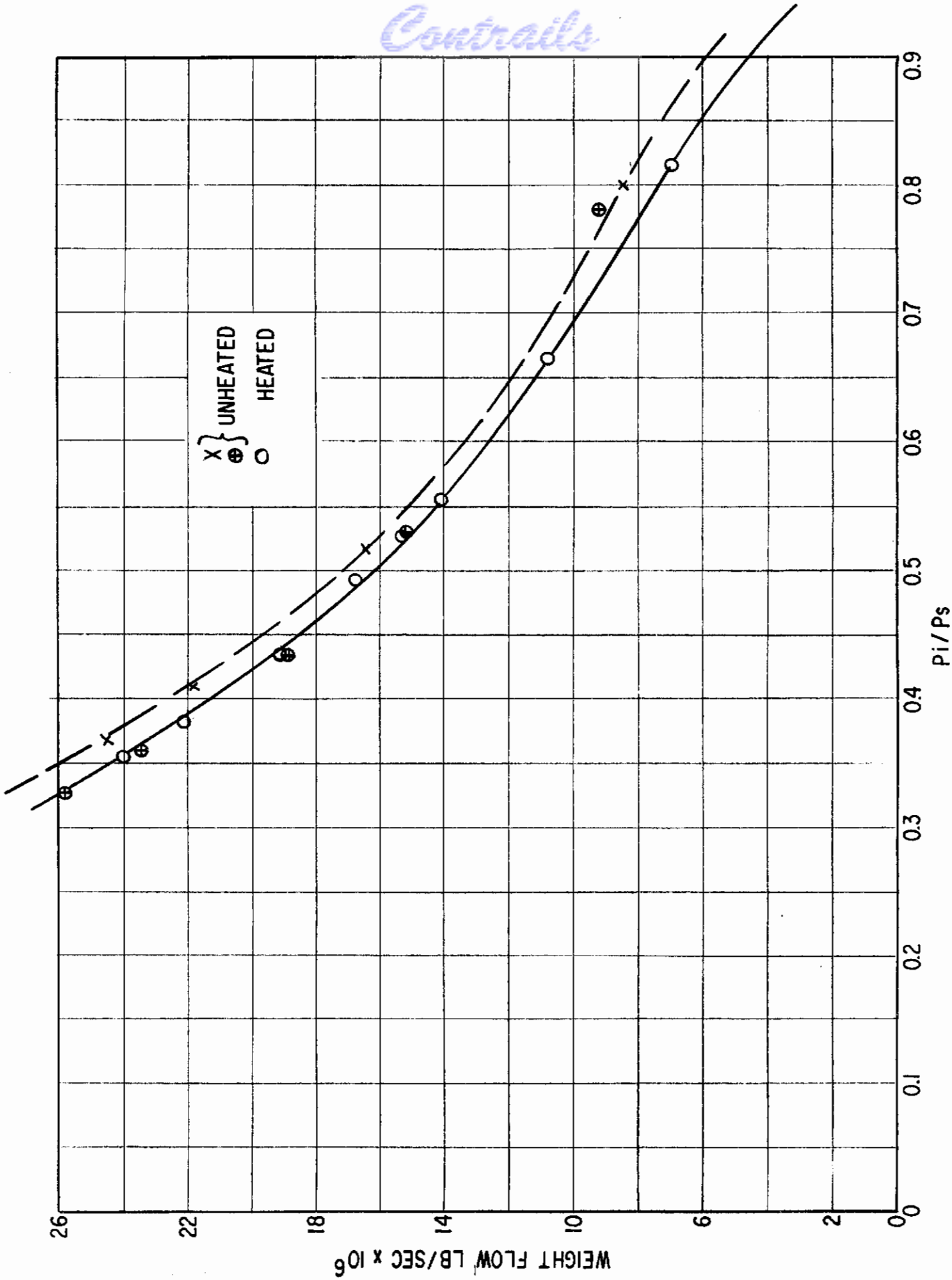

Figure 53. Flow Calibration Curve - Erosion Test

4. Visual inspection of the impingement test piece showed absolutely no effect due to either heat or gas flow.

Twenty hours were accumulated at 1950°F with several additional running hours at lower temperatures. The general conclusion is that no problems would be expected in this area on a short term basis.

Rotor Stability Tests

The stability range definition was felt primarily for the test equipment of Figure 19 built for this program. However, prior to these evaluations, a pretest procedure for the first test series was instituted as follows:

1. Thrust Bearing

   a. Assembly and leak test of pressure manifold
   b. Flow calibration of orifice group
   c. Finish machining and adjustment of thrust bearing capacitance probe

2. Turbine Nozzle Box Plate

   a. Pressure-flow calibration of turbine nozzles.

3. Bronze Bearing Inserts

   a. Flow check of all orifices (inherently compensated configuration)
   b. Final fitting and match-marking of inserts to bearing support rings
   c. Assembly into support rings
   d. Final measurement of bores

4. Bearing Support Rings

   a. Install jacking screws
   b. Final fitting and match-marking to housing

5. Shafts, Steel

   a. Dynamic balancing
   b. Final measurement of diameters and lengths (three shafts to provide three different clearances)

6. Calibration of Journal Bearing Loader (in housing) With Measured Weights

7. Adjustment of Shaft End Play

   a. Axial measurement of all components afecting shaft end play
   b. Grind spacer rings to proper thickness to achieve .001 inch end play

8. Assembly of Journal Bearings in Housing

9. Calibration of Thrust Loader With Measured Weights Applied to End of Shaft

    a. Subassembly of housing, journal bearings, thrust loader, and shaft, thrust bearing not installed.

10. Final Fit and Adjustment of Rig Support Bracket

11. Assembly of Rig for First Test

    a. Align nozzle box plate to housing and install dowels
    b. Align thrust bearing and loader plates to housing and install tiebolts

12. Installation of Rig in Test Facility

    a. Mount rig in bracket
    b. Install and adjust all probes
    c. Connect gas supply lines from control panel (low temperature tubing)
    d. Connect all pressure taps (thermocouples not required)

13. Conduct test of First Combination of Orifice Diameter and Clearance

14. Disassemble and Change Clearance (different shaft)

    a. Repeat for third shaft

15. Disassemble and Change Orifice Configuration

The experimental program as currently defined is made up of the following major divisions, in chronological order:

1. Room temperature evaluation of 360 degree hybrid bearings.

    a. Determination of static stiffness and verification of the effects of clearance, orifice size, mode of compensation, and supply pressure on the stiffness for each configuration to be evaluated.

    b. Determination of stability and verification of the predicated stability criteria.

    c. This portion will be performed with the bronze bearings and steel shafts, allowing the high temperature test pieces to be reserved for high temperature tests.

2. Room temperature evaluation of flexure mounted hybrid pad bearings.

   a. Determination of pad film stiffness.
   b. Determination of flexure radial and angular stiffness.
   c. Exploration for instabilities.

3. High temperature evaluation of 360 degree bearing.

   a. Optimization of bearing parameters for a design point temperature, based on the refined criteria determined by room temperature evaluation, and finishing of the high temperature test piece.

   b. Operation at the design point temperature, verification of design point performance.

   c. Determination of the effects on stiffness and stability of operation at off-design temperatures.

   d. Determination of latitude of stability optimization criteria for operation over an extended temperature range.

4. High temperature evaluation of flexure mounted hybrid pad bearing.

   a. Greatly dependent on the results of room temperature evaluation. Changes in flexure stiffness due to change in material properties with temperature may be very significant. Testing in this area is not yet completely defined.

The test data for the first phase are to be collected to verify and refine the criteria implied by Figure 13. To this end, the data must include variations in the feeding parameters Λ_s and the degree of inherent compensation δ, where δ is the ratio of orifice radius to twice the bearing radial clearance for orifices drilled directly into the bearing bore ($\delta = a/2C$). The degree of compensation refers to the minimum or controlling restriction in the flow system. For orifices drilled directly into the bore, there are two possible restrictions: the orifice area and the clearance annulus around the orifice. This is illustrated below.

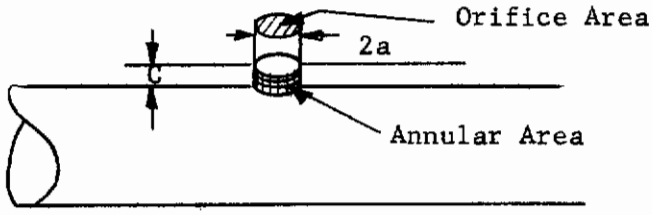

The orifice area is πa^2 and the annular area $\pi 2ac$. The ratio of the orifice area to annular area is

$$\frac{\pi a^2}{\pi 2ac} = \frac{a}{2c}$$

When the ratio is 0.5 or less, the orifice is the controlling restriction. Where the ratio is two or greater, the annular area controls. The configuration defined by the data in Figure 61 with a δ value of 1.66 is between the two limits and is, therefore, dependent on both restrictions.

Three test shafts permit three clearance ranges for a given bearing configuration. Each shaft-bearing combination is evaluated for a series of pressure ratios. After such a test series, the orifice is changed and the process is repeated. The data collected, at least for the initial tests, was as follows:

1. Static Load-Deflection and Flow Determination at Desired Pressure Ratios
2. Critical Speeds at Each Pressure Ratio
3. Whirl Threshold at Each Pressure Ratio
4. Whirl Ratio at Each Threshold Point
5. Load-Deflection Tests at Various Speeds for a Selected Pressure Ratio
6. Whirl Threshold at Various Eccentricity Ratios. A Selected Pressure Ratio
7. Flow versus Speed at a Selected Pressure Ratio and Zero Eccentricity
8. Determine Mode (Conical or Translatory) of Whirl

Since the bearing is inherently compensated, the measured stiffness is compared with the calculated stiffness for an inherently compensated bearing. This is shown on Figure 54. The measured stiffness is lower than the calculated except for very low pressure ratios. However, there is reasonable agreement. The flow characteristics shown on Figure 55 agree much more closely. It should be noted that these flows are below the 40 pound per hour limit set for this program, and that low temperature performance will yield the maximum flow condition.

For each pressure ratio, the speed at which fractional-frequency whirl occurred was determined. In order to see if this was following the trend of Figure 13, these data were plotted on a similar coordinate system. Although these data were taken at various pressure ratios, Figure 56 indicates that the general trend is correct. It is expected that there may be a family of such curves when the data is separated with respect to pressure ratio. However, this will not be possible until the various shaft clearance combinations are completed.

It is generally accepted that the stability should be improved at higher eccentricity ratios. Therefore, some evaluation was devoted to determining the threshold speed variation with increasing eccentricity ratio. Figure 57 shows the variation of threshold speed with eccentricity ratio. At a pressure ratio of six, a significant variation was noted. These data are compared with the predictions of Reference 8 on Figure 58. The trend is qualitatively predicted; however, the theoretical data was for low eccentricity values only.

Some of the data collected were intended to determine whether certain variations should be considered in future evaluations. Figure 59 shows how mass flow varies with speed. The maximum variation in flow was in the order of 3-1/2 percent. Figure 60 shows the variation of mass flow with eccentricity ratio. Again, the variation is small. Therefore, it was decided that flow determinations would be limited to check tests in future evaluations.

Finally, a determination was made to compare the load capacity and stiffness as a function of speed. This is shown on Figure 61. There is very little variation. This is to be expected since the compressibility number Λ is small, less than 1.

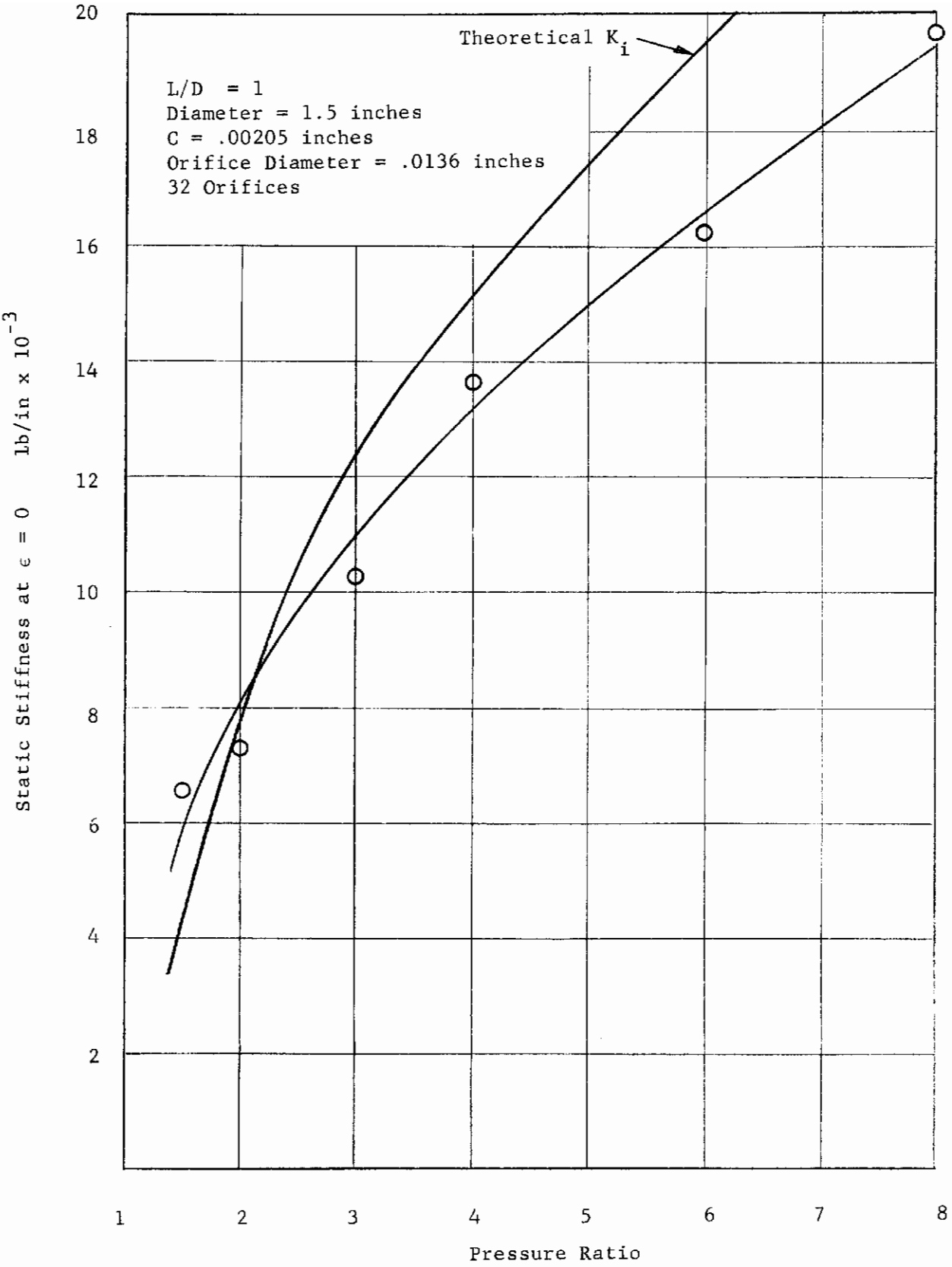

Figure 54. Double Row Hydrostatic Bearing Stiffness versus Pressure Ratio

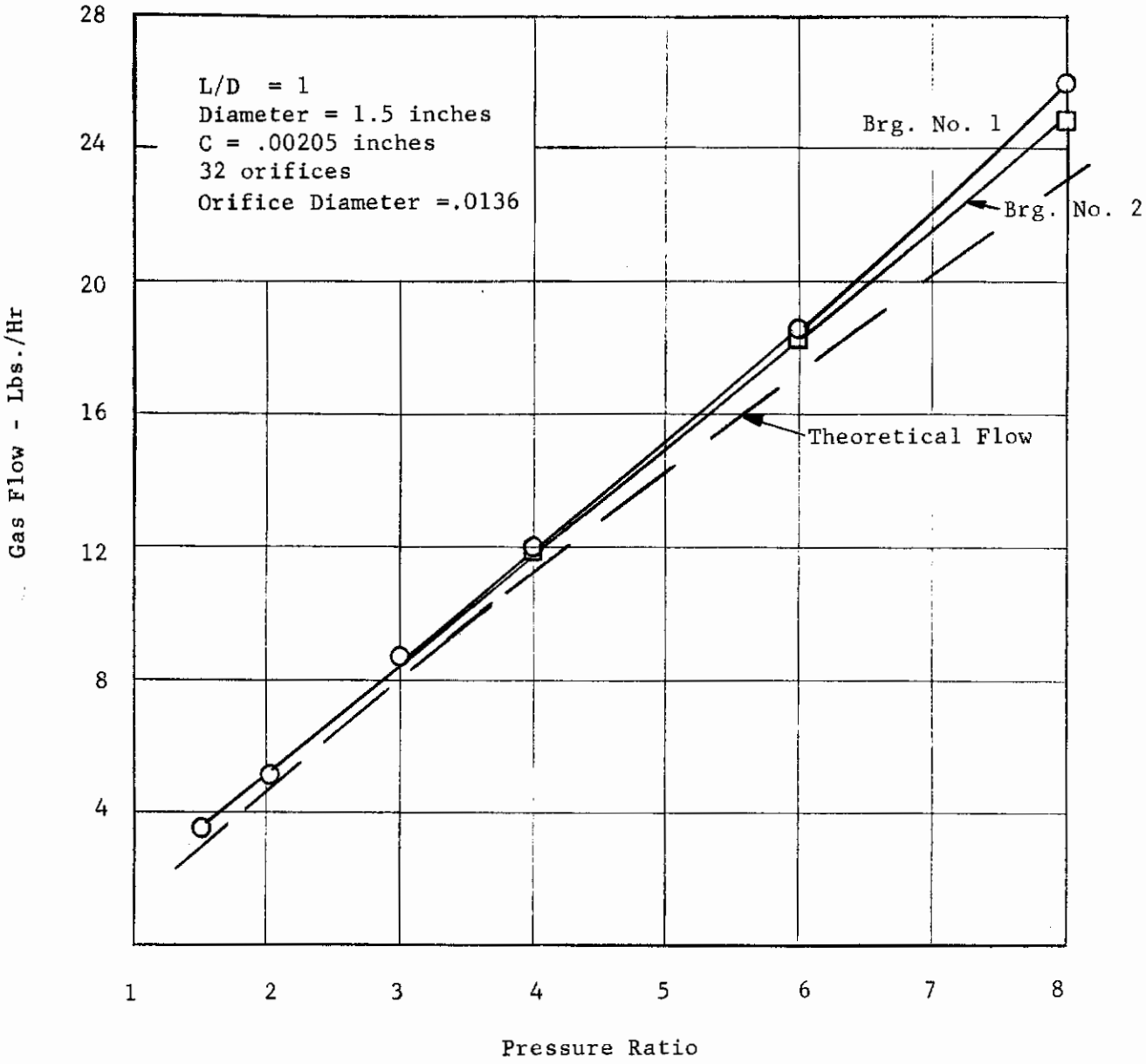

Figure 55. Double Row Hydrostatic Bearing Flow versus Pressure Ratio

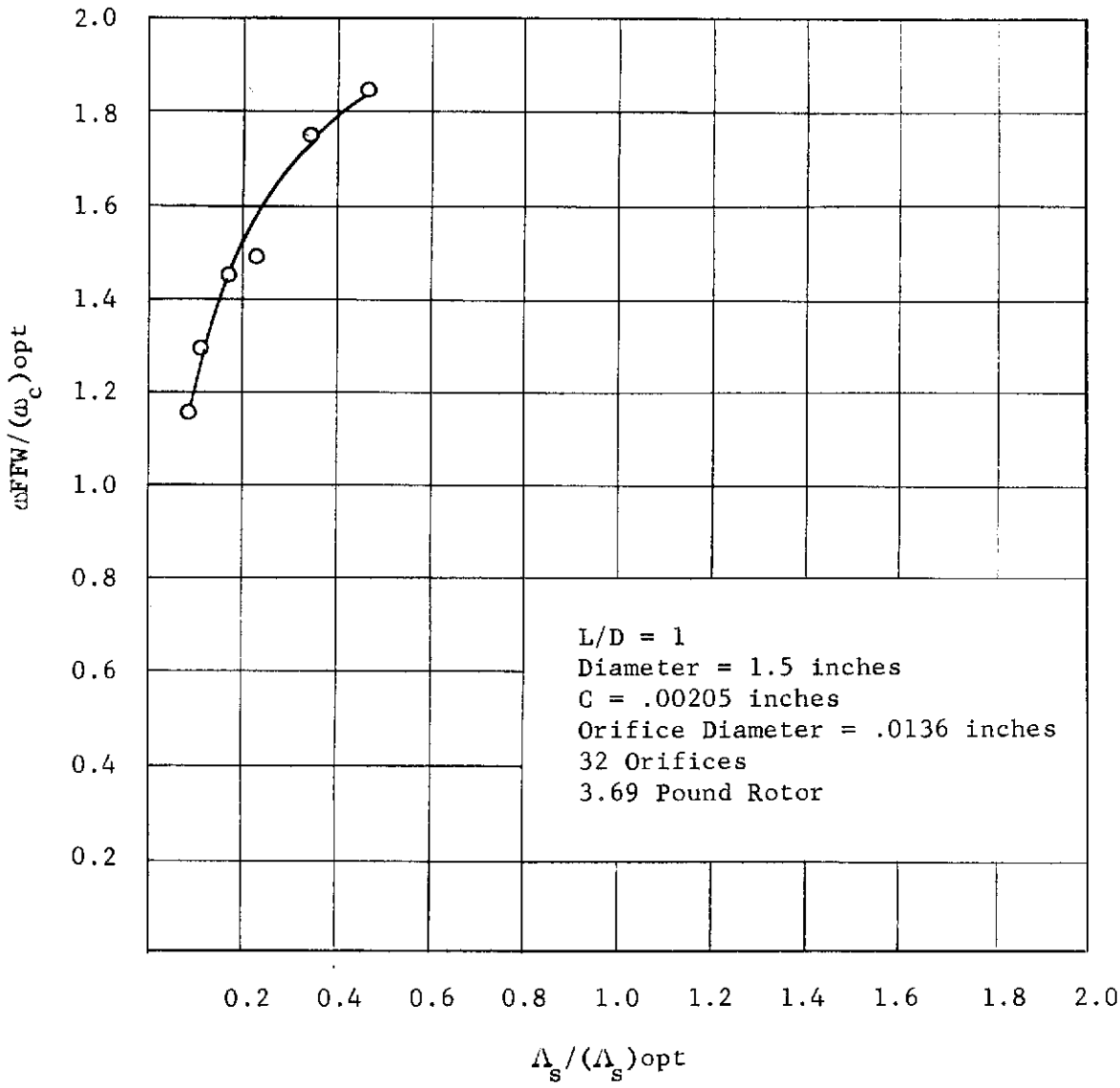

Figure 56. Speed Ratio versus Feeding Parameter Ratio

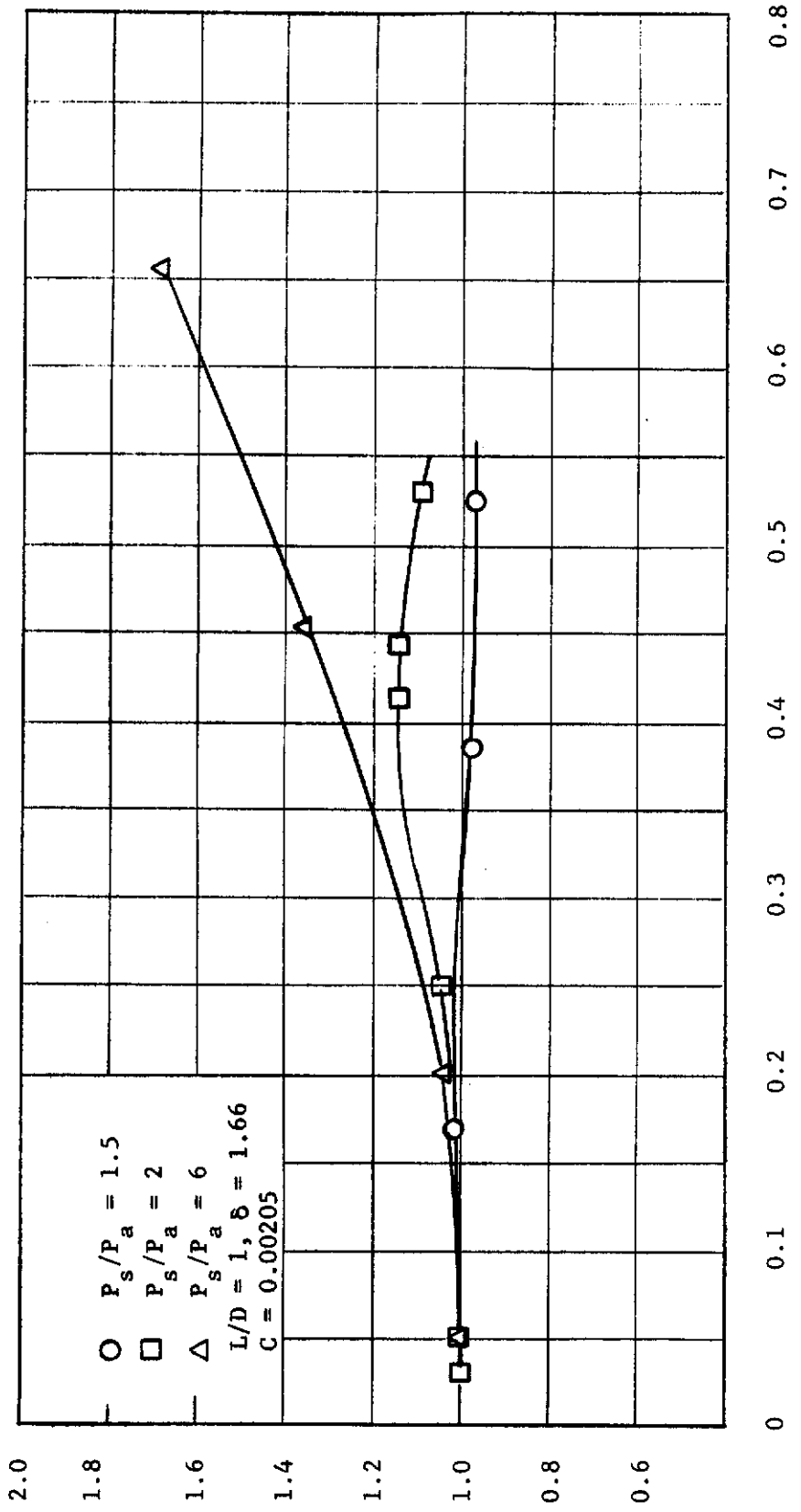

Figure 57. Effect of Eccentricity Ratio on Whirl Speed

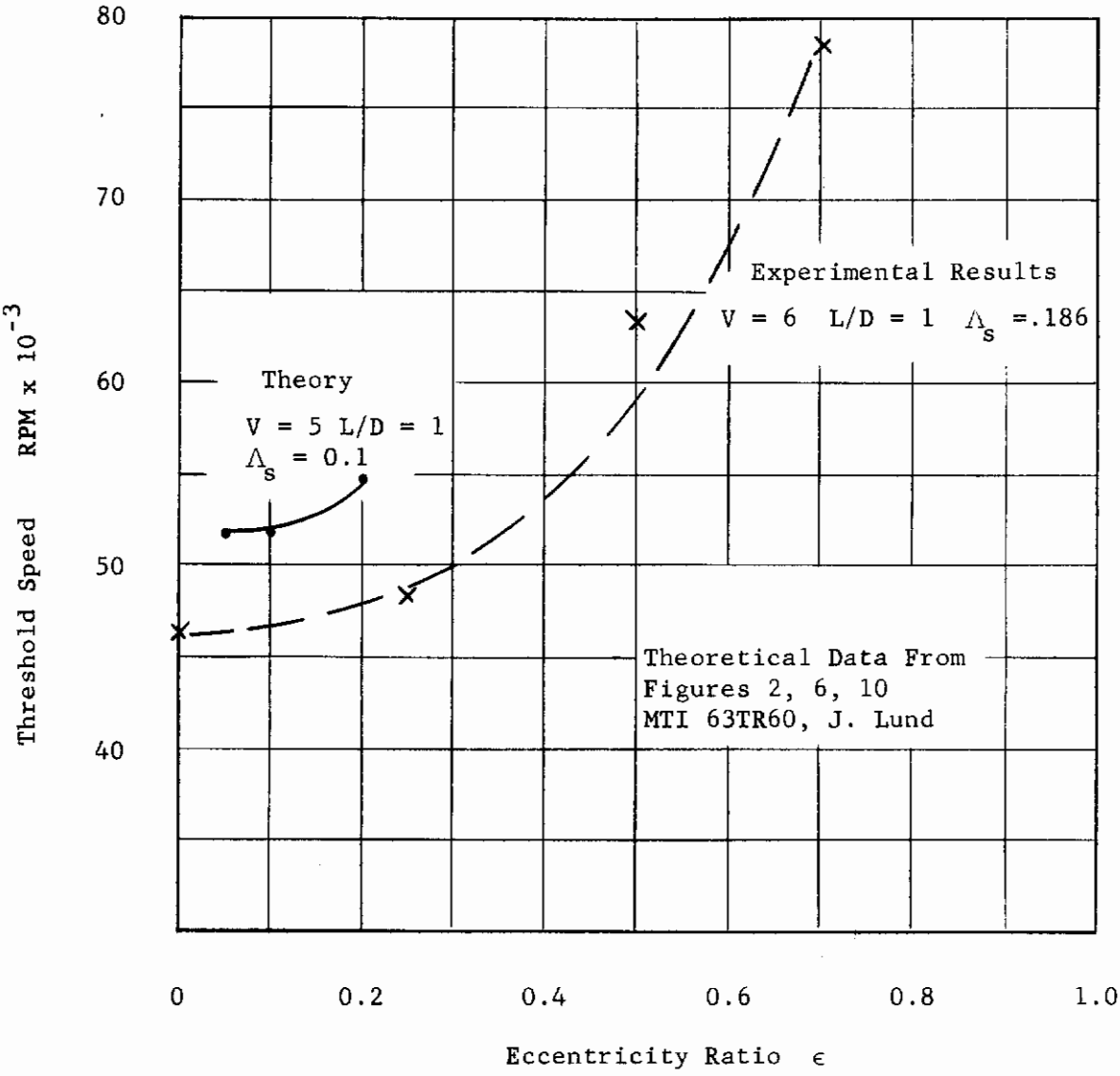

Figure 58. Effect of Eccentricity Ratio on Whirl Speed

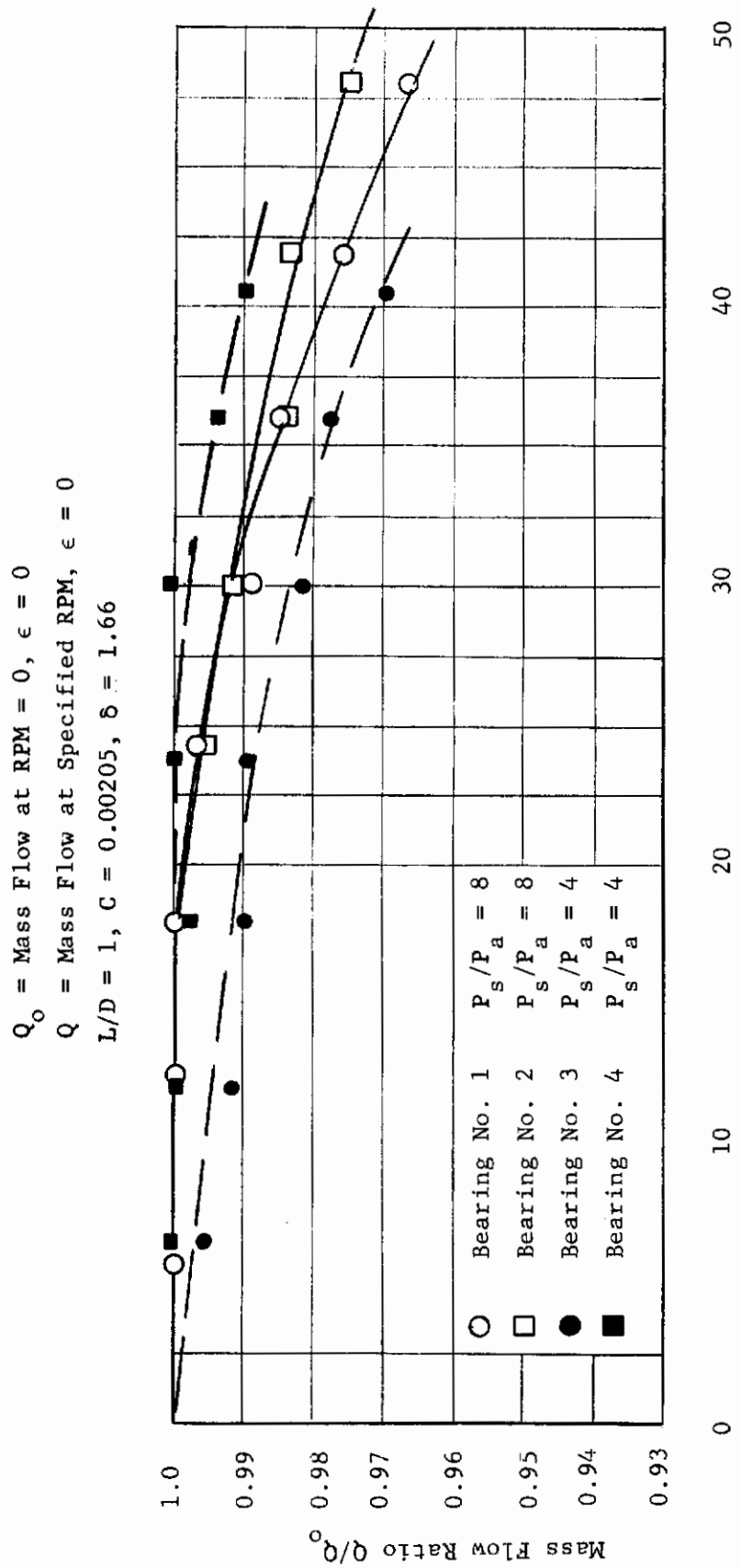

Figure 59. Flow versus Shaft Rotational Speed

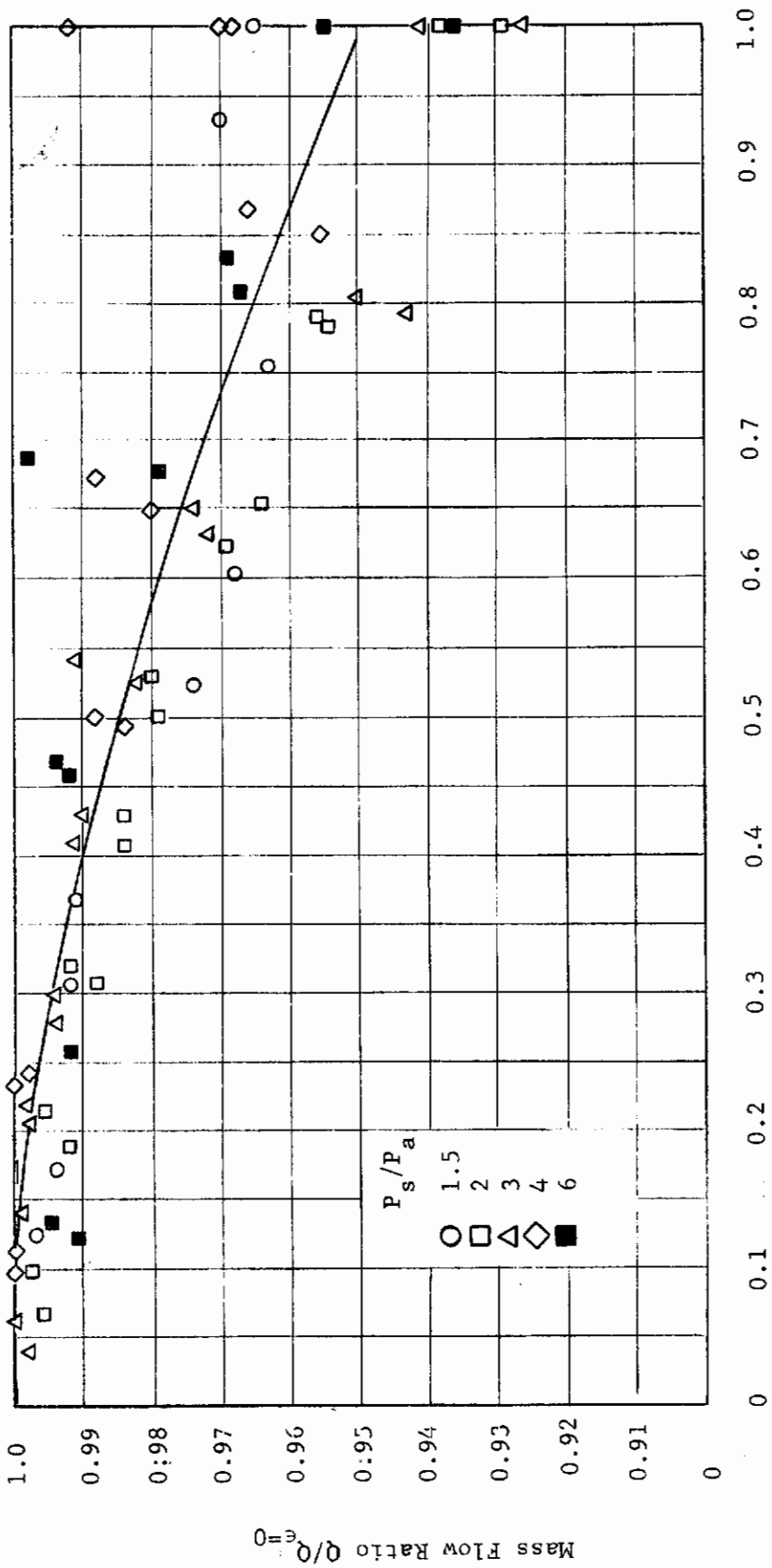

Figure 60. Mass Flow versus Eccentricity Ratio

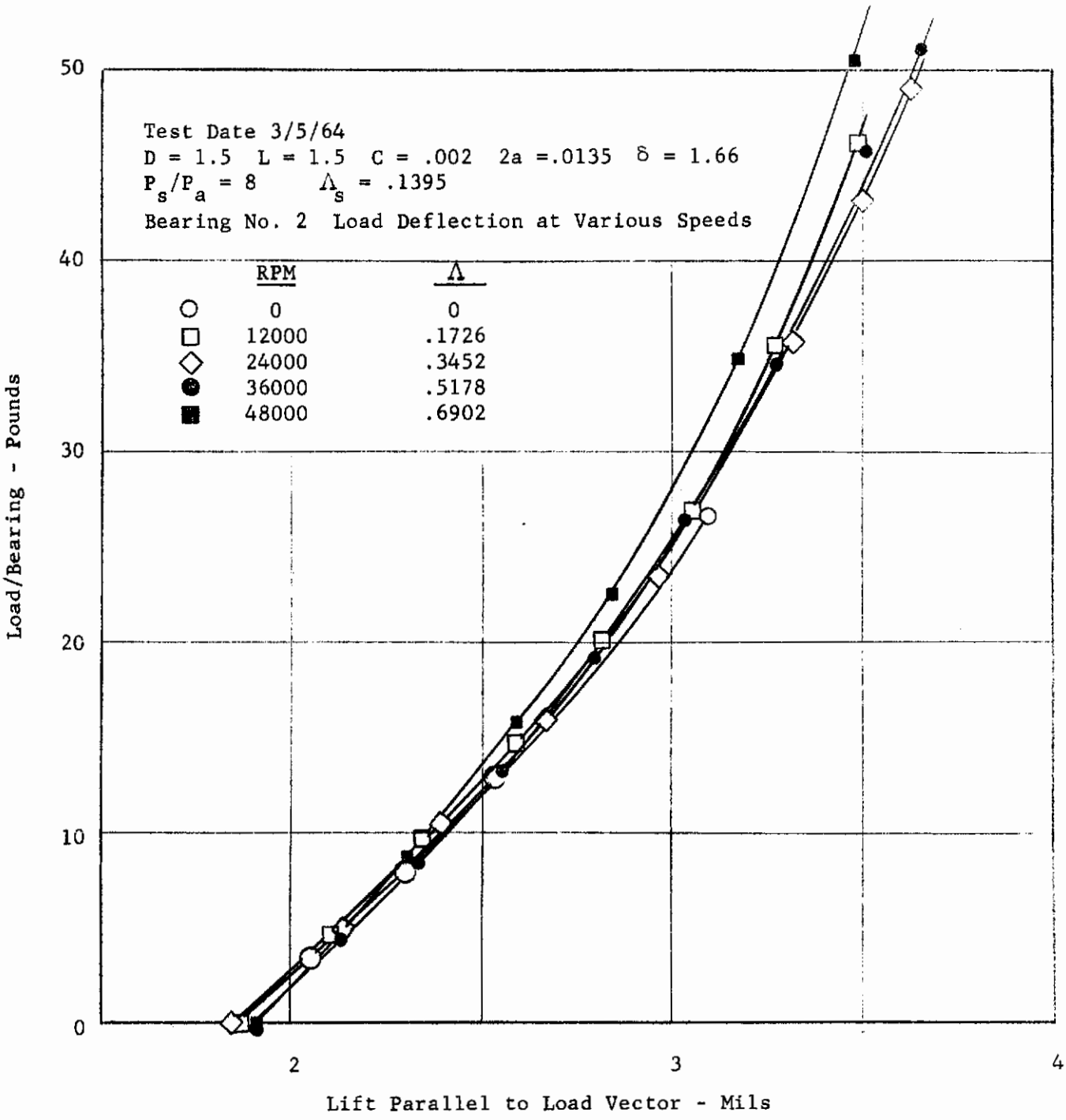

Figure 61. Load-Deflection as a Function of Speed

REFERENCES

1. J. Meacher, "Gas Lubrication of Bearings at Very High Temperatures, High Speeds, and Low Lubricant Flow Rates," ASD-TDR-62-310, February 1962.

2. L. Licht and H. G. Elrod, Jr., "An Analytical and Experimental Study of the Stability of Externally-Pressurized, Gas-Lubricated Thrust Bearings," Contract Nonr-2342(00), Task NR 061-113, February 1961.

3. J. W. Lund, "On the Hybrid Gas Lubricated Journal Bearing," Contract No. Nonr 3730 (00), Task No. NR 061-131, March 1962.

4. J. W. Lund, "The Hydrostatic Gas Journal Bearing with Journal Rotation and Vibration." ASME Paper No. 63-LubS-4, June 1963.

5. L. W. Winn and B. Sternlicht, "The Load Carrying Capacity and Stability of Hybrid Gas Bearings." Report for ONR, November 3, 1962.

6. H. H. Richardson, "Static and Dynamic Characteristics of Compensated Gas Bearings." Trans. ASME, Vol. 80, 1958, pp. 1503-1509.

7. R. H. Larson and H. H. Richardson, "A Preliminary Study of Whirl Instability for Pressurized Gas Bearings." Journal of Basic Engineering, Trans. ASME. Vol. 84, Series D, No. 4, December 1962, pp. 511-520.

8. J. W. Lund, "Hybrid Gas Journal Bearing Stability," MTI-63TR60, December 27, 1963.